

Aus der Klinischen Kooperationseinheit Dermato-Onkologie
der Klinik für Dermatologie, Venerologie und Allergologie,
Medizinischen Fakultät Mannheim
Leiter: Prof. Dr. med. Jochen Sven Utikal

SOX10 downregulation in tumor cells affects extracellular vesicle
production and function in the tumor microenvironment

Inauguraldissertation
zur Erlangung des medizinischen Doktorgrades
der
Medizinischen Fakultät Mannheim
der Ruprecht-Karls-Universität
zu
Heidelberg

vorgelegt von
Peng Yuan
aus
Anhui, China
2021

Dekan: Prof. Dr. med. Sergij Goerd
Referent: Prof. Dr. med. Jochen Sven Utikal

Für meine liebe Familie

CONTENTS

	Page
LIST OF ABRREVIATIONS.....	1
1 INTRODUCTION	5
1.1 The function of SOX10 in neural crest development and melanogenesis	5
1.2 The function of SOX10 in tumors	6
1.3 The function of exosomes in tumor microenvironment	8
1.3.1 The definition of exosomes.....	8
1.3.2 The biogenesis, transportation and uptake of exosomes	8
1.3.2.1 The biogenesis of exosomes	9
1.3.2.2 The transportation of exosomes	10
1.3.2.3 The uptake of exosomes.....	11
1.3.3 Exosomal cargoes in cancer cells	12
1.3.3.1 Nucleic acids in exosomes.....	13
1.3.3.2 Proteins in exosomes.....	14
1.3.3.3 Lipids in exosomes	16
1.3.4 The role of exosomes in SOX10 ^{high} tumors	16
1.4 Objective	19
2 MATERIALS AND METHODS.....	20
2.1 Materials.....	20
2.1.1 Antibodies.....	20
2.1.2 Buffers	21
2.1.3 Cell culture reagents.....	21
2.1.4 Chemicals.....	22
2.1.5 Database	23
2.1.6 Instruments.....	23
2.1.7 Kits	24
2.1.8 Primer oligos.....	24

2.1.9 Others.....	25
2.1.10 Software	26
2.2 Methods.....	26
2.2.1 Cell culture and conditioned media collection.....	26
2.2.2 SOX10 knockdown systems in cell lines	27
2.2.3 Western blotting.....	28
2.2.4 β -galactosidase assay for microscope and flow cytometry.....	29
2.2.5 Isolation of exosomes from cell culture supernatant and interstitial fluid of murine brain tumors.....	30
2.2.6 Characterization and quantification of exosomes	32
2.2.7 Uptake of exosomes and functional assay on macrophages.....	33
2.2.8 Evaluation of the migration of tumor cells	35
2.2.9 Statistics	35
3 RESULTS.....	36
3.1 Cancer drugs induce the downregulation of SOX10 in BRAF ^{V600} melanoma cells and RTK I glioblastoma cells	36
3.2 SOX10 downregulation induces a β -galactosidase (β -gal)-positive phenotype and increased exosome production in melanoma and glioblastoma cell lines	41
3.3 SOX10 KD cells affect the phenotype of macrophages via exosomes	50
3.4 SOX10 KD exosomes induce pro-inflammatory phenotype of macrophages via the TLR8-NF- κ B pathway	60
4 DISCUSSION AND OUTLOOK	65
4.1 Discussion	65
4.2 Outlook.....	68
5 SUMMARY	69
6 REFERENCES	70

7 CURRICULUM VITAE 84

8 ACKNOWLEDGEMENT 86

LIST OF ABRREVIATIONS

BCL2	B-cell lymphoma 2 protein
BRAFi	BRAF inhibitors
CDK2	Cyclin-dependent kinase 2
CE	Cholesteryl ester
Cer	Ceramide
CHMP4C	Charged multivesicular body protein 4c
CHOL	Cholesterol
circRNA	Circular RNA
CM	Conditioned media
CRISPRi	Short palindromic repeats interference
DAG	Diacylglycerol
DCT	Dopachrome tautomerase
DGK α	Diacylglycerol kinase α
Dom	Dominant megacolon
dsRNA	Double strand RNA
ECM	Extracellular matrix
EMT	Epithelial-to-mesenchymal transition
ER	Endoplasmic reticulum
ESCRT	Endosomal sorting complexes required for transport
ESE	Early-sorting endosomes
EVs	Extracellular vesicles
FACS	Fluorescence—activated cell sorting
GB	Glioblastomas
gDNA	Genomic DNA
GSCs	Glioma stem cells
HexCer	Hexosylceramide
HLA	Human leukocyte antigen
HMG	High-mobility group
hnRNPs	Nuclear ribonucleoproteins
HRS	Hepatocyte growth factor-regulated tyrosine kinase substrate

HSP86	Hot shock protein 86
IFN γ	Interferon- γ
IL	Interleukin
ILVs	Intraluminal vesicles
KD	Knockdown
KO	Knockout
LDLR	Low-density lipoprotein receptor
LINEs	Long interspersed nuclear elements
lncRNAs	Long non-coding RNAs
LPS	Lipopolysaccharides
LTR	Long terminal repeats
MAPK	Mitogen-activated protein kinase
M-CSF	Macrophage colony-stimulating factor
MEKi	MEK inhibitors
MES	Mesenchymal
MHC	Major histocompatibility complex
miRNAs	MicroRNAs
MITF	Microphthalmia-associated transcription factor
MMP9	Matrix metalloproteinase 9
MVBs	Mutivesicular bodies
MW	Molecular weight
NCCs	Neural crest cells
nSMase2	Neutral sphingomyelinase 2
NT	Non-targeting
PA	Phosphatidic acid
PAX3	Paired box gene 3
PBMC	Peripheral blood mononuclear cell
PC O/P	PC ethers
PD-L1	Programmed death-ligand 1
PE	Phosphatidylethanolamine
PE O/P	PE ethers
PG	Phosphatidylglycerol
PI3K	Phosphoinositide 3-kinase

PLD2	Phospholipase D2
PMEL	Premelanosome protein
PS	Phosphatidylserine
rRNAs	Ribosomal RNAs
RTK I	The receptor tyrosine kinase I
SASP	Senescence associated secretory phenotype
shRNA	Short-hairpin RNA
SINEs	Short interspersed nuclear elements
SM	Sphingomyelin
SNARE	SNAP Receptor
snoRNAs	Small nucleolar RNAs
snRNAs	Small nuclear RNAs
SOX	SRY-related HMG box
SRP-RNAs	Signal recognition particle RNAs
SRY	Sex determining region Y
ssRNAs	Single strand RNAs
TAG	Triacylglycerol
TAMs	Tumor-associated macrophages/microglia
TCGA	The Cancer Genome Atlas Program
TfR	Transferrin receptor
TGF β	Transforming growth factor beta
TGF β RI	TGF β receptor I
TLR	Toll-like receptors
TMZ	Temozolomide
tRNAs	Transfer RNAs
TSG101	Tumor susceptibility gene 101
t-SNARE	Target SNARE
TYPR1	Tyrosinase-related protein 1
TYR	Tyrosinase
USP32	Ubiquitin-specific protease 32
UTR	Untranslated region
VEGFa	Vascular endothelial growth factor A
VPS4B	Vacuolar protein sorting-associated protein 4B

LIST OF ABRREVIATION

v-SNARE	Vesicle SNARE
VTA1	Vesicle trafficking 1
W4	Waardenburg-Shah syndrome type 4
β-gal	Beta-galactosidase

1 INTRODUCTION

1.1 The function of SOX10 in neural crest development and melanogenesis

The sex-determining region Y (SRY)-related high-mobility group (HMG) box 10 (SOX10) protein belongs to the SOX family, which are transcription factors responsible for the regulation of cell development and cell fate determination during embryogenesis (Jiang et al., 2013). The SOX proteins are characterized by the 79 amino-acid HMG box domain, which functions in recognizing and binding the C[A/T]TTG[T/A][T/A] motifs at the minor groove of DNA (Haseeb and Lefebvre, 2019; Zhao and Koopman, 2012). There are 20 members of the SOX family, including nine subgroups such as *SOXA*, *SOXB1-2*, and *SOXC-H*. The classification is based on the HMG domain sequences, protein structures, gene organization, and cell development functions (Bowles et al., 2000). SOX10 is a part of the SOXE family, which also includes SOX8 and SOX9. SOXE proteins mediate processes such as melanogenesis (Harris et al., 2010), neural crest development and differentiation (Weider and Wegner, 2017), sex determination and chondrogenesis (Lefebvre and Dvir-Ginzberg, 2017; Li et al., 2014b). SOX10 is particularly important in melanogenesis and neural crest development.

SOX10 was first identified as an essential player in neural system development and melanogenesis in the “dominant megacolon” (Dom) spontaneous mouse mutant model (Southard-Smith et al., 1998). Dom mice harbor *Sox10* gene mutations and were used to investigate Waardenburg-Shah syndrome type 4 (W4), a disease, which is often connected with symptoms such as sensorineural deafness and hypopigmentation (Bondurand et al., 2007; Southard-Smith et al., 1998). The mutated *Sox10* in the W4 syndrome indicates that the dysfunction of *Sox10* impairs neural cell and melanocyte development. To specify the function of SOX10 during neural crest development, *Sox10* mutant mouse models were further utilized to investigate murine embryo development. Researchers found that loss of *Sox10* function did not affect the presence of neural crest-derived embryonic structures at the pre-migration state of neural crest cells (NCCs) (Britsch et al., 2001; Herbarth et al., 1998; Southard-Smith et al., 1998). However, the dysfunction of *Sox10* in post-migratory NCCs induced apoptosis before NCCs were differentiated into glia cells in the peripheral neural system, and the surviving NCCs also failed to differentiate into glia cells. This indicates that SOX10 may affect the survival and the differentiation of post-migratory NCCs (Paratore et al., 2001). During the differentiation of NCCs, SOX10 also plays a role in

the development of melanocytes. The function relies on a synergistic action with paired box gene 3 (PAX3) protein to modulate the expression of microphthalmia-associated transcription factor (MITF) (Bondurand et al., 2007; Potterf et al., 2000), and MITF further activates pigmentation-related genes such as *TYR*, *TYRP1*, *DCT*, *PMEL*, which encode tyrosinase, tyrosinase-related protein 1, dopachrome tautomerase and premelanosome protein, respectively. These proteins will initiate the transformation of tyrosine to the melanin pigments, thus leading to the maturation of melanocytes (Bertolotto et al., 1998; Yasumoto et al., 1994). Of note, SOX10 alone can also directly modulate the expression of *TYR*, *TYRP1* by binding the evolutionary conserved distal enhancers of these genes, despite the synergy with MITF (Murisier et al., 2006, 2007). Besides, the SOX10-MITF pathway also mediates the expression of B-cell lymphoma 2 (*BCL2*) and cyclin-dependent kinase 2 (*CDK2*), which promote the survival and proliferation of melanocytes (Du et al., 2004; McGill et al., 2002). Therefore, SOX10 was proposed to play essential roles in the tumorigenesis and development of melanoma and glioma due to its critical function in modulating the differentiation, survival, and proliferation of melanocytes and glia cells.

1.2 The function of SOX10 in tumors

SOX10 has been reported to be expressed in melanoma, glioma, triple-negative breast cancer, ovarian epithelial tumors, and bladder cancers (Feng et al., 2017; Kwon et al., 2016; Sun et al., 2014; Wu et al., 2020; Yin et al., 2017). Data of the skin cutaneous melanoma cohort from The Cancer Genome Atlas (TCGA) show that over 95% of melanoma have strong expression of SOX10 (Fig.1).

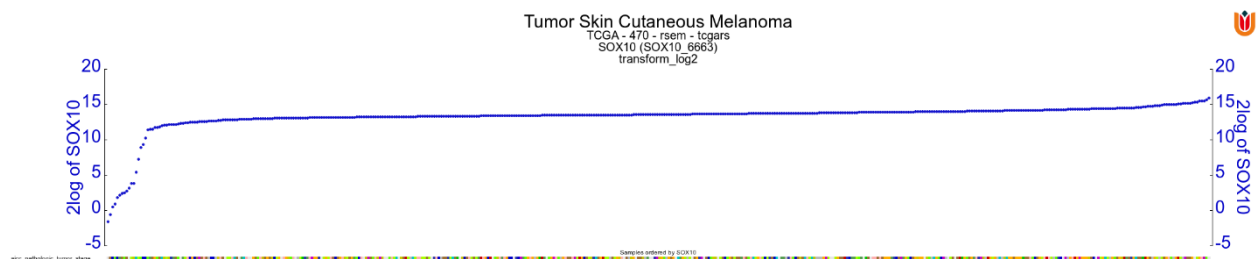


Fig.1 SOX10 expression in the TCGA melanoma cohort. The plot was generated using the R2 genomics analysis and visualization platform. Left and right Y-axis are log₂ expression SOX10, blue dots are SOX10 levels of single patients.

High expression of SOX10 is correlated with the formation and maintenance of melanoma, and high SOX10 expression also enhances tumor invasiveness during

disease progression (Graf et al., 2014; Shakhova et al., 2012). Interestingly, the loss of SOX10 in melanoma may also lead to worse outcomes in patients treated with standard therapies. Sun *et al.*, reported that acquired SOX10 downregulation induced the upregulation of epidermal growth factor receptor and resistance to targeted therapies in BRAF^{V600E} mutant melanoma (Sun et al., 2014); however, the occurrence of SOX10 downregulation in patients was not well investigated. To note, BRAF^{V600E} mutant patients account for 30-50% of all melanoma cases, and inhibitors of BRAF (BRAFi) and downstream MEK (MEKi) are used in standard treatment for BRAF^{V600E} mutant patients (Vanni et al., 2020). Unfortunately, patients frequently develop therapy resistance within about 12 months, and the mechanisms are not entirely understood (Luebker and Koepsell, 2019).

In gliomas, SOX10 is usually expressed in low-grade tumors such as grade II astrocytomas and grade II oligodendrogliomas rather than grade IV glioblastomas (Ferletta et al., 2007). However, a specific subtype of glioblastoma, known as the receptor tyrosine kinase I (RTK I), also displays high SOX10 expression. This RTK I subtype was identified based on tumor-DNA methylation patterns and overlaps with the proneural glioblastoma subtype that was defined based on transcriptome features (Wu et al., 2020). Analogous to the treatment-related effects observed in melanoma, radiation treatment of Sox10^{high} glioblastoma in an allograft mouse model induced Sox10 downregulation in the murine tumor cells (Lau et al., 2015). Although the function of SOX10 in glioblastoma is still unclear, our group recently found that lower SOX10 may predict worse overall and progression-free survival in patients with RTK I glioblastoma. Furthermore, the knockdown (KD) of SOX10 in RTK I glioblastoma induced an RTK I-to-mesenchymal transition that was related to worse outcome (Wu et al., 2020). In conclusion, therapy-associated downregulation of SOX10 appears to be associated with shorter survival of melanoma and glioblastoma patients.

In melanoma cells, SOX10 downregulation in tumor cells has been shown to result in the expression of the senescence marker beta-galactosidase (β -gal) (Sun et al., 2014; Wang et al., 2017), and increased cytokine release, analogous to the senescence-associated secretory phenotype (SASP) observed in senescent normal and tumor cells. Cytokines, chemokines, and extracellular vesicles (EVs) are thought to play important roles in modulating the tumor microenvironment and tumor progression. In

glioblastoma, similar to melanoma, our group also found that knocking down SOX10 in the RTK I cell line LN229 induces a β -gal-positive phenotype and upregulated the secretion of cytokines, such as CCL2, CXCL1, etc., (unpublished data). It is still unclear, how SOX10 suppression in tumor cells affects exosome production and the cells of the tumor microenvironment.

1.3 The function of exosomes in the tumor microenvironment

1.3.1 The definition of exosomes

Exosomes are a subtype of extracellular vesicle (EV) that contributes to intercellular communication (Vader et al., 2014). Exosomes can be distinguished from other EVs by their size, density, morphology, and molecular composition (Colombo et al., 2014; S et al., 2013). Exosomes range from 40-160 nm in size, distinguishing them from larger EVs such as the microvesicles (100-1000 nm) and apoptotic bodies (50-5000 nm)(Momen-Heravi et al., 2013). With the help of asymmetric-flow field-flow fractionation, exosomes can be further sub-classified into exomeres (35-50 nm), small exosomes (60-80 nm), and large exosomes (larger than 90 nm) (Kalluri and LeBleu, 2020; Zhang et al., 2018a). In addition to size distribution, exosomes can also be defined by their density of 1.10-1.18 g/ml, which differs from that of other EVs such as apoptotic bodies and microvesicles (Yu et al., 2018). More importantly, exosome can also be differentiated by their biomarkers, which they acquire through their specific biogenesis pathway.

1.3.2 The Biogenesis, transportation, and uptake of exosomes

The biogenesis of exosomes relies on the endosomes. Initially, the cytoplasm membrane invaginates and forms *de novo* early-sorting endosomes (ESE), which can fuse with existing intracellular ESEs, and/or accept mass such as lipids, proteins and nucleic acids from the endoplasmic reticulum (ER) or trans-Golgi network. During this process, the membrane of endosomes will invaginate and form intraluminal vesicles (ILVs). These early endosomes will eventually transform into multivesicular bodies (MVBs). There are two destinations for MVBs. They either are digested by lysosomes and autophagosomes, leading to the degradation and clearance of the internal cargoes, or fuse with the cytoplasm membrane and release the ILVs (now the exosomes) to the extracellular space.

1.3.2.1 The biogenesis of exosomes

During MVB formation, endosomal sorting complexes required for transport (ESCRT)-dependent and ESCRT-independent pathways participate in the inside-budding process. The ESCRT-dependent pathway involves four ESCRT protein complexes, ESCRT-0, ESCRT-I, ESCRT-II, and ESCRT-III, and the associated ATPase VPS4 complex (Henne et al., 2013). Among the ESCRTs and associated proteins, expression of the ESCRT-0 proteins hepatocyte growth factor-regulated tyrosine kinase substrate (HRS) and tumor susceptibility gene 101 (TSG101), ESCRT-I protein signal transducing adapter molecule 1 (STAM1), and ESCRT-III proteins charged multivesicular body protein 4C (CHMP4C), vacuolar protein sorting-associated protein 4B (VPS4B), vesicle trafficking 1 (VTA1), and ALIX was found to correlate with the exosome production. For example, in HeLa cells, the knockdown of CHMP4C, VPS4B, VTA1, and ALIX induced increased exosome production, while knockdown of HRS and TSG101 reduced exosome production (Colombo et al., 2013). To note, targeting ESCRTs and the associated proteins may not altogether abolish the formation of ILVs in MVBs (Stuffers et al., 2009), which indicates that ESCRT-independent pathways may compensate for the effects of ESCRT loss under certain circumstances.

Exosome formation and cargo sorting processes are regulated by the non-ESCRT ceramide-dependent pathway. Ceramide is composed of sphingosine and a fatty acid and is an essential component of lipid rafts (Sokolowska and Blachnio-Zabielska, 2019). Ceramide can induce lateral-phase separation in the cytoplasm, and the cone-shaped structure of ceramide may spontaneously curve the endosomal membrane to facilitate the inward budding of endosomes and ILV formation (Zhang et al., 2019). The biogenesis of ceramide relies on the hydrolysis of sphingomyelin (SM) and the removal of the large head group via neutral sphingomyelinase 2 (nSMase2) (Trajkovic et al., 2008). Inhibition of nSMase2 via KD or knockout (KO) of the corresponding gene (SMPD3) or by the nSMase2 inhibitors GW4869 and Cambinol, has successfully reduced exosome production in both normal cells and cancer cell lines (Catalano and O'Driscoll, 2020; Lang et al., 2016; Poggio et al., 2019; Sackmann et al., 2019). This finding supports the hypothesis that the ceramide-dependent pathway is involved in exosome production. In addition to the ceramide-dependent pathway, the tetraspanin-dependent pathway also plays an important role in exosome biogenesis. The

tetraspanins, such as CD63, CD9, and CD81 were reported enriched in many exosomes and thus were commonly used as biomarkers for exosomes. Although the function of tetraspanins in MVB formation is unclear, abolishing CD63 and CD9 expression can inhibit exosome production in specific cell lines such as HEK293 or bone marrow dendritic cells (Chairoungdua et al., 2010; Hurwitz et al., 2018).

1.3.2.2 The transport of exosomes

Followed by the formation of ILVs, MVBs are either sorted to lysosomes for degradation or directed to the cytoplasm membrane to release ILVs. Although it is unclear how cells determine the fate of MVBs, it is known that the intracellular trafficking of MVBs relies on the tubulin cytoskeleton and motor molecules (kinesins, dynein, and actin-related molecules) (Hessvik and Llorente, 2018; Sinha et al., 2016; Wen et al., 2016). The expression levels of Rab GTPases, which control many intracellular and intercellular membrane trafficking processes, are closely correlated with exosome production. In a short hairpin RNA (shRNA) screen targeting multiple GTPases, Ostrowski et al. reported that the KD of Rab2b, Rab5b, Rab9a, Rab27a, and Rab27b inhibited exosome secretion. They found that KD of Rab27a induced the enlarged and accumulated MVBs in the cytoplasm, and KD of Rab27b inhibited the transport of MVBs from the perinuclear area to the cell periphery. Rab27a and Rab27b silencing prevented MVE docking to the cytoplasm membrane, inhibiting exosome release (Ostrowski et al., 2010). Of note, the suppression of Rab27a to reduce exosome production has been widely applied in tumor microenvironment research on the modulation of tumor pro-metastatic niches, blocking the delivery of exosomal programmed death-ligand 1 (PD-L1) to T cells, and prohibiting the tumor-supportive stromal cells from modulating the tumor microenvironment (Bobrie et al., 2012; Hoshino et al., 2013; Peinado et al., 2012; Poggio et al., 2019; Webber et al., 2015). These studies suggest that Rab27a could be a potential therapeutic target when tumor-derived exosomes mediate pro-tumorigenic clinical effects. In addition to Rab27, the expression of Rab11, Rab35, and Rab7 were also reported to positively correlate with exosome production; however, KD of these small GTPases failed to reduce exosome production and even increased exosome production in some cell lines (Baietti et al., 2012; Hsu et al., 2010; Koles et al., 2012). Post-translational modification of MVB-related proteins may also affect the secretion of exosomes. For example, ubiquitination and ubiquitination-like modifications (ISGylation) on MVB proteins (TSG101, Rab27a,

and Rab7) induced the aggregation of MVBs in the cytoplasm and eventually led to the degradation of MVBs by lysosomes. In contrast, inhibition of Rab7 ubiquitination via ubiquitin-specific protease 32 (USP32) may increase exosome production (Peng et al., 2020; Sapmaz et al., 2019; Song et al., 2019; Villarroya-Beltri et al., 2016). All in all, intracellular trafficking of MVBs is greatly dependent on the cytoskeleton, the intracellular vesicle transport system, and post-translational modifications of MVB-related proteins that modulate the trafficking processes and exosome quantity.

Following the docking of MVBs at the cytoplasm membrane, the release of exosomes is further controlled by membrane fusion processes. Membrane fusion is mediated by a trans-SNARE Receptor (SNARE) complex SNAREpin, which consists of two types of SNARE proteins, vesicle SNARE (v-SNARE) and target SNARE (t-SNARE) (Koike and Jahn, 2019). The SNARE proteins are found in the vesicle and cytoplasm membranes, and the fusion process is activated by the formation of SNAREpin (Peng et al., 2020). Notably, SNAREpin assembly relies on the interaction of Rab GTPases such as Rab27a with Sec/Munc proteins (SEC1/MUNC19) (Ostrowski et al., 2010; Peng et al., 2020). In addition, the octameric exocyst complex that tethers exocytic vesicles to the plasma membrane is also crucial in the fusion process (Ahmed et al., 2018). As soon as the fusion initiates, ILVs will be released from the parent cells to the intercellular space.

1.3.2.3 The uptake of exosomes

The uptake of exosomes by cells requires several processes such as receptor-/raft-mediated endocytosis, micropinocytosis, and phagocytosis. Receptor-/raft mediated endocytosis mainly involves clathrin-mediated endocytosis and caveolae/raft-dependent endocytosis. Clathrin-mediated endocytosis relies on low-density lipoprotein (LDLR) and transferrin (TfR) receptors on the surfaces of recipient cells that bind the corresponding ligands on the exosomes. As soon as the ligand-receptor binding occurs, clathrins will be recruited to the surface of recipient cells, induce an inward invagination of the plasma membrane (Mayor et al., 2014; Tian et al., 2014), and the exosomes are subsequently internalized by the recipient cells. The receptor-/raft dependent endocytosis involves the caveolae-dependent, noncaveolar dynamin-dependent, and non-caveolar dynamin-independent pathways. The caveolae is regarded as a specific subdomain of lipid rafts, and caveolae-dependent endocytosis

internalizes vesicles with sizes of 50-100 nm due to the naturally curvy morphology of the plasma membrane (Ni et al., 2020). The formation of caveolae relies on caveolin-1 (CAV1), which is regulated by kinases such as Src-family tyrosine kinase and phosphatases such as serine/threonine protein phosphatases PP1 and PP2A (Cohen, 2002; Glenney, 1989; Kiss and Botos, 2009; Lee et al., 2000). However, the regulatory role of CAV1 in exosome uptake is still controversial. For example, neurons can upregulate CAV1 to improve the uptake of endothelial cell-derived exosomes, while it was also reported that CAV1 inhibited the internalization of exosomes in B cells (Nanbo et al., 2013; Svensson et al., 2013; Yue et al., 2019). Interestingly, exosomes also carry CAV1, whereas the function of exosomal CAV1 is not entirely understood (Ni et al., 2020). In addition, the dynamin-dependent pathway can work in caveolae-dependent or caveolae-independent manner, and the latter may rely on flotillin-1 and cholesterol (Glebov et al., 2006; Schneider et al., 2007). Small GTPases such as Cdc42 and ARF6 can also regulate endocytosis via a non-caveolar dynamin-independent pathway by influencing polymerization of the actin cytoskeleton (Mayor and Pagano, 2007; Mayor et al., 2014; Nabi and Le, 2003), which is required to target the internalized exosome to either the lysosomes the cytoplasm membrane for recycling (McKelvey et al., 2015). Phagocytosis and macropinocytosis also depend on actin for the invagination process. Phagocytosis relies on FcR and complement receptors, scavenger receptors, or toll-like receptors, which are highly expressed in phagocytes such as macrophages and dendritic cells, to activate the phosphoinositide 3-kinase (PI3K) pathway. Once PI3K pathway has been activated, the cytoplasm membrane composition and actin filament will change and reshape regional structures to encapsulate the ligand-contained exosomes (Uribe-Querol and Rosales, 2020). In contrast, macropinocytosis is a ligand-independent endocytosis process controlled by Na^+ - H^+ exchange and PI3K pathways (Fitzner et al., 2011; Tian et al., 2014). Both clathrin and non-clathrin-dependent pathways modulate the uptake of exosomes by the acceptor cells and thereby mediate intercellular communication.

1.3.3 Exosomal cargoes in cancer cells

Exosomes contain proteins, nucleic acid, and lipids. These cargoes are essential for intercellular communication and the maintenance of cellular homeostasis. In cancer, the exosome cargoes have been reported to mediate various pro- and anti-tumor effects in tumor development. Here, I will introduce the most common cargoes found

in tumor exosomes.

1.3.3.1 Nucleic acids in exosomes

RNA and DNA are very abundant in exosomes and have been characterized by high-throughput sequencing (Balaj et al., 2011; Kahlert et al., 2014; Koppers-Lalic et al., 2014; Kurywchak and Kalluri, 2017; Nolte-'t Hoen et al., 2012; Takahashi et al., 2017; Thakur et al., 2014; Valadi et al., 2007; Yang et al., 2017). Although DNAs may stem from the non-vesicle secretome rather than EVs, the abundance of RNAs is still a hallmark of exosomes.

Exosomal RNAs include mRNAs and diverse non-coding RNAs. mRNA has been reported to account for 5-20% of total RNAs in healthy human serum- and urine-derived exosomes (Li et al., 2014a). In cancer cell lines from melanoma and glioblastoma, this ratio can reach up to 20-35% (Wei et al., 2017; Wu et al., 2017). Non-coding RNAs account for most of the nucleic acids in exosomes and include ribosomal RNAs (rRNAs), microRNAs (miRNAs), vault RNAs, long non-coding RNAs (lncRNAs), Y-RNAs circular RNA (circRNA), small nuclear RNAs (snRNAs), transfer RNAs (tRNAs), small nucleolar RNAs (snoRNAs), signal recognition particle RNAs (SRP-RNAs), 3' untranslated region (UTR) transcripts of protein-coding genes, and repetitive elements such as long interspersed nuclear elements (LINEs), short interspersed nuclear elements (SINEs), and long terminal repeats (LTR). Non-coding RNAs have been utilized as novel diagnostic and prognostic biomarkers for cancer, inflammation, and autoimmune diseases (Malla et al., 2017; Nedaeinia et al., 2017; Valentino et al., 2017; Zhang et al., 2016). For example, the expression of the small RNAs miR-17, miR19a, miR-21, miR-126 and miR-149 is higher in metastatic sporadic melanoma patients than familial melanoma patients and unaffected control subjects (Yin et al., 2019). miR-1238 is a prognostic biomarker for assessing the effect of chemotherapy protocols in glioblastoma (Yin et al., 2019);, and the combination of the mRNAs KRTAP5-4 and MAGEA3, and lncRNA BCAR4 is a promising diagnostic indicator for colorectal cancer (Dong et al., 2016).

Among the various non-coding RNAs, miRNAs were frequently studied regarding their tumor-supportive or suppressive functions in the tumor microenvironment (Sun et al., 2018). Although miRNAs are commonly regarded as the most important small-RNA

constituents in exosomes, they are not always the most predominant (Huang et al., 2013; Koppers-Lalic et al., 2014; Nolte-'t Hoen et al., 2012; Tosar et al., 2015). For example, in human glioma and chronic lymphatic lymphoma cell lines, Y-RNAs (HY1, HY3 and HY4), that have been proposed to modulate the innate immune response of myeloid cells via Toll-like receptor signaling (Haderk et al., 2017), are more abundant than the total miRNAs (Haderk et al., 2017; Wei et al., 2017). The sorting of non-coding RNA into exosomes includes selective and unselective processes. On the one hand, the sorting process relies on unselective MVB formation to encapsulate cytoplasmic RNAs into the lumen of ILVs. On the other hand, exosome-bound heterogeneous nuclear ribonucleoproteins (hnRNPs), 3'UTR, miRISC (Ago2), membrane proteins, and RNA-binding proteins mediate the selective sorting of RNAs in motif-dependent or independent manner. For example, the sumoylation on hnRNPA2B1 enhances the packing of miR-522 and miR-1246 into exosomes through GGAG/UGCA motif-dependent sorting by hnRNP (Santangelo et al., 2016; Villarroya-Beltri et al., 2013; Wei et al., 2021; Wu et al., 2018; Zhang et al., 2020).

In addition to RNA, the genomic DNA (gDNA) was also detected in exosomes derived from cancer or healthy cells subjected to DNA damage (Kahlert et al., 2014; Takahashi et al., 2017; Yang et al., 2017; Yokoi et al., 2019). However, these findings were challenged by a study that investigated the DNA content of vesicle and non-vesicle secretomes derived from colorectal cancer cell lines. In particular, Jeppesen *et al.* suggested that cells can directly secrete gDNA and histones via autophagy and exosome-independent pathways (Jeppesen et al., 2019). However, additional functional studies on exosomal gDNA indicated that the secretion of gDNA constitutes an outward delivery of harmful or redundant DNA to maintain cellular homeostasis. In line with this hypothesis, exosome secretion induced accumulation of cytoplasmic DNA in donor cells (Takahashi et al., 2017) (Lian et al., 2017). These studies also supported that gDNA could be a conditional rather than constitutive content of exosomes.

1.3.3.2 Exosomal proteins

Proteins are highly abundant in exosomes and are associated with the essential functions of ILVs formation, MVB transportation, and exosome secretion. They commonly include cytoplasmic and plasma membrane proteins, while proteins of the endoplasmic reticulum (ER), Golgi body, mitochondria, and nuclear-associated

proteins are less abundant (They et al., 2002). The exosomal proteins can be roughly categorized into MVB-related proteins, membrane-transport and fusion proteins, tetraspanins, heat shock proteins, adhesion molecules, cytoskeleton proteins, enzymes, and antigen-presenting molecules (Beach et al., 2014; Reddy et al., 2018). These proteins not only included those which participated in the biogenesis, transportation, and uptake of exosomes but also cargoes irrelevant for exosome production. For example, the heat shock proteins such as HSP90, HSP70, HSP27, and HSP60 were found in both the lumen and surface of exosome and mediated the immune response in tumor microenvironment (Reddy et al., 2018); The exosomal adhesion molecules include integrins, ICAM-1, CD11 family, etc., which mediate exosome-cell, exosome-extracellular matrix and exosome-EV interaction (Buzas et al., 2018). Exosomes derived from melanoma, colon cancer, pancreatic cancer and mammary cancer cell lines such as B16-F10, LIM1251, PAN02 and 4T1 were found to carry cytoskeleton proteins such as actins, myosin, tubulins, keratin, respectively (Mathivanan et al., 2010; Zhang et al., 2018a). However, these proteins could also be absent in classical CD9, CD63, and CD81-positive exosomes derived from the cell lines DKO-1 and Gli36 (Jeppesen et al., 2019), demonstrating that exosomes derived from different cell lines display extensive heterogeneity. Exosome cargoes are also abundant with enzymes such as pyruvate kinase isozymes M1/M2, enolase, phosphoglycerate kinase 1, glucose-6-phosphate isomerase, membrane-type 1 matrix metalloproteinase, and various of ATPase. In cancer, these enzymes not only reprogram the metabolic function in the recipient cells such as cancer-associated fibroblasts, adipocytes, endothelial cells, macrophages and mesenchymal stem cells, but directly modulate the extracellular matrix, enhancing tumor motility and invasiveness (Mu et al., 2013; Sanderson et al., 2019; Yang et al., 2020); The antigen-presenting major histocompatibility complex (MHC) I and II also are found on exosomes, with their quantity typically corresponding their expression level in the host cells (Admyre et al., 2003). The human MHC molecules such as the human leukocyte antigen (HLA)-DR1 are often used as exosome biomarkers. Similar to the function of the MHC on cells, exosomal MHC also participate in antigen presentation (Utsugi-Kobukai et al., 2003), and mediate the immune response such as the initiation of T-cell priming, differentiation of mature T-cells, and the development of effector functions (Li et al., 2019). In addition to the proteins commonly found on exosomes, proteins that are specifically expressed or upregulated in host cells can also be presented on

exosomes and exert function on recipient cells. For example, upregulated PD-L1 in melanoma, prostate cancer and colorectal cancer will also presents in the corresponding exosomes, inhibit the function of T cells in the tumor microenvironment, suppress immune surveillance and promotes tumor progression (Chen et al., 2018; Poggio et al., 2019). In summary, exosomes carry various proteins inherited from host cells that not only reflect the biogenesis process but also the characteristics of the host cells per se.

1.3.3.3 Exosomal lipids

Lipids are very abundant in the bilayer membrane of exosomes, including cholesterol (CHOL), SM, phosphatidylserine (PS), phosphatidylethanolamine (PE), PE ethers (PE O/P), diacylglycerol (DAG), PC ethers (PC O/P), hexosylceramide (HexCer), ceramide (Cer), and phosphatidylglycerol (PG), while cholesteryl ester (CE) and triacylglycerol (TAG), which assemble the lipid droplets and lipoproteins, are largely absent (Skotland et al., 2017). The absence of CE and TAG can be used to determine whether the isolated exosomes were contaminated by lipid droplets and lipoproteins. The relative frequencies of these lipids differ between exosomes and cells. For example, HexCer, CHOL, SM, and PS are enriched in exosomes, while PC and PE are less abundant in exosomes than cells. In addition, the outer leaflet of exosomal membranes contains more SM and PC, and the other lipids are enriched in the inner membrane (Skotland et al., 2017; van Meer et al., 2008). Unlike nucleic acids and proteins, the functions of exosomal lipids in intercellular vesicle trafficking are still little understood (Egea-Jimenez and Zimmermann, 2020).

1.3.4 The role of exosomes in SOX10^{high} tumors

As mentioned in section 1.2, SOX10^{high} tumors are most commonly found among melanoma and RTK I glioblastoma. In these tumors, exosomes are thought to be mediators of intercellular signaling that remodels the tumor microenvironment, accelerates tumor metastasis and facilitates immune escape.

In melanoma, tumor-derived exosomes promoted the tumorigenesis of less malignant cells by delivering miRNA-221/222, which activates the PI3K/AKT pathway (Felicetti et al., 2016) and inhibits the function p27Kip1/CDKN1B, promoting c-KIT receptor-dependent tumor progression (Felicetti et al., 2008). Autocrine and paracrine exosomal

micro-RNAs let-7i, let-7a and miR-191 induced epithelial-to-mesenchymal transition (EMT) in melanoma through the activation of mitogen-activated protein kinase (MAPK) signaling pathways (Xiao et al., 2016), promoting the metastatic potential of melanoma cells. Melanoma-derived exosomes were also reported to be enriched with proteases such as uPAR, ADAMs and Hadase, which can digest the component of ECM such as type I and IV collagens, laminins and fibronectin (Tucci et al., 2018).

Melanoma-derived exosomes also affect stromal cells such as fibroblasts and endothelial cells. Exosomes can drive the transformation of normal fibroblasts into cancer-associated fibroblasts, which support tumor progression and invasiveness by modulating the ECM, secreting soluble factors such as vascular endothelial growth factor A (VEGFa), matrix metalloproteinase 9 (MMP9) and fibroblast growth factor (FGF), and inhibiting T-cell function (Sahai et al., 2020; Zhou et al., 2018). The transformation of fibroblasts is believed correlated with the overexpression of miR-155 in exosomes by either activating JAK/STAT3 signaling or glucose metabolism of normal fibroblasts (Shu et al., 2018; Zhou et al., 2018). In addition to fibroblast, endothelial cells can also be affected by exosomes. For example, melanoma exosomes can directly deliver miR-9 to endothelial cells, and thereby activate the JAK/STAT pathway and promote angiogenesis and cell migration (Zhuang et al., 2012). Exosomes also induce the expression of angiogenic factors such as VEGFa and interleukin-6 (IL6) in tumor and stromal cells, leading to increased angiogenesis and metastasis of melanoma to distal organs such as lymph nodes, brain and liver (Olejarz et al., 2020).

Recently, many publications have stressed the importance of melanoma-derived exosomes for tumor-cell immune escape. The exosomes can directly affect the function of immune cells such as antigen-presenting cells (APC) and CD8⁺ T cells. For example, melanoma cells were shown to transport MHC-I molecules to APCs and downregulate the co-stimulatory molecules CD86 and CD40 that are required for T-cell activation and induced immune suppression (Duchler et al., 2019). Melanoma cells also loaded overexpressed PD-L1 on exosomes which directly contacted CD8⁺ T cells and led to the suppression of T-cell function (Chen et al., 2018). On the other hand, tumor-derived exosomes can suppress the function of T-cells in an indirect way. Exosomal proteins and small RNAs can induce monocytes or macrophages into pro-inflammatory and immune-suppressive phenotypes via toll-like receptors (TLR). TLRs

are very abundant in monocytic cells, including TLR1/2/4/5/6/10 at the cell surface and TLR3/7/8/9/11/12/13 in intracellular endosomes. TLRs function as pattern-recognition receptors to recognize microbe-specific and self-derived molecular signatures such as pathogen-associated molecular patterns and damage-associated molecules patterns, respectively (Kawasaki and Kawai, 2014). The activation of TLRs can activate downstream NF- κ B, interferon regulatory factors (IRFs), and MAPK pathway to induce the expression of pro-inflammatory cytokines, type I/II interferons, and ultimately modulate the tumor immune-microenvironment. Specifically, melanoma-derived proteins such as HSP86 activate TLR4 signaling on monocytes and induce a pro-inflammatory phenotype and PD-L1 upregulation. The activated monocytes can then inhibit the proliferation of CD8⁺ T cells and, therefore, the adaptive immune response to tumor cells (Fleming et al., 2019). Alternatively, the pro-inflammatory monocytes can also be activated via TLR7/8 targeting exosomal small RNAs such as miR-21, let-7, and Y-RNAs, and result in pro- as well as anti-tumor responses in lung cancer, glioma, and chronic lymphocytic leukemia (Buonfiglioli et al., 2019; Fabbri et al., 2012; Haderk et al., 2017; Lunavat et al., 2015). Of note, these three small RNAs are also abundant in melanoma (Lunavat et al., 2015).

SOX10^{high} glioblastoma constitutes about 10-15% of all primary glioblastoma. The cancer cell line encyclopedia (CCLE) includes 66 cell lines categorized as glioma, but only four of these, LN229, KS-1, SNB75, and snu-466, exhibit high SOX10 expression at mRNA level. It was reported that LN229-derived EVs facilitate the transformation of human astrocytes in combination with viral oncogenes (SV40, RasG12V and TERT)(Zeng et al., 2020); LN229 also increased exosome production and pro-oncogenic miR-21 delivery when cells were treated with the DNA alkylating agent Temozolomide (TMZ) (Kosgodage et al., 2019).

In summary, SOX10^{high} tumor-derived exosomes impact cancer progression and modulate the tumor microenvironment in direct and indirect ways. As discussed above in section 1.2, preliminary evidence indicates that the downregulation of SOX10 likely affects the production of extracellular vesicles by SOX10^{high} tumors. Thus, studying the exosome-dependent effects of SOX10 downregulation in melanoma and glioblastoma is a scientifically and potentially clinically significant research topic.

1.4 Objective

My overall goal is to address the potential role of SOX10 in exosome-mediated tumor-macrophage communication and tumor progression in melanoma and glioblastoma. To this end, I will use cancer cell lines and macrophages derived from peripheral blood-derived mononuclear cells (PBMCs) to perform drug treatment experiments, gene and protein expression analysis, exosome isolation and characterization, pharmacologic inhibition of signaling pathways, and functional assays. Specifically, I will address the following questions.

- Do drugs used in standard melanoma and glioblastoma therapy induce the downregulation of the transcription factor SOX10?
- Does the loss of SOX10 impact the production of exosomes by melanoma and glioblastoma cells?
- Can exosome-dependent signaling by melanoma cells induce phenotypic transformation of tumor-associated macrophages?

2 MATERIALS AND METHODS

2.1 Materials

2.1.1 Antibodies

Antibody	Clone/activity	Distributor
ALIX	3A9	Cell Signaling Technology, Danvers, MA, USA
Anti-goat IgG, HRP-linked Antibody	n/a	Santa Cruz, Dallas, TX, USA
Anti-mouse IgG, HRP-linked Antibody	n/a	Santa Cruz, Dallas, TX, USA
Anti-rabbit IgG, HRP-linked Antibody	n/a	Santa Cruz, Dallas, TX, USA
Calnexin	C5C9	Cell Signaling Technology, Danvers, MA, USA
CD63	MX-49.129.5	Novus Biologicals, Denver, CO, USA
CD81	M38	Thermo Fisher Scientific, Waltham, MA, USA
CD9	D3H4P	Cell Signaling Technology, Danvers, MA, USA
GAPDH	CB1001	Calbiochem, San Diego, CA, USA
NF- κ B p65 XP®	D14E12	Cell Signaling Technology, Danvers, MA, USA
Phospho-NF- κ B p65 (Ser536)	93H1	Cell Signaling Technology, Danvers, MA, USA
SOX10	EPR4007	Abcam plc., Cambridge, UK
TSG101	4A10	GeneTex, Alton Pkwy Irvine, CA, USA
α -Tubulin	DM1A	Sigma-Aldrich, Munich, Germany
β -Actin	SP124	Sigma-Aldrich, Munich, Germany

2.1.2 Buffers

Material	Distributor/Recipe
NEBuffer 10x	New England Biolabs, Ipswich, MA, USA
Optiprep homogenization buffer	0.25M sucrose(HPLC), 6mM EDTA, 10mM Tris/HCl, pH7, in 200ml ddH2O
Optiprep working buffer	0.25M sucrose(HPLC), 1mM EDTA, 60mM Tris/HCL, pH7.4, in 200ml ddH2O
RIPA buffer, 10X	Abcam plc., Cambridge, UK
Stripping buffer	0.2 M glycine, 3 nM SDS, in ddH2O (pH2.2), 1:100 (v/v) Tween 20
T4 DNA Ligase Buffer	New England Biolabs, Ipswich, MA, USA
TBS 10X	20mM Trizma, 137mM NaCl in ddH2O (pH 7.6)
TBST	TBS, 1:1000 (v/v) Tween 20

2.1.3 Cell culture reagents

Material	Distributor
rhTGF-b1	Life Technologies, Carlsbad, USA
IL4 Recombinant Human Protein	Life Technologies, Carlsbad, USA
IFN-gamma, human recombinant	Biocat
Lipopolysaccharides	Sigma-Aldrich, Munich, Germany
Human M-CSF, research grade	Miltenyi Biotec, Bergisch Gladbach, Germany
Material	Distributor
Biocoll	Biochrom GmbH
BSA	Sigma-Aldrich, Munich, Germany
Dulbecco's Modified Eagle Medium, high glucose	Thermo Fisher Scientific, Waltham, MA, USA
Foetal Calf Serum (FCS)	Sigma-Aldrich Chemie GmbH, Munich, Germany
Leucosep™ tubes, 50 mL	Greiner Bio-One International GmbH, Kremsmünster, Austria
MEM Non-Essential Amino Acids Solution	Life Technologies, Carlsbad, USA
Multiwell plates, 12-well, 24-well, 48-well	TPP Techno Plastic Products AG, Trasadingen, Switzerland
Pasteur pipettes / VWR® Disposable Transfer pipettes	VWR International, Radnor, PA, United States
PBS Dulbecco's	Life Technologies, Carlsbad, USA
Penicillin / Streptomycin (10.000 U/ml)	Biochrom AG, Berlin, Germany
RPMI 1640 (2mM Glu)	Life Technologies, Carlsbad, USA

2.1.4 Chemicals

Material	Distributor
2-mercaptoethanol	Sigma-Aldrich, Munich, Germany
Acti-stain 670 phalloidin	Tebu-bio, Peterborough, United Kingdom
Agarose	Roth, Karlsruhe, Germany
AgeI restriction endonuclease	New England Biolabs, Ipswich, MA, USA
BLpI restriction endonuclease	New England Biolabs, Ipswich, MA, USA
BstXI restriction endonuclease	New England Biolabs, Ipswich, MA, USA
Chloroquine diphosphate salt	Sigma-Aldrich, Munich, Germany Cayman Chemical, Ann Arbor, Michigan, United States
CU-CPT8m	
EcoRI restriction endonuclease	New England Biolabs, Ipswich, MA, USA
Ethanol	Merck, Darmstadt, Germany
Ethylenediaminetetraacetic acid	Sigma-Aldrich, Munich, Germany
Galunisertib	Selleck chemicals, Houston, Texas United states
Halt Protease and Phosphatase Inhibitor Cocktail (100X)	Life Technologies, Carlsbad, USA
<u>Lysogeny broth</u>	Roth, Karlsruhe, Germany
Methanol	Roth, Karlsruhe, Germany
NuPAGE™ MOPS SDS Running Buffer (20X)	Thermo Fisher Scientific, Waltham, MA, USA
Paraformaldehyde	Roth, Karlsruhe, Germany
Pierce™ ECL Plus Western Blotting-Substrat	Thermo Fisher Scientific, Waltham, MA, USA
Pierce™ ECL Western Blotting Substrate	Thermo Fisher Scientific, Waltham, MA, USA
ProLong Glass Antifade Mountant with NucBlue Stain-2 mL	Life Technologies, Carlsbad, USA
Puromycin	Merck, Darmstadt, Germany
Sodium chloride	Merck, Darmstadt, Germany
Sodium dodecyl sulfate (SDS)	Roth, Karlsruhe, Germany
T4 DNA Ligase	New England Biolabs, Ipswich, MA, USA
Tris-Base	Sigma-Aldrich, Munich, Germany
Trisoxon-x100	Sigma-Aldrich, Munich, Germany
Tween 20	Sigma-Aldrich, Munich, Germany
Vemurafenib (PLX4032) 10mg	Selleck chemicals, Houston, Texas United states

2.1.5 Database

Database	Website
CRISPR web design tool	http://crispr.mit.edu
NCBI RefSeq database	https://www.ncbi.nlm.nih.gov/refseq/
R2 genomics analysis and Visualizaion platform	https://hgserver1.amc.nl/cgi-bin/r2/main.cgi

2.1.6 Instruments

Instrument	Distrubutor
BD-FACSAria	BD Biosciences, Heidelberg, Germany
Beckman Optima L-70 ultracentrifuge	Beckman Coulter GmbH, Krefeld, Germany
Centrifuge Heraeus Fresco 17, tabletop centrifuge	Thermo Fisher Scientific, Waltham, MA, USA
Centrifuge Heraeus Sepatech Varifuge 3.0R	M&S Laborgeräte GmbH, Wiesloch, Germany
Eppendorf Mastercycler® Thermal Cycler S	Eppendorf, Hamburg, Germany
FACS Canto IITM	BD Biosciences, Heidelberg, Germany
INTAS Imager	INTAS Science Imaging Instruments, Göttingen, Germany
Leica LSM510 confocal microscope	Carl Zeiss Microscopy, Jena, Germany
Leica LSM510 confocal microscope	Carl Zeiss Microscopy, Jena, Germany
Mithras LB940 Plate Reader	Berthold Technologies, Bad Wildbad, Germany
NanoDrop® ND-1000 Spectrometer	NanoDrop, Wilmington, USA
NanoSight LM10	NanoDrop, Wilmington, USA
Pipettes (20µl, 100µl, 200µl, 1000µl)	Gilson, Middleton, Germany
Pipettes (2µl, 10µl, Multistepper)	Eppendorf, Hamburg, Germany
QuantStudio™ 5 Real-Time PCR System	Thermo Fisher Scientific, Waltham, MA, USA
SDS-PAGE Gel Apperatus	Bio-Rad Laboratories, Inc., Hercules, USA
SP8 Leica confocal microscope	Carl Zeiss Microscopy, Jena, Germany
Steri-Cycle CO ₂ Cell Culture Incubator	Thermo Fisher Scientific, Waltham, MA, USA
SW40T rotor	Beckman Coulter GmbH, Krefeld, Germany
Vi-CELL XR 2.03	Beckman Coulter GmbH, Krefeld, Germany
Western Blot Transfer Device	Bio-Rad Laboratories, Inc., Hercules, USA
ZEISS EM 910	Carl Zeiss Microscopy, Jena, Germany
ZEISS EM 912	Carl Zeiss Microscopy, Jena, Germany

2.1.7 Kits

Kit	Distributor
CellEvent™ Senescence Green Flow Cytometry Assay Kit	Life Technologies, Carlsbad, USA
EndoFree Plasmid Maxi Kit	Qiagen, Hilden, Germany
LEGEND MAX™ Human IL-1β ELISA Kit	BioLegend, San Diego, CA, USA
LEGEND MAX™ Human IL-8 ELISA Kit	BioLegend, San Diego, CA, USA
Micro BCA™ Protein Assay Kit	Thermo Fisher Scientific, Waltham, MA, USA
Pierce™ BCA Protein Assay Kit	Thermo Fisher Scientific, Waltham, MA, USA
QIAprep Spin Miniprep Kit	Qiagen, Hilden, Germany
QuantiTect Reverse Transcription Kit	Qiagen, Hilden, Germany
RNeasy Mini Kit	Qiagen, Hilden, Germany
Senescence B-Galactosidase Staining Kit	Cell Signaling Technology, Danvers, MA, USA
Tumor Dissociation Kit, mouse	Miltenyi Biotech, Bergisch Gladbach, Germany

2.1.8 Primer oligos

Primers	Species	Strand	Sequence
pLKO-Tet-on-nontarget	human	Sense	CCGGCAACAAGATGAAGAGCACCAACTCGAGTTGGTGCTCTT CATCTTGTTGTTTT
		Antisense	AATTA AAAACAACAAGATGAAGAGCACCAACTCGAGTTGGTGC TCTTCATCTTGTTG
pLKO-Tet-on-shSOX10-2	human	Sense	CCGGCCGGGCTGCTGAACGAAAGTGACAACTCGAGTTGTCAC TTTCGTT CAGCAGCCCGTTTTT
		Antisense	AATTA AAAACCGGGCTGCTGAACGAAAGTGACAACTCGAGTT GTCAC TTTTCGTT CAGCAGCCCGG
shNT	human	Sense	CCGGCAACAAGATGAAGAGCACCAACTCGAGTTTCTCAGACA AAGAATGAGGTTTTTG
		Antisense	AATTCA AAAACAACAAGATGAAGAGCACCAACTCGAGTTTCTC AGACAAAGAATGAGG
sgNT	human	Sense	TTGGCGCCAACG TGCCCTGACGGGTTTAAGAGC
		Antisense	TTAGCTCTTAAACCGTCAGGGCACGTTTGGCGCCAACAAG
shSOX10-2	human	Sense	CCGGGCTGCTGAACGAAAGTGACAACTCGAGTTGTCAC TTTT GTT CAGCAGCTTTTTG
		Antisense	AATTCA AAAAAGCTGCTGAACGAAAGTGACAACTCGAGTTGTCA CTTTTCGTT CAGCAGC
shSOX10-2	human	Sense	CCGGGCAGCCAGTATATACGACACTCTCGAGAGTGTCGTATA TACTGGCTGCTTTTTG
		Antisense	AATTCA AAAAAGCAGCCAGTATATACGACACTCTCGAGAGTGTC GTATATACTGGCTGC

MATERIALS AND METHODS

sgSOX10-1	human	Sense	TTGATTCAGGCTCCGTCCTAACGGTTTAAGAGC
	human	Antisense	TTAGCTCTTAAACCGTTAGGACGGAGCCTGAATCAACAAG
sgSOX10-4	human	Sense	TTAGCTCTTAAACAAGGTGTGCGGTCCAGCTCGCAACAAG
	human	Antisense	TTAGCTCTTAAACAAGGTGTGCGGTCCAGCTCGCAACAAG
sgSOX10-6	human	Sense	TTGAGTCTCGGGCTGTCCGGCCAGTTTAAGAGC
	human	Antisense	TTAGCTCTTAAACTGGCCGGACAGCCCGAGACTCAACAAG
shSOX10-1	human	Sense	CCGGGCTGCTGAACGAAAGTGACAACTCGAGTTGTCACTTTC GTTTCAGCAGCTTTTTG
	human	Antisense	AATTCAAAAACCTCATTCTTTGTCTGAGAACTCGAGTTTCTCA GACAAAGAATGAGG
shSox10	mouse	Sense	CCGGTTGCTCCAGCGATACCTTAATCTCGAGATTAAGGTATCG CTGGAGCAATTTTTG
	mouse	Antisense	AATTCAAAAATTGCTCCAGCGATACCTTAATCTCGAGATTAAG GTATCGCTGGAGCAA

2.1.9 Others

Material	Distributor
0.22 µm Millex® Syringe Filter Units	Merck KGaA, Darmstadt, Germany
C-chip counting chamber	VWR, Leicestershire, UK
Eppendorf® Safe-Lock microcentrifuge tubes (1.5 mL, 2.0 mL)	Eppendorf, Hamburg, Germany
FACS tubes	Becton, Dickinson and Company (BD), Franklin Lakes, USA
Falcon tubes (15 mL, 50 mL)	Becton, Dickinson and Company (BD), Franklin Lakes, USA
NEB® Stable Competent E. coli	New England Biolabs, Ipswich, MA, USA
NuPage 4-12% Bis-Tris Gel	Thermo Fisher Scientific, Waltham, MA, USA
NuPage electrophoresis system	Thermo Fisher Scientific, Waltham, MA, USA
pLKO.1 puro plasmid	Addgene, Watertown, MA 02472, USA
pU6-sgRNA EF1Alpha-puro-T2A-BFP plamid	Addgene, Watertown, MA 02472, USA
Tet-pLKO-puro plasmid	Addgene, Watertown, MA 02472, USA

2.1.10 Software

Software	Distributor/Open source
BD FACS Diva	BD Biosciences, San Jose, USA
Flowjo v10.7	BD Biosciences, San Jose, USA
GraphPad Prism 9	GraphPad Software, 2365 Northside Dr. Suite 560, San Diego, CA 92108
Imagej(Fiji)	Open source
NanoSight LM10 NTA 2.3 software	Malvern Instruments Ltd, Worcestershire, UK

2.2 Methods

2.2.1 Cell culture and conditioned media collection

The human melanoma BRAF^{V600E} mutant cell lines A375 and HT144 (generously provided by Prof. Viktor Umansky, German Cancer Research Center (DKFZ), and the human glioblastoma cell line LN229 (p53 mutant, PTEN wt, p16 del) was obtained from ATCC (Cat#CRL-2611). A375 and HT144 cell lines were cultured in DMEM supplemented with 10% FCS, Penicillin/Streptomycin, and MEM non-essential amino acid (NEAA). LN229 was cultured in DMEM supplemented with 10% FCS, Penicillin/Streptomycin, and glutamine. HEK293T cells for lentivirus production were in antibiotic-free DMEM supplemented with 10% FCS. All the cells were cultured in multi-well plates, T-25, T-75, or T-150 tissue culture flasks under 5% CO₂, and all cell lines have been tested for mycoplasma contamination (by Eurofins Genomic, Luxembourg, or the in-house PCR-based verification).

For exosome collection, I cultured cells with prepared exosome-free media. In detail, the FCS was centrifuged under 100,000 x g using the SW40T rotor and Beckman Optima L-70 ultracentrifuge to separate the EVs, then the FCS were sterilized by 0.22 µm pore size filter in tissue culture hood followed by being applied to the DMEM media supplemented with antibiotics.

The PBMCs were isolated from blood buffy coat samples, purchased from the Institute for Clinical Transfusion Medicine and Cell Therapy (IKTZ, Heidelberg, Germany). The buffy coats were first diluted 1:4 by PBS then were subjected to Ficoll density gradient

separation. In detailed, the Biocoll density solution (1.077g/ml) was applied to the Leucosep™ tubes and centrifuged under 1,000 x g for 5 minutes followed by adding the diluted buffy coats on the top of the solution. After applying 30 mL diluted buffy coats on the top of density solution, the tubes were centrifuged at room temperature (RT) for 20 minutes under 1,000 x g, without break, then four phases will present from the top to bottom which are plasm phase, PBMC phase, Biocoll phase and the erythrocytes/granulocyte phase respectively. The PBMC phase was carefully removed to a new 50 mL Falcon tube, and washed by ice-cold PBS for 2 times under 300 x g centrifugation at 4 °C. Then the washed PBMCs pellets were suspended in serum-free PRMI-1640 and counted by Vi-cell XR for the cell density. 1.5 and 3 x 10⁷ viable PBMCs were then seeded in each well of 12 or 6-well plates and incubated under 37°C, 5% CO₂ for 3-4 hours until cells were sufficiently attached to the bottom. Next, the attached cells were washed 4-5 times with warm PBS followed by being cultured in the complete RPMI (PRMI-1640, 10% FCS, glutamine Penicillin/Streptomycin, 2-mercaptoethanol, HEPES buffer) with 20ng/ml M-CSF reconstituted in 0.1% bovine serum albumin (BSA). The cells were subsequently cultured for 7-8 days until the small adherent PBMCs transformed into the spindle or roundish shapes. To visualize exosomes in the macrophages, PBMCs were seeded on small coverslips placed in 12-well plates. The coverslips were pretreated by 70% ethanol and dried in the tissue culture hood then were embedded in wells of a 12-well plate, followed by sterilization under ultraviolet light for 1 hour before PBMCs were added.

2.2.2 SOX10 knockdown systems in cell lines

The LN229, A375, and HT144 cell lines were transduced with a Cas9 endonuclease Dead (dCas9) constructs containing the blue fluorescent protein (BFP) and the human influenza hemagglutinin (HA) tags, then the BFP positive cells were sorted using a single-cell sorter BD-FACSAria. The sorted cells were further diluted into single cell suspension and cultured in 96-well plates to a density of 0.5 cell/well for single cell cloning. After 1-2 weeks, I selected and expanded 5 clones of each cell line and selected the strongest HA-positive clones by Western blots for single guide RNA (sgRNA) transduction. The sgRNA sequences were designed by CRISPR web design tool. In detail, I targeted a -50 to +200 bp genomic window relative to the transcription

start site of SOX10 defined by the NCBI RefSeq database and 2 sgRNAs sequences were selected from the tool. Next, synthetic sgRNA oligonucleotide primers were cloned into a 5' BstXI-BIPI 3' digested backbone of a pU6-sgRNA EF1Alpha-puro-T2A-BFP expression plasmid. The plasmids were subsequently transfected into NEB® Stable Competent E. coli for amplification. The amplified plasmids were then isolated using the Qiagen plasmid mini prep kit followed by the Sanger sequencing (services was provided by Eurofins Genomics). After validating the sequence of the plasmids, they were further expanded in LB buffer and isolated by the Qiagen plasmid maxi prep kit. Next, I transfected the HEK293T cells with the plasmids to produce lentiviruses which were obtained and concentrated by ultracentrifugation of the cell supernatant. Finally, the stable dCas9-expressing cell lines were transduced with lentivirus containing gRNAs targeting SOX10, or lentivirus containing negative guide RNA using a multiplicity of infection (MOI) of 2.5. The successfully transduced cells were selected with puromycin (1 µg/ml) for 48-120 h, followed by qRT-PCR and Western blotting to test the KD efficiency. In addition to the CRISPRi system, the lentivirus-shRNA KD systems used cDNA constructs of shRNA (purchased from Addgene) which were cloned into pLKO.1 puro and Tet-pLKO-puro plasmids respectively. The preparation of lentivirus is similar as the CRISPRi system and tumor cells were treated with the non-targeting (NT) shRNA and SOX10 shRNA-containing lentivirus and selected by puromycin (1 µg/ml) for 4-7 days. To note, the inducible SOX10 KD cell lines required further addition of 1 µg/ml doxycycline to the medium for at least 7 days after puromycin selection to induce the expression of shRNA, and the media were DMEM containing 4.5 g/l glucose (D5921, Sigma) supplemented with 10% tetracycline-free fetal bovine serum (Clontech).

2.2.3 Western blotting

The cells were transduced with lentivirus, treated with inhibitors or exosomes, then the supernatant was discarded, and cells were washed by ice-cold PBS. Next, the PBS was discarded, and cells were lysed in modified RIPA lysis buffer (0.5% sodium dodecyl sulfate) supplemented with 1X protease and phosphatase inhibitors cocktail (100X in stock). The cells were then sheared and centrifuged under 10.000 x g at 4°C for 20 minutes for obtaining clear protein supernatant. The concentration of protein was quantified by BCA assay then were diluted to 0.5 µg/µl with NuPAGE™ LDS Sample

Buffer and reducing agent followed by being boiled at 95 °C for 5 min. In the end, a total of 2.5-10 µg of protein samples were loaded and resolved on 4–12% Bis-Tris protein gels according to the manufacturer's instructions. After polyacrylamide gel electrophoresis, the proteins on the gel were transferred to a methanol-activated and transfer buffer-wetted PVDF membrane. The membrane was blocked in 5% skim-milk or BSA in TBS-T at RT for 1 h with gentle shaking. The membranes were incubated with anti-SOX10, anti-p65, anti-phospho-p65, anti-β-Actin, anti-α-Tubulin antibodies in 5% skimmed milk or BSA in TBS-T at 4 °C overnight with gentle shaking. To note, the phosphorylated antibodies must be blocked in 5% BSA before the primary antibody incubation to avoid strong background. On the next day, the membrane was washed with TBS-T for 10 min three times, then the membrane was incubated in the corresponding horseradish peroxidase (HRP) conjugated secondary antibodies (anti-mouse-HRP, anti-rabbit-HRP and anti-goat-HRP) for 1 h with gentle agitation at room temperature. At last, the membranes were washed in TBS-T for 10 minutes three times again before the addition of ECL reagents or ECL plus reagents to excite the signals. The membranes were subsequently detected by INTAS imaging machine. α-Tubulin and β-Actin were used as loading control and ImageJ was used to proceed unobvious differences between samples.

2.2.4 β-galactosidase assay for microscopy and flow cytometry

For β-galactosidase(β-gal) staining for microscopy, the cells were seeded in 12-well plates in monolayer and reached around 90% cell confluence. X-gal was prepared to 20 mg/ml and mixed with the staining solutions which were offered by the kit. The ratio of each solution was according to the manufacturer's recommendation, and the final β-gal solution was adjusted to pH 5.9-6.1 and evaded from light. Then the cells were washed once by PBS and fixed by the fixative solution offered by the kit for 10-15 minutes at RT, followed by two-time washes by PBS. Next, β-gal solution was added to the cells and the plates were sealed by parafilm overnight at 37 °C. The β-gal positive cells could be observed and showed blue stains under the microscope.

For quantifying the ratio of β-gal cells, I utilized flow cytometry by using CellEvent™ Senescence Green Flow Cytometry Assay Kit. The cells were cultured and detached by trypsin, then cells were washed with PBS followed by 300 x g centrifugation to get cell pellets. The cell pellets were fixed by 2% PFA and incubated for 10 minutes at RT

then cells were washed with 1% BSA and pelleted by centrifuge. Next, the cell pellets were resuspended by the working solution with 1X senescence green probe and incubated for 1-2 hours at 37 °C in a CO₂-free incubator in the dark. After being washed by 1% BSA two times, cells were resuspended in 1% BSA for flow cytometry using 480nm laser and 530nm filter to detect β-gal positive cells.

2.2.5 Isolation of exosomes from cell culture supernatant and interstitial fluid of murine brain tumors.

The cell culture supernatant was harvested from NT and SOX10 KD cells cultured in exosome-free media. The supernatant was centrifuged at 300 x g for 10 minutes to deplete cells and then was further centrifuged under 10,000 x g at 4°C for 20 minutes to further deplete the cells, debris, and large vesicles. To pellet exosomes, the proceeded supernatant was applied to a serial 100,000 x g centrifugation using SW40T rotor and SW28 rotor. To be in detail, the supernatant was centrifuged at 100,000 x g for 1 and a half hours in polyallomer tubes, then the supernatant was discarded to get the unpurified exosome pellets or preserved for exosome-free CM. If the exosomes needed to be stained with PHK26 dye, the pellet was resuspended in 50 µl 0.22 µm pole filtered PBS and mixed with the 1:50 diluted dye for 30 min at RT in the dark. Then the resuspended exosomes were further diluted by the filtered ice-cold PBS up to 7mL for the next-step centrifugation. The second centrifugation requires a diluted Optiprep™ density gradient solution, which is composed of the original Optiprep™ solution, the working solution, and homogenization buffer (recipes have been listed in the section 2.1.2). After mixing the three solutions and buffer according to the manufacturer's introduction, 20% Optiprep™ solution was made with 1.11-1.12 g/ml density, and 4 mL solution was carefully laid onto the bottom of a new polyallomer tube, followed by 7 mL exosome-contained solution being carefully piled at the top of the Optiprep™ solution to create a liquid phase separation. Next, the tubes were centrifuged under 100,000 x g at 4°C again for 1 and a half hours. After this process, the exosomes were restricted in the lower liquid phase, thus 6.5mL liquid on the top was carefully removed and 3.5mL density gradient solution was harvested and transferred to a new polyallomer tube. In the third step, the 3.5mL solution was adjusted to 11mL by the filtered PBS and centrifuged under 100,000 x g at 4°C for 1 and a half hours to pellet exosomes. After a careful removal of all liquid in the tube, the

pellets were finally resuspended in ice-cold PBS for further experiments. Of note, for optimized electron microscopy imaging, the resuspended exosomes should be kept at 4°C overnight, otherwise will be kept at -80°C.

Exosomes from murine SOX10 KD and NT tumors of a murine glioblastoma model established by DKFZ colleagues (Costa et al., 2021; Wu et al., 2020) were isolated from interstitial fluid provided to me by my colleague Ka Hou Man. In this model, the murine cell line mGB1, is cultured in DMEM/F12 Medium containing N2 Supplement, L-Glutamine, 20ng/ml Epidermal growth factor (EGF), 20ng/ml Fibroblast growth factor 2 (FGF2), and antibiotics. Lentiviral particles with pLKO.1-shNT (non-target control) and pLKO.1-shSox10 are produced to generate mGB1-NT and mGB1-shSox10 cells. Then the mGB1 NT and SOX10 cells are selected with puromycin at 1 ng/ml for at least 5 days. After the efficiency of KD was verified by qRT-PCR, the cells are orthotopically injected to the mouse brain. For intracranial injection, 200,000 cells (shNT and shSox10, in 1 µl volume) are injected into adult C57B6 /J mice (8 weeks female) brain under anesthesia with isoflurane. The tumor sizes are monitored by MRI scanning monthly since the eighth week post-injection. Mice are sacrificed when the evaluated sizes of tumors are above 50 µL measured by T2 MRI. The harvested brains are washed with ice-cold PBS and tumors carefully resected to avoid large contaminations from the normal brain area. Tumor samples are finely minced and dissociated using a tumor dissociation kit following the manufacturer's recommendation. Briefly, enzyme mix (enzymes D, R and A) is applied to tumor samples and the tumors are mechanically disrupted by GentleMACS dissociator, followed by incubation at 37 °C for 15 minutes in a tube rotator. After two rounds of mechanical and enzymatic dissociations, tissues are further triturated using serological pipettes and passed through 70 µm cell strainers twice to generate single-cell suspension. During all the tissue disassociation, the disassociation and washing buffer is preserved, followed by 300 x g centrifugation, at RT to deplete the cells and debris. The disassociation and washing buffer was applied to the 3-step serial ultracentrifugation described above. In total, materials from 6 KD and 3 NT mice were included in my study.

2.2.6 Characterization and quantification of exosomes

The characterization of exosomes relies on the morphology, size distribution, and the exosome-specific biomarkers. The morphology of exosomes was assessed by transmission electron microscopy of LN229, HT144, and A375 exosomes. Experiments were performed by Dr. Karsten Richter and according to protocols established by the Imaging and Flow Cytometry Core Facility, Central Unit Electron Microscopy, German Cancer Research Center (DKFZ), Heidelberg, Germany. In brief, exosomes were absorbed on carbon-coated, glow-discharged Formvar grids (400 mesh). Followed two washes with distilled water, the exosomes were fixed with 1% (v/v) glutaraldehyde and negatively stained with 2% uranyl acetate. For detection, samples were embedded in methylcellulose/ uranyl acetate, and pictures were taken via ZEISS EM 910 or EM 912 instruments. The size distribution of exosomes was performed for exosomes via the nanoparticle tracking analysis (NTA) system using a NanoSight LM10 equipped with a 405 nm laser. Exosomes were 1:100 to 1:400 diluted in 0.22 μ m-filtered PBS before measurement to obtain sample concentrations and size distribution. The measurement was according to the manufacturer's instruction and identical parameters were used for comparing samples. For the detection of exosome biomarkers, microBCA assay and Western blotting were used to quantify the protein level and the biomarker expression. In brief, exosomes and the corresponding parental cells were lysed in 1X RIPA buffer for 1 hour at 4 °C with continuous shaking. Samples were then centrifuged at 17,000 x g for 20 min at 4 °C, and the supernatant was transferred to new tubes. Protein lysates of cells were quantified via BCA™ Protein Assay Kit and exosome protein was measured by the microBCA™ Protein Assay Kit according to manufacturer's instructions. The standard BSA was diluted from 400 to 5 μ g protein/mL and 0.5 to 200 μ g protein/mL for BCA assay and microBCA assay respectively. Samples were then 1:25 or 1:5 diluted to reach the total sample volume that each assay requires. For standard or sample, the same volume was transferred into microplate wells of a 96-well plate and the corresponding working reagent was subsequently added. Next, samples were shortly mixed and incubated for two hours at 37 °C in the dark. Then, light absorbance at 562 nm was analyzed using a Mithras LB 940 Multimode Microplate Reader and the optical density (OD) values were recorded. Based on the OD value of BSA standard and samples, the concentration of protein can be calculated and 5 μ g protein of cell and exosome lysates were input in Western blotting. The primary antibodies used to distinguish exosome and whole-cell lysate

were anti-TSG101 (1:250), anti- CD63 (1:100), anti-CD9 (1:100), anti-CD81 (1:100), anti-Alix (1:100), anti-Calnexin (1:200), anti-GAPDH (1:1000), anti- β -Actin (1:1000). ECL or ECL plus detection reagent was applied and X-ray films were exposed and developed.

To quantify exosomes, the exosome concentration or protein amount determined by NTA and microBCA, respectively, was multiplied by the dilution factors and normalized to the cell numbers which were counted during the harvest of supernatant. For the normalization of murine tumor-derived exosomes, tumor volume recorded in T2 MRI, were used.

2.2.7 Uptake of exosomes and functional assay on macrophages

For evaluating the exosome uptake in macrophages, 1×10^9 PHK26 stained vesicles evaluated by NTA were applied to coverslips embedded in a 12-well tissue culture plate with differentiated macrophages. The incubation with exosomes was sustained for 2 hours, 4 hours, 8 hours, and 24 hours, the coverslips removed, transferred to a new 12-well plate and washed with PBS twice. Then the cells were fixed with 4% PFA for 10 minutes at RT followed by 2 washes of PBS. Permeabilization buffer was then added to the coverslips and incubated for 5 minutes at RT followed by two more washes. The coverslips were taken out of the plate and laid on a parafilm and 100nM anti-F-actin Phalloidin dye was applied to the fixed cell and incubated 30 minutes at RT in the dark. To remove the Phalloidin solution, coverslips were washed 3 times in PBS, then the mounting media drops containing DAPI were added to a clean glass slide, and the coverslips were flipped and carefully laid on the top of the mounting media. The slides and coverslips were then kept at RT in the dark over night until the mounting media dried and fixed the coverslips to the slides. Finally, the imaging of stained macrophages was performed with a SP8 Leica confocal microscope applying identical parameters for laser intensity and color compensation. To localize the PHK26 signal in the macrophages, the Z-stack images of several planes of focus were obtained, the images combined and analyzed by ImageJ.

For the functional assay, 2.5-5 μ g exosomes were applied to cells and incubated for 8 hours, the supernatant harvested and centrifuged at 300 x g for 10 minutes to deplete

cells, and then preserved by freezing at -80°C . For tumor cell-derived CM treatment on macrophages, the complete CM was centrifuged under $300 \times g$ then $10,000 \times g$ to deplete cell debris and large vesicles, and the exosome-free CM were further centrifuged under $100,000 \times g$ to deplete exosomes and to preserve cytokines. The CM was then sterilized by $0.22 \mu\text{m}$ filter and mixed with fresh media and applied to the macrophages for 48 hours. After the treatment, the cells were gently washed by PBS and lysed with RLT buffer. To isolate the total RNA from the macrophage lysis, RNeasy Mini kits were used. In brief, cell lysates were applied to RNA mini spin columns and centrifuged at $17,000 \times g$ to trap RNA on the binding membrane. Then, the membrane was washed with RW1 buffer once and RPE buffer twice, followed by elution of the RNA with $50\mu\text{L}$ RNase-free water. A Nanodrop spectrophotometer was used to quantify the total RNA and evaluate its purity based on 260nm and 280nm absorbance. The RNA was then reverse-transcribed into cDNA by the QuantiTect Reverse transcription Kit according to the manufacturer's recommendations. In brief, 500ng RNA were input and 6:1 mixed with the genomic DNA wipeout reagent for 2 minutes at 42°C . The RNA was then mixed with primers and reverse transcriptase master mix and incubated at 42°C for 30 minutes, followed by 95°C for 3 minutes. The cDNA was then diluted in $50\mu\text{L}$ RNase-free water for quantitative-real time-PCR (qRT-PCR). qRT-PCR was done on a QuantStudio™ 5 Real-Time 384-well PCR System with primers synthesized by Sigma-Aldrich. The cDNA was mixed with the 0.2 nM primers of the targeted gene and Sybr green master mix, and a total $10 \mu\text{L}$ mix with 3 technical replicates were used per gene and sample. The system then yielded the cycle threshold (Ct) value and ΔCt values normalized to housekeeping genes such as $\beta\text{-Actin}$ and GAPDH . The $-\Delta\Delta\text{Ct}$ was used to evaluate the relative expression of a gene in a sample.

The frozen supernatant was used to evaluate the quantity of particular cytokines produced by the macrophages. I used the LEGEND MAX™ ELISA Kit to evaluate the level of IL1 β and CXCL8 according to the manufacturer's instruction.

2.2.8 Evaluation of the migration of tumor cells

To evaluate the migration of tumor cells after treated with CM of exosome-educated macrophages, I seeded 5,000 HT144 and 10,000 A375 cells in 24 well plates overnight and exchanged the media with macrophage-conditioned media that was 1:1 mixed with exosome-free fresh media. Complete fresh media were used as control. Cells were then cultured for 24 hours and transferred into serum-free media for another 24 hours for cell-cycle synchronization. Then the cells were suspended by trypsin and counted using C-chip counting chambers. Next, 2,000 cells from each treatment condition were resuspended in 100 μ L serum-free media and seeded in the 8.0 μ m-pore inserts chamber of Corning Transwell plates, followed by placing the inserts in an empty 24-well plate. 500 μ L fresh 5% FCS media were added to the ambient space of the chambers and cells were incubated for 24 hours. Then cells that did not migrate were cleaned off the membrane with a cotton wool stick and both sides of the chamber were fixed with methanol for 10 minutes at RT. To stain the migrated cells, insert chambers were rinsed in hematoxylin for 15 minutes and subsequently rinsed in water, 80% ethanol, and 100% ethanol in rotation, each step requiring 2 minutes at RT. Finally, the inserts were dried overnight in the ventilation hood, and cells were counted the next day, by vertically and horizontally selecting 10 fields, each, and counting cells which were stained brown or deep purple at 20x magnification.

2.2.9 Statistics

Statistical comparison of data was performed with unpaired or paired Student's t-test for quantification of exosomes, cell count, and $-\Delta\Delta C_t$ value. The tests were performed by GraphPad Prism 9, the significance-threshold for P-values was set in <0.05 . For comparing the significance of linear fold change of gene expression in qRT-PCR, the paired Wilcoxon signed-rank test was used due to the asymmetrical distribution of the data.

3 RESULTS

3.1 Cancer drugs induce the downregulation of SOX10 in BRAF^{V600} melanoma cells and RTK I glioblastoma cells

To investigate the clinical relevance of SOX10 downregulation in melanoma and glioblastoma, I first reviewed published data. For melanoma, I identified two studies, including RNA-seq data of BRAFi and MEKi-treated patients who had acquired drug resistance (Hugo et al., 2015; Sun et al., 2014). Out of a total 20 of biopsies, 65% showed therapy-associated downregulation of SOX10 (Fig.1). This suggests that drug-induced SOX10 downregulation commonly occurs in the long-term BRAFi and MEKi treatment.

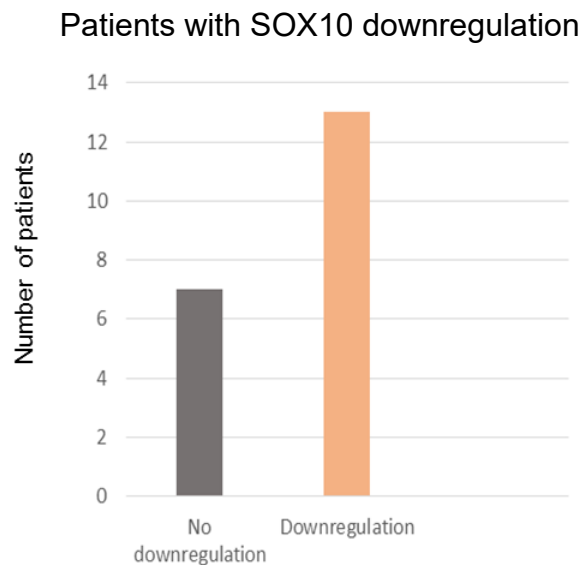


Fig 1. Therapy-associated SOX10 downregulation in melanoma. Numbers of patients that showed no, or less than 10% downregulation (grey bar; n=7), or more than 10% downregulation (orange bar; n=13) of SOX10 in bulk-tumor RNA-Seq data after BRAFi, MEKi, or combination treatment. Data of two studies on patients who exhibited tumor-progressive features during treatment were combined (Hugo et al., 2015; Sun et al., 2014) .

To investigate whether SOX10 downregulation can be recapitulated *in vitro*, I treated the BRAF^{V600E} mutant melanoma cell lines A375 and HT144 with the BRAFi Vemurafenib for different periods. Interestingly, the shorter, 2-day treatment did not suppress SOX10 expression (Fig.2A), even though treated cells did grow slower than control cells. In contrast, the longer, 6-day treatment with Vemurafenib concentrations ranging from 0.5 to 2 μ M resulted in SOX10 downregulation (Fig.2B). These results

suggest that the therapy-associated SOX10 downregulation observed in melanoma patients could be a secondary rather than direct effect of Vemurafenib treatment.

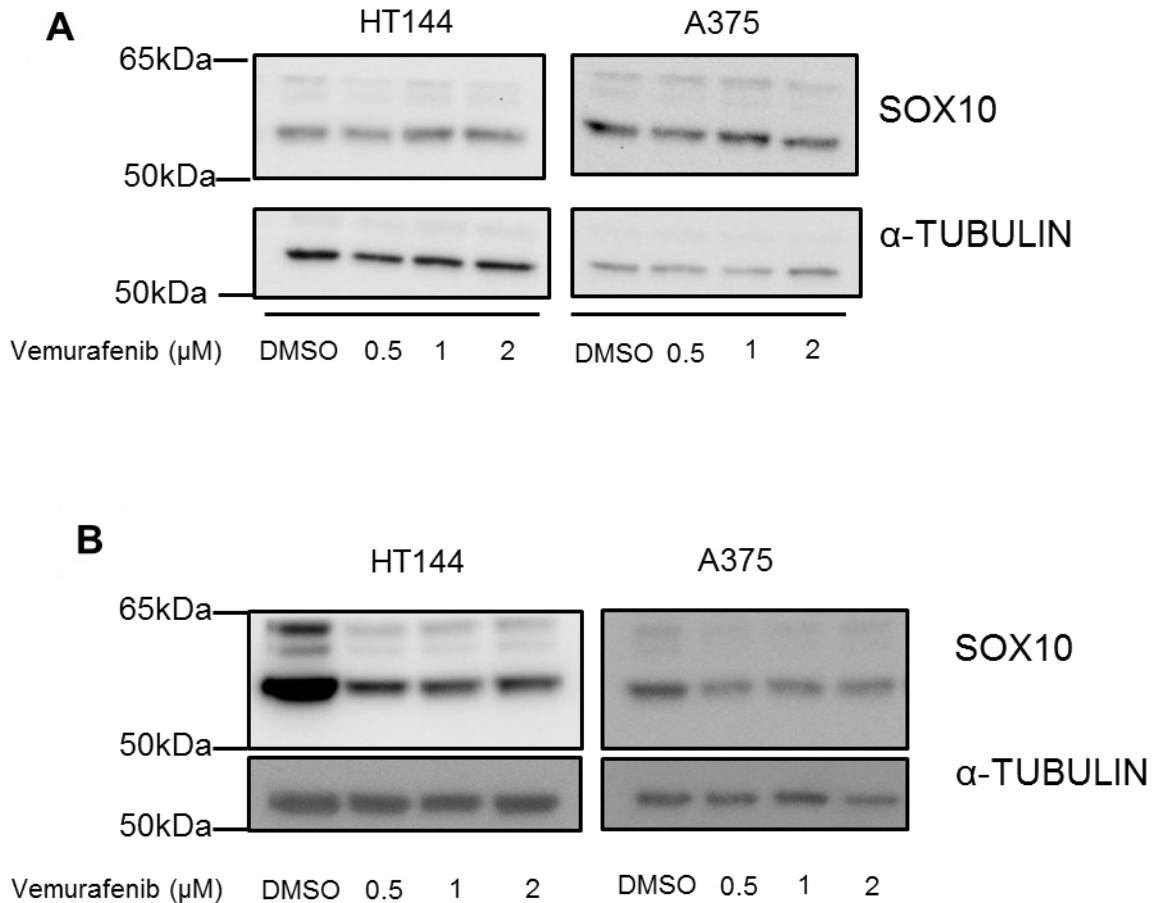


Fig 2. Suppression of SOX10 protein expression in melanoma cell lines by Vemurafenib treatment, as analyzed by Western blotting. A) 2 day-treatment; B) 6-day treatment. Experiments were performed at least two times for each cell line and time period. Representative images are shown.

I also performed qRT-PCR to determine whether SOX10 suppression occurs at the transcriptional or post-transcriptional level. The analysis revealed that treatment with

2 μ M Vemurafenib reduced *SOX10* mRNA levels by 51% and 80% in A375 and HT144, respectively (Fig.3A), indicating transcriptional repression. The expression of *SOX10* has been shown to be suppressed by transforming growth factor-beta ($TGF\beta$) signaling in neural crest stem cells and laryngeal squamous cell carcinoma(Cui et al., 2019; John et al., 2011).

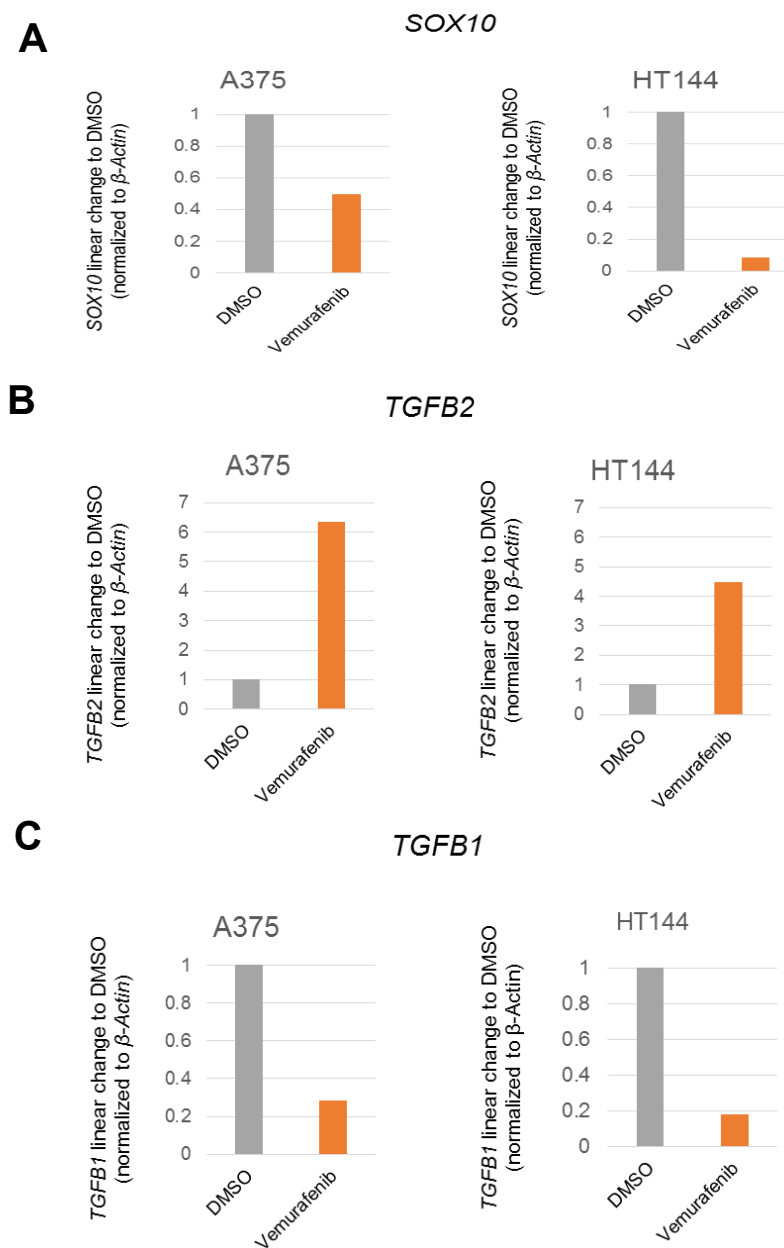


Fig.3 Vemurafenib-dependent changes of (A) *SOX10*, (B) *TGFB2*, and (C) *TGFB1* expression. RNA-expression was determined by qRT-PCR after 6-day treatment with 2 μ M Vemurafenib in the cell lines HT144 and A375. Ratios were computed relative to expression in control cells treated with 0.04% DMSO and normalized to the housekeeping gene β -actin.

Therefore, I reasoned that Vemurafenib might induce the upregulation of TGF β family-associated factors such as the TGF β isoforms TGF β 1 and TGF β 2. By qRT-PCR, I found that concurrent with SOX10 downregulation (Fig. 3A), TGF β 2 levels indeed were upregulated in the A375 and HT144 cell lines (Fig. 3B), while TGF β 1 was downregulated (Fig. 3C). These results are consistent with the reported significant upregulation of TGF β 2 after Vemurafenib treatment in the colo858 cell line (Fallahi-Sichani et al., 2017).

To determine whether inhibitors of TGF β signaling can rescue SOX10 suppression, I applied the TGF β receptor I (TGF β RI) inhibitor Galunisertib (LY2157299) combined with Vemurafenib to HT144 and A375. Immunoblotting confirmed that Galunisertib rescued SOX10 protein downregulation by Vemurafenib, whereas Galunisertib per se did not affect SOX10 expression (Fig. 4A and 4B). These results are lending additional support to the hypothesis that Vemurafenib-induced SOX10 suppression is mediated by TGF β signaling.

In contrast to melanoma, no studies have been published regarding SOX10 expression in glioblastoma after standard therapies, such as TMZ and radiotherapy, in human patients or cell lines. However, Lau et al. have shown that radiation induces Sox10 downregulation in a Sox10^{high} proneural mouse glioma model (Lau et al., 2015); SOX downregulation depended on JAK2/STAT3 pathway signaling, which co-operates with TGF β signaling to induce EMT in cancer cells (Liu et al., 2014). This study suggests that standard glioblastoma therapies possibly induce SOX10 downregulation. Therefore, I asked whether TMZ could also induce SOX10 downregulation in glioblastoma. In collaboration with my colleague Ka Hou Man, I performed TMZ treatment of SOX10^{high} RTK I cell line LN229. I found consistent SOX10 downregulation at RNA and protein levels (Fig.5A and Fig.5B), similar to my observations in the context of Vemurafenib treatment of melanoma cell lines.

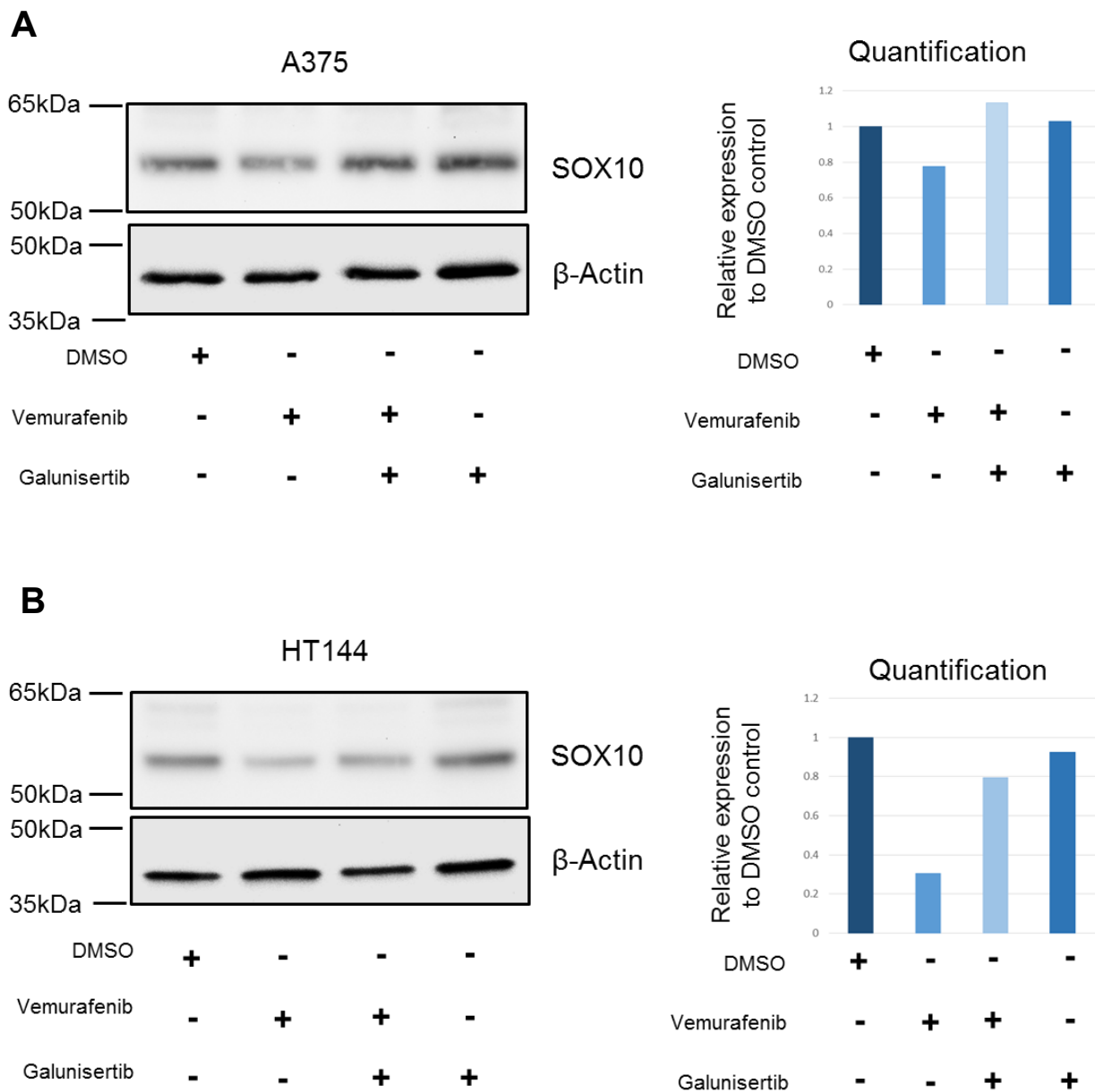


Fig 4. TGFBR1i inhibits SOX10 downregulation induced by Vemurafenib. Visualization by Western blotting of SOX10 protein expression in A) A375 and B) HT144 melanoma cells under different treatment conditions. The concentrations of Vemurafenib, Galunisertib, and DMSO were 2 μ M and 10 μ M, and 0.04%, respectively. On the right, the densitometric quantification of band intensities using Image J software is shown. Band intensities were normalized to the respective β actin loading controls and are displayed relative to DMSO controls.

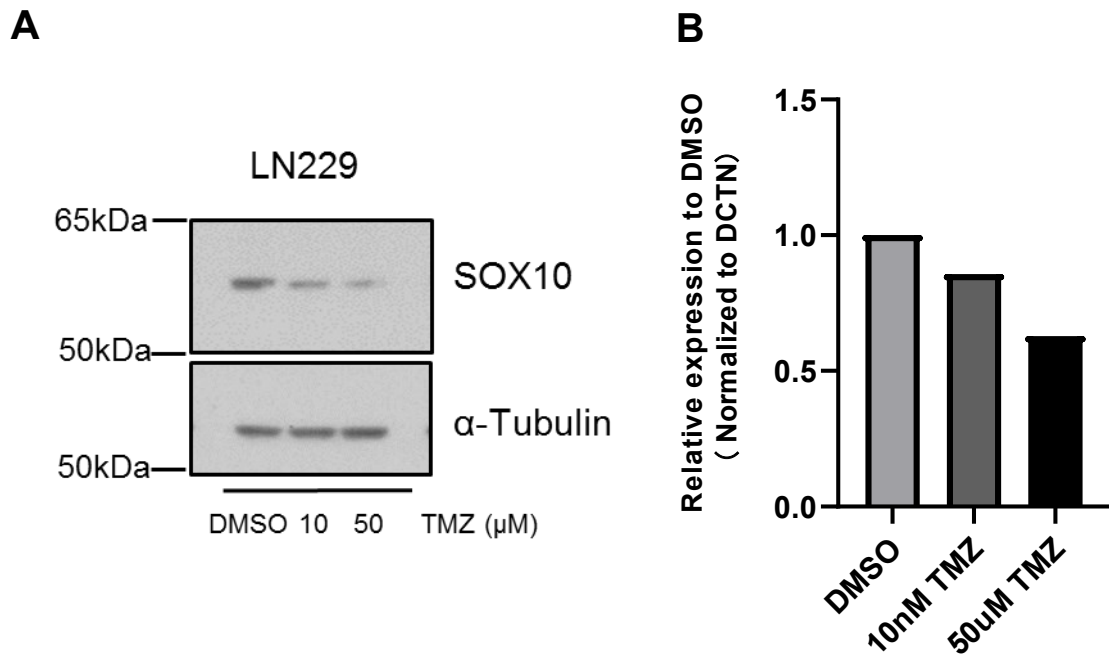


Fig 5. Temozolamide (TMZ) induces SOX10 downregulation in glioblastoma cells. A) Representative Western blot of SOX10 expression in LN229 glioblastoma cells treated with DMSO, 10 μ M, and 50 μ M TMZ for 5 days. The experiments were repeated twice and showed similar results; B) SOX10 mRNA levels in TMZ-treated LN229 cells, relative to DMSO-treated controls. This result was independently confirmed by my colleague Ka Hou Man (data not shown).

3.2 SOX10 downregulation induces a β -galactosidase (β -gal)-positive phenotype and increased exosome production in melanoma and glioblastoma cell lines

To understand the function of SOX10 downregulation in melanoma and glioblastoma cells, I utilized lentivirus-mediated shRNA and clustered regularly interspaced short palindromic repeats interference (CRISPRi) to inhibit the expression of SOX10 in the HT144, A375, and LN229 cell lines. Both knockdown systems successfully reduced SOX10 expression (Fig.6A and B). In melanoma cells, SOX10 KD suppressed cell proliferation by about 50% (Fig.6C). In line with these data, our group has previously shown suppression of cell proliferation by about 30% after SOX10 KD in LN229 glioblastoma cells (Wu et al., 2020).

To investigate the functional phenotype of the SOX10 downregulated tumor cells, I tested whether SOX10 KD induces a β -gal positive phenotype. The appearance of β -gal positive cells has been reported in the context of SOX10 KD in melanoma (Sun et al., 2014), and this phenotype was often connected with senescence-associated secretory phenotype (SASP). Although the β -gal positive cells resulting from SOX10

KD do not enter a classic senescent state, they do exhibit senescence-like features such as reduced cell proliferation and increased cytokines excretion (Cristofalo, 2005; Severino et al., 2000). As expected, microscopy and fluorescence-activated cell sorting (FACS) identified more β -gal positive cells and more cells with enlarged, flattened, or elongated morphology among the SOX10 KD compared to the non-targeting (NT) control cells (Fig.7).

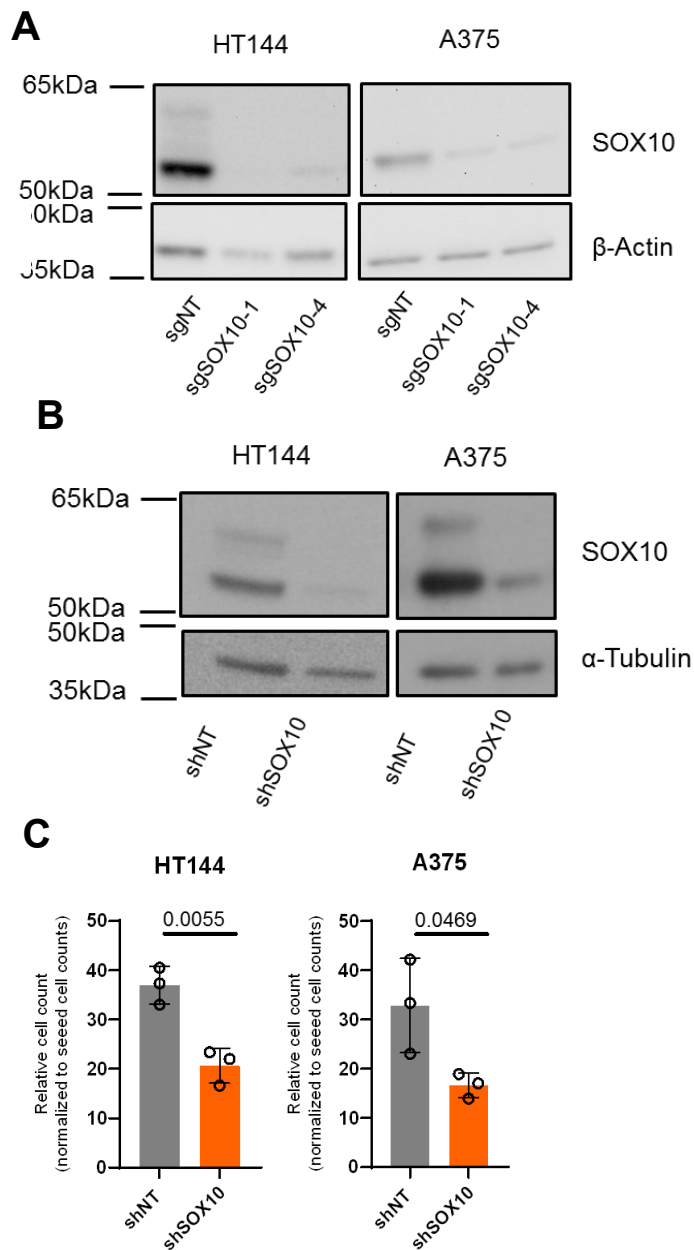


Fig 6. SOX10 KD suppresses cell proliferation in HT144 and A375 melanoma cells. A and B) CRISPRi (A) and shRNA (B) systems efficiently knock down SOX10 expression in A375 and HT144 respectively; C) Cell counts 4 days after seeding are shown for shRNA-knockdown and control cells. Cell counts were normalized to the count of initially seed cells. N = 3 biological replicates. Error bars represents standard variations. P-values were calculated by two-tailed unpaired Student's t-test.

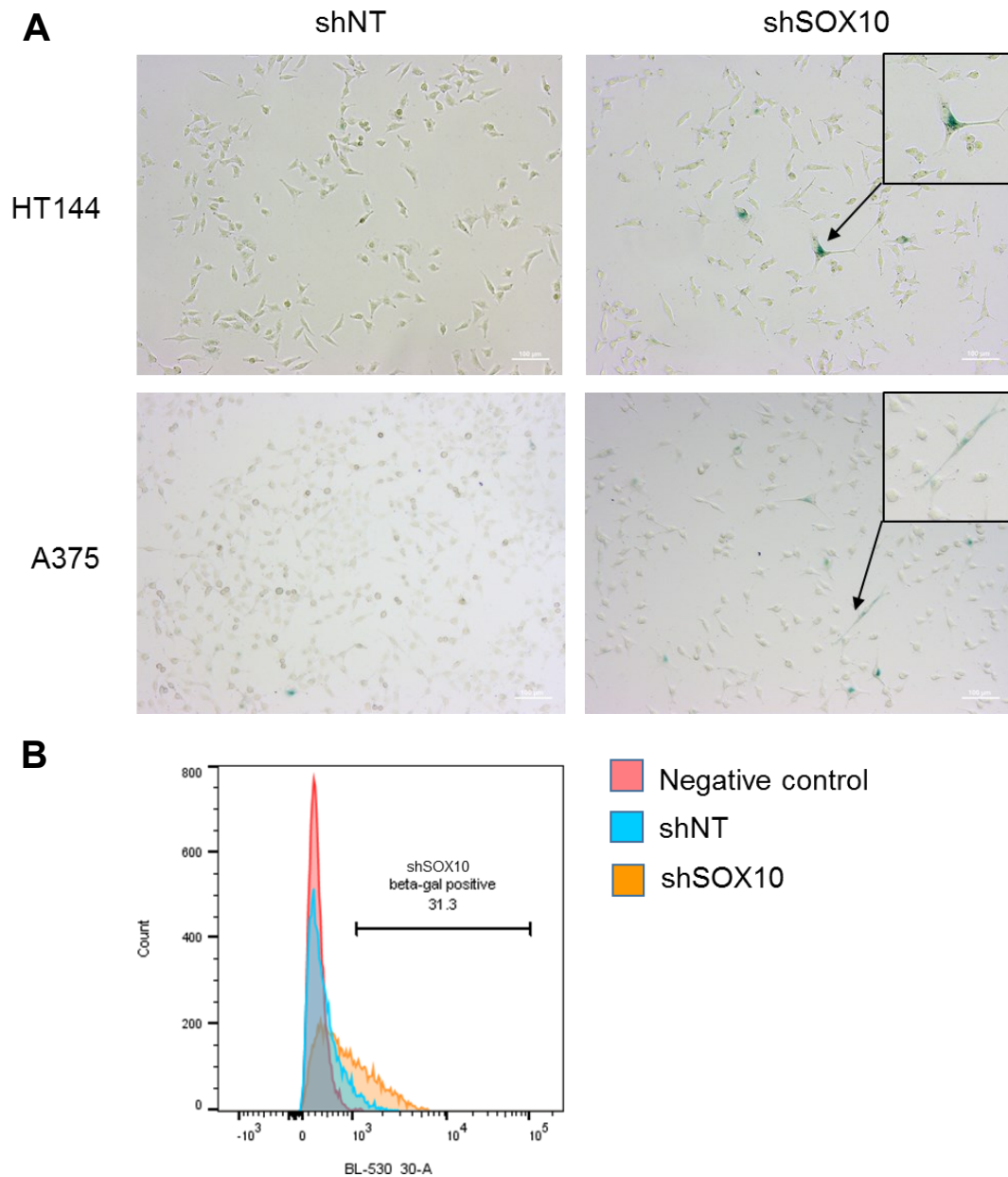


Fig 7. SOX10 KD in A375 and HT144 melanoma cells induces β -gal expression and cell morphology changes. A) Cells were fixed stained for β -galactosidase and imaged by bright field microscopy. Scale bars correspond to 100 μ m. Insets show magnifications of β -gal positive cells. B) Quantification of β -gal positive cells in HT144 SOX10 KD (orange) and shNT control cells (blue) by fluorescence-activated cell sorting (FACS). The fluorescence intensity in the 530/30 filter is shown on the X-axis and cell counts are shown on the Y-axis. The percentage of β -gal positive cells (31.3%) is noted above the horizontal line that indicates the positive range beyond the threshold defined by the negative control (red). In the repeat experiment, the proportion of β -gal positive cells was 20.8%.

Since it was reported that β -gal expression can be associated with increased production of EVs such as exosomes (Lehmann et al., 2008), I isolated exosomes from NT and SOX10 KD cell lines via a 3-step ultracentrifugation protocol (Fig.8).

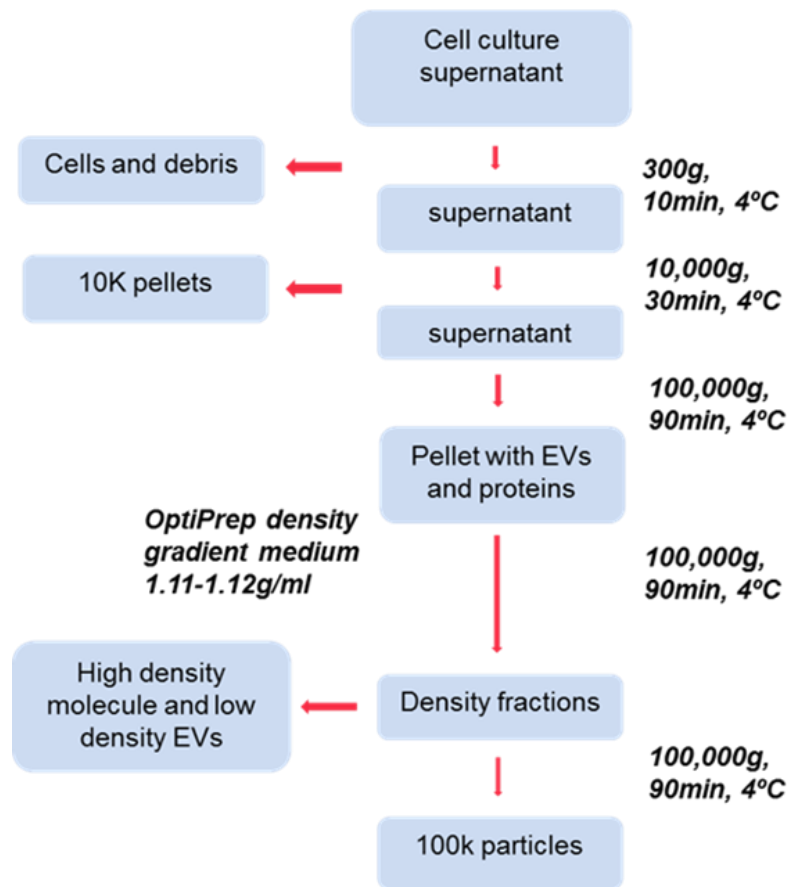
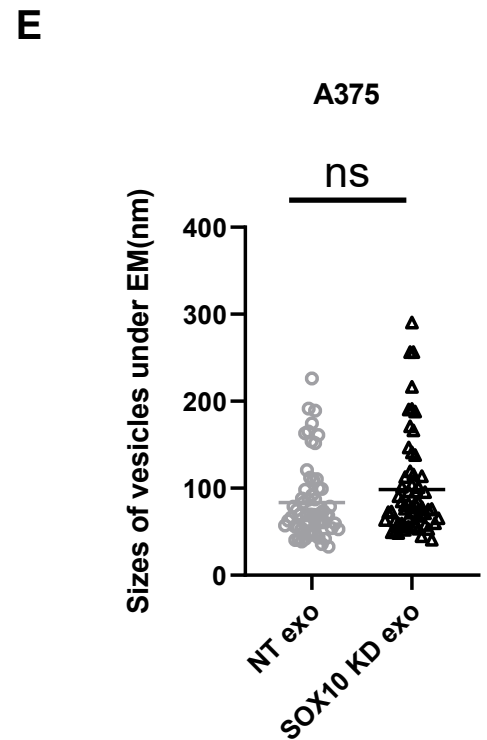
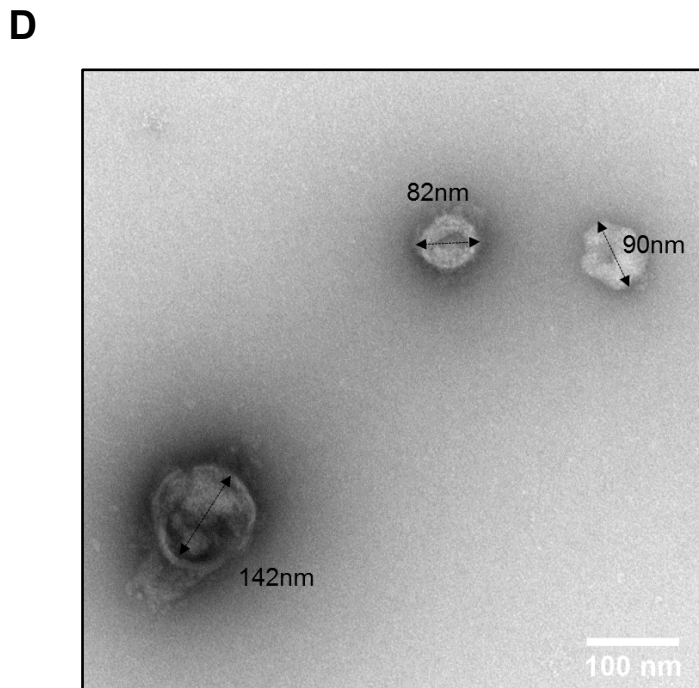
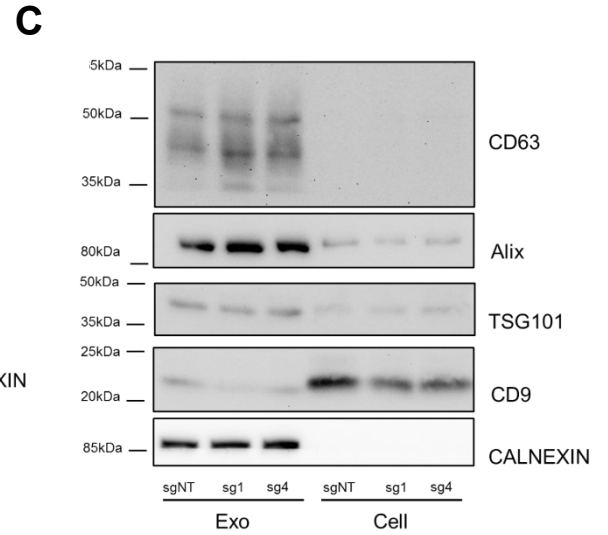
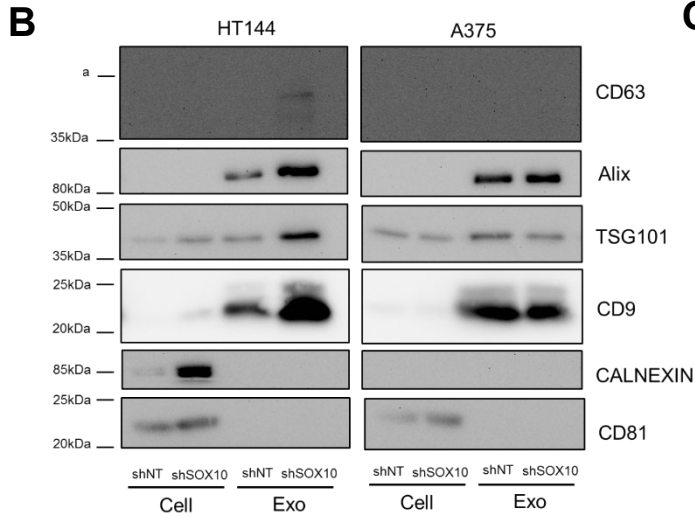
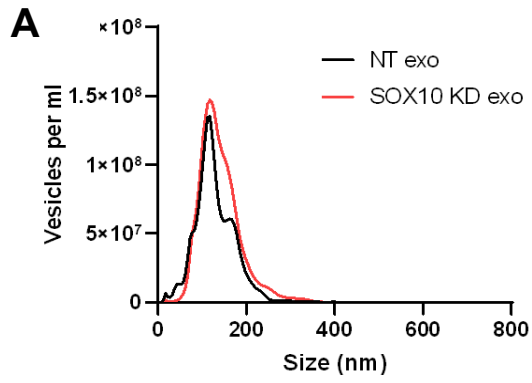


Fig.8 Schematic workflow for exosome isolation and purification. Cell culture conditioned media were isolated and consecutively centrifuged at 300xg and 10,000xg to separate cells, debris and big vesicles. Then the supernatant was further ultra-centrifuged 3 times at 100,000xg to collect all exosomes. In the second ultracentrifugation step, 1.11 to 1.12g/ml OptiPrep density gradient solution was used to further purify exosomes and avoid contamination from RNPs and low-density vesicles.

Conditioned media (CM) collected from cell culture were subjected to 300 x g and 10000 x g centrifugations to eliminate most cell debris and large EVs such as microvesicles. Subsequently, the supernatant was centrifuged under 100,000 x g, and the EVs contained pellets were applied to an Optiprep™ density gradient (1.11-1.12g/ml) for a second 100,000 x g ultracentrifugation to minimize the contamination from larger vesicles and proteins such as ribonucleoprotein. Finally, the exosome-containing density gradient media was subjected to the third 100,000 x g ultracentrifugation to remove the density-gradient media and concentrate the purified exosomes.

To characterize the exosomes, I utilized Nanosight (NTA) analysis, immunoblotting, and electron microscopy (EM) to identify the exosome features, size distribution, exosome biomarkers, and the micro structure. Nanosight analysis demonstrated that most of the vesicles had sizes of 30-200nm, and that there was no significant difference between NT and SOX10 KD exosomes (Fig.9A). For Western blotting, I used several exosome positive markers such as ALIX, TSG101, CD9, CD63, CD81 and a traditional negative marker, CALNEXIN, which is usually positive in whole cell lysate rather than exosomes. The melanoma exosomes were consistently positive for ALIX, TSG101 and CD9, and CALNEXIN negative, however CD81 and CALNEXIN were missing in all exosomes while positive in whole cell lysate (Fig.9B). For LN229, the exosomes were enriched with ALIX, TSG101 and CD63. Unexpectedly, CALNEXIN was also positive in exosomes while absent in whole cell lysates (Fig.9C). These results indicate that CALNEXIN may not always be a suitable negative marker for exosome identification.

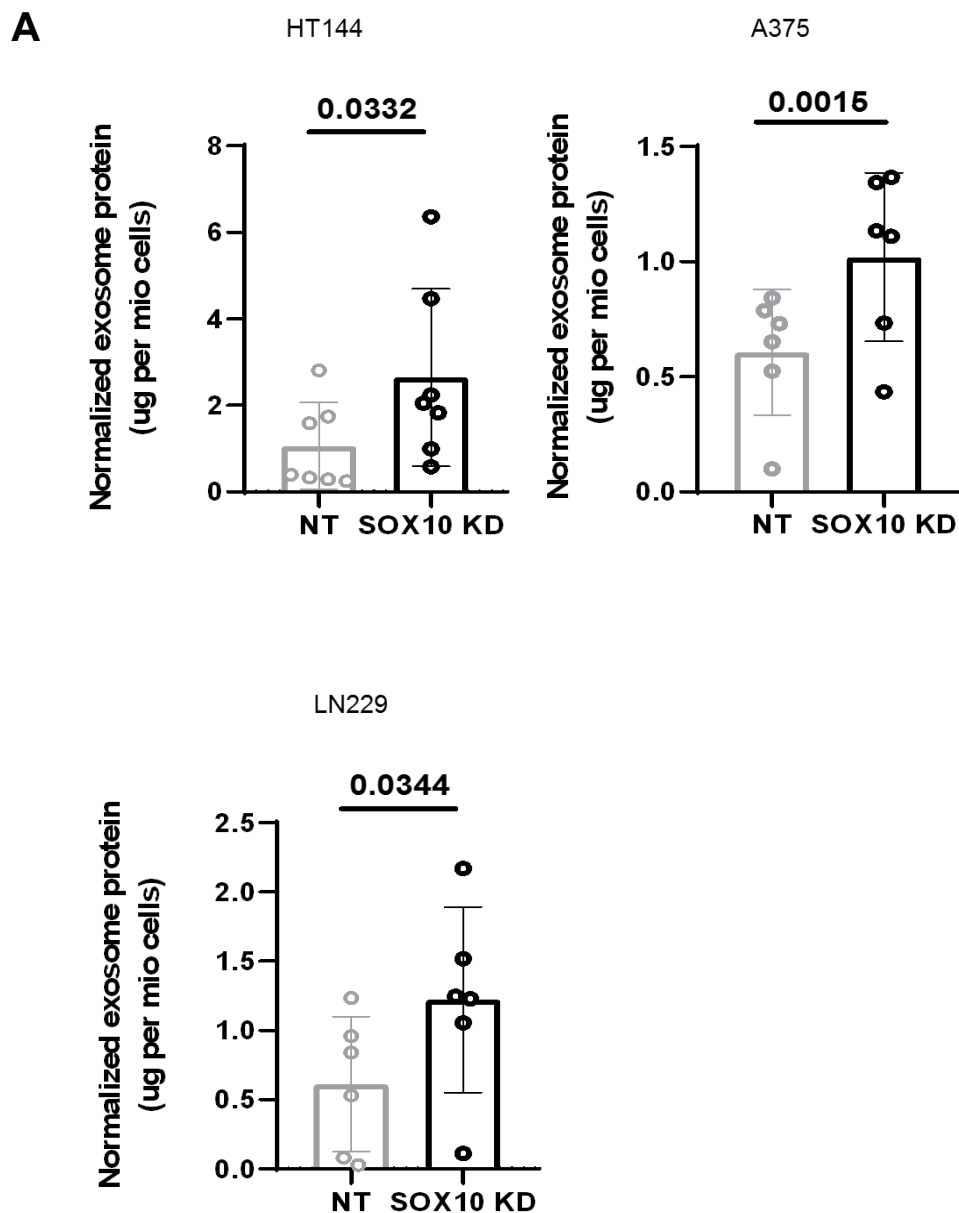
Fig 9 (next page). Characterization of cell line-derived exosomes. A) Size-distribution analysis of exosomes derived from control and SOX10 KD A375 cells; B) Western blot analysis (input 2.5 µg protein) of the expression of exosome positive and negative markers from exosomes (EXO) and whole-cell lysates (Cell) of A375 and HT144 shNT control cells and shSOX10 KD cells; C) Western blot analysis of exosome marker expression from EVs and whole cell lysates of the LN229 cell line. sg1 and sg4 denote two guide SOX10-targeting RNAs that were used for the CRISPRi knockdowns. guiding RNAs. sgNT denotes the non-targeting guiding RNA used as control; D) Electron microscopy image of freshly prepared exosomes derived from a A375 sgSOX10 cell line. The diameters of each vesicle are marked with arrows and their lengths calculated via ImageJ. scale bar: 100nm. E) The distribution of exosome sizes under EM, n=60 vesicles each for the A375 NT and SOX10 KD exosome samples. ns, not significant.



Next, I characterized the exosomes by transmission electron microscopy, showing that the majority of the freshly prepared EVs were 30-200nm in size. There were no differences in the average sizes of vesicles from NT and SOX10 KD cells, consistent with the NTA results (Fig 9D and E).

After validating that the isolation protocol is an efficient purification method, I further investigated whether SOX10 downregulation affects the production of exosomes. Interestingly, by using total protein quantification and EM, I acquired consistent results that SOX10 KD cells produce more exosomes than NT cells (Fig.10).

In addition, I also confirmed that Vemurafenib treatment induced exosome production by the HT144 melanoma cell line, stronger, consistent with the effect of SOX10 KD (Fig.11).



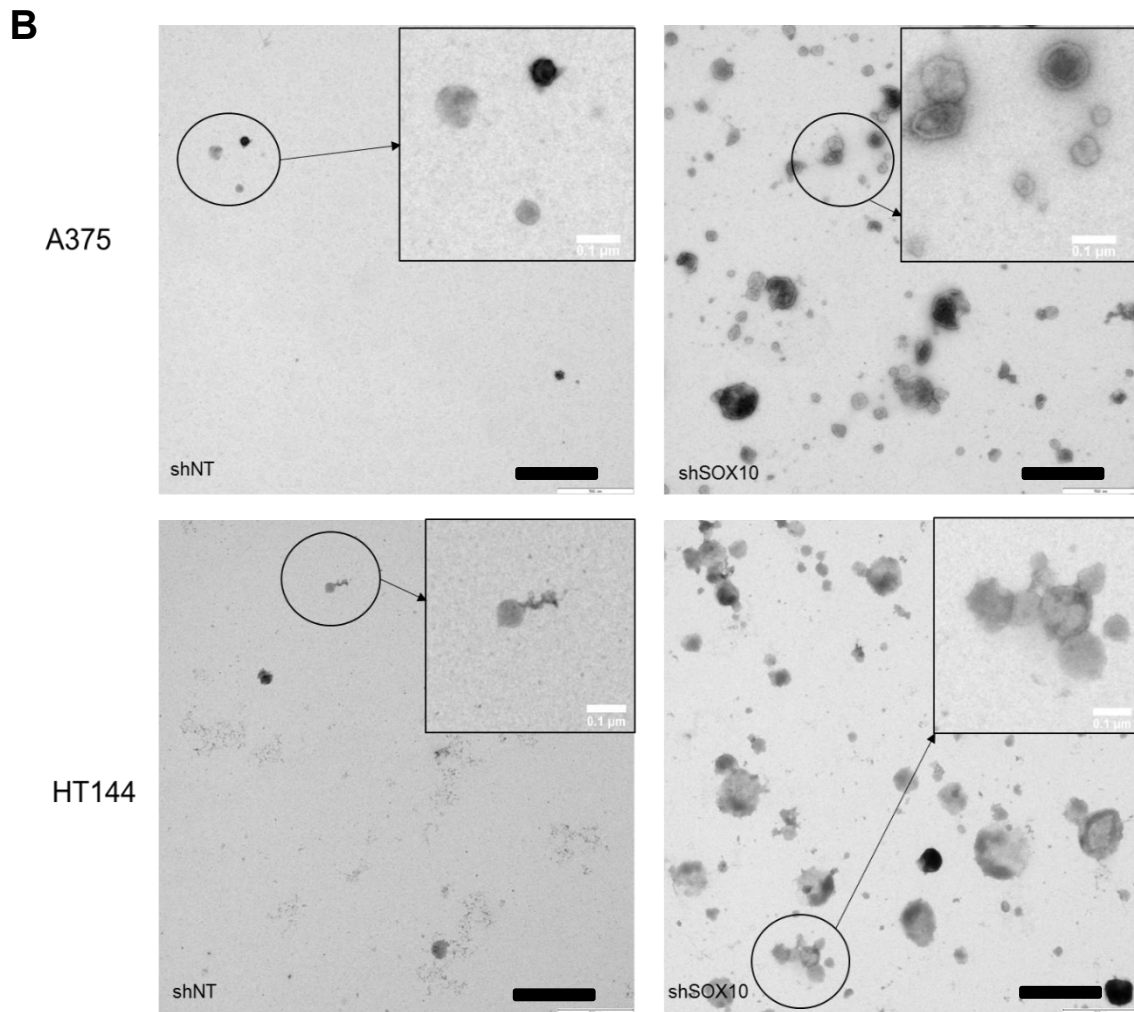


Fig10. SOX10 KD increase exosome production. A) Three histograms present the normalized exosomes quantity between NT and SOX10 KD cell lines in HT144, A375 and LN229. The label beside Y-axis means the amount of NT and SOX10 KD exosomes were quantified by microBCA then was normalized to total cell numbers at harvest time point. HT144 (n=7), A375 (n=6), LN229 (n=7). The height of bars are mean value of the normalized exosome quantity, and the error bars represent the standard deviation. P value were obtained by two-tailed paired Student's t-test and the values were labelled at the top of the two bars of each histogram; B) Representative electron microscopy images of NT and SOX10 KD exosomes from A375 and HT144 (Dr.Karsten Richter, Core Facility Unit Electron Microscopy of the German Cancer Research Center). The black scale bar at the right bottom corner of the each big image is 500 nm. Insets show magnifications of vesicle details. Scale bar: 100 nm.

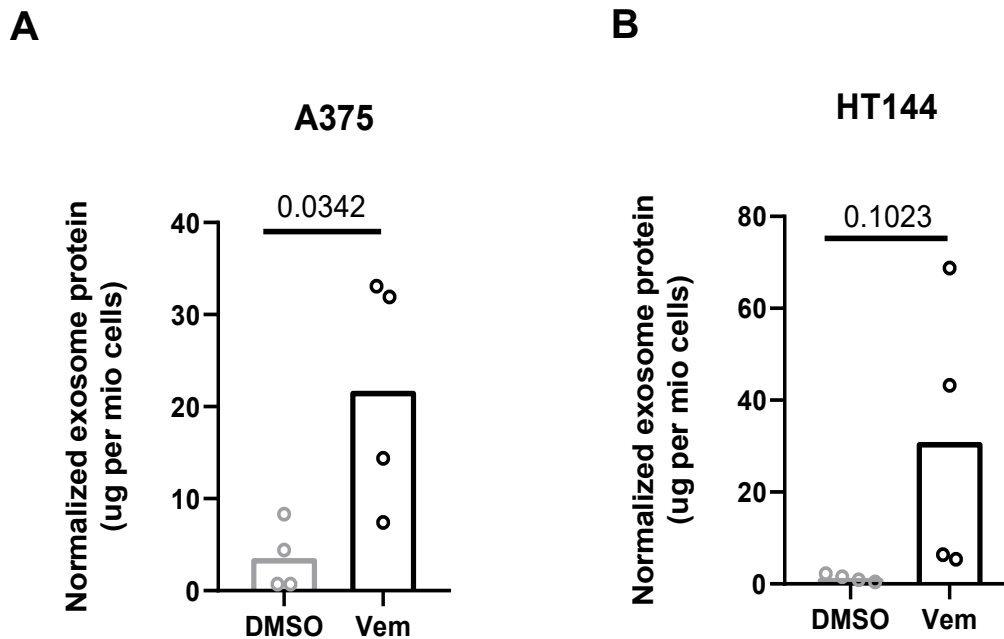


Fig.11 Vemurafenib induces increased exosome production in HT144 and A375. A) The histogram presents the normalized exosomes quantity between DMSO and 2 μ M Vemurafenib (Vem) in A375; B) The histogram presents the normalized exosomes quantity between DMSO and 2 μ M Vemurafenib (Vem) in HT144. The label beside Y-axis means the amount of NT and Vemurafenib-treated exosomes were quantified by microBCA then was normalized to total cell numbers at harvest time point. 4 biological replicates were performed for each cell line. The height of the bars represent mean value of the normalized exosome quantity. P-values were obtained by two-tailed unpaired Student's t-test and indicated at the top of the two bars of each histogram.

Besides the *in vitro* work, I also sought to validate whether SOX10 KD cells produce more exosomes *in vivo*. To address this question, I analyzed material of a syngeneic graft mouse model that my colleague Ka Hou Man is using to generate brain tumor in mice. In brief, Sox10 was knocked down in the SO10^{high} murine glioma stem cells (GSCs) mGB1 by shRNA and the Sox10 KD and NT GSCs were orthotopically transplanted into wildtype (wt) C57BL/6 mice. Previously, our group has reported that in this mouse model, Sox10 KD tumors proliferated faster than the NT tumors and Sox10 KD tumor conferred shorter life span to the host mice (Wu et al., 2020). Basing on this, I worked with my colleagues Ka Hou Man and Pavle Boskovic to disassociate the Sox10 KD and NT tumors, from which I isolated EVs from the interstitial media in order to compare the quantity of exosomes. Both NT and Sox10 KD tumor-derived exosomes were Cd63 positive in Western blotting analysis while lacking cytoplasmic markers such as β -Actin and Gapdh (Fig.12A). Next, I quantified the total exosomes

from 3 NT tumors and 6 Sox10 KD tumors and normalized the exosome numbers by the corresponding tumor volumes recorded by magnetic resonance imaging (MRI). In line with my cell line data, exosome production appeared higher in SOX10 KD than control tumors (Fig.12B).

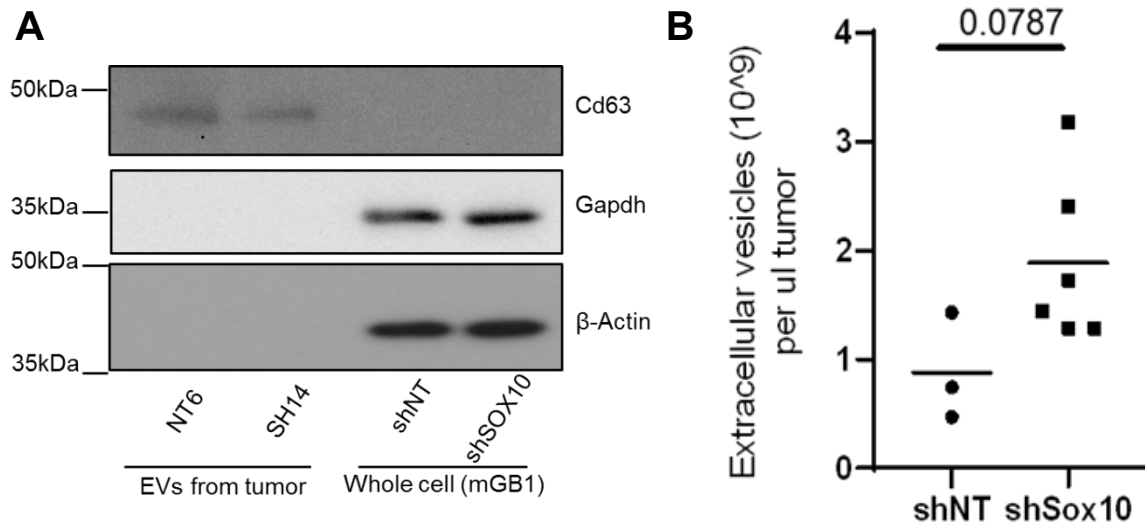


Fig.12 Sox10 KD tumors produce more exosomes than NT. A) Western blot of exosomes isolated from the interstitial fluid of disassociated tumors and whole cell lysate from the transplanted mGB1 cell line. NT6 and SH14 represent one NT tumor and Sox10 KD tumor. Cd63 was used as positive markers for exosomes, unfortunately other markers didn't show bands in both exosome and cell lanes. Gapdh and β -Actin were used as cell markers. The position and MW of protein electrophoresis markers was labelled at the right of each blots and the names of each protein were marker at the right of the blots. B) Nanosight analysis of the quantity of vesicles from NT tumors (n=3) and Sox10 KD tumors (n=6). Vesicle quantities were normalized by the tumor volume (μ l) evaluated by MRI, horizontal line represent the mean value and each dots represent one tumor. P values were calculated by two-tailed unpaired Student's t-test.

3.3 SOX10 KD cells affect the phenotype of macrophages via exosomes

Since in the tumor microenvironment of melanoma and glioblastoma, myeloid cells such as macrophages and resident microglia can be transformed into tumor-associated macrophages/microglia (TAMs) (Geribaldi-Doldan et al., 2020; Harjes, 2021), I asked the question whether the secretome of SOX10 KD cells affects the phenotypic transition of myeloid cells. I first tested whether conditioned media of SOX10 KD cells affected the phenotype of human blood derived macrophages. For this purpose, I differentiated PBMCs into macrophages with 20 ng/ml M-CSF, a

concentration that was reported to avoid strong polarization of macrophages (Hamidzadeh et al., 2020). Subsequently, I performed M1 and M2 polarization of these macrophages. M1 polarization was induced by interferon γ (IFN γ) and lipopolysaccharides (LPS), and M2 polarization by interleukin-4 (IL4), treatment.

These are standard methods for polarizing macrophages (Orecchioni et al., 2019). I then validated the polarization states by comparing the expression of cytokine genes such as IL1 β , CXCL8, CCL4, TNF, etc., between the unpolarized and polarized macrophages. qRT-PCR analysis revealed that the gene expression of the unpolarized macrophages typically fell between that of the M1 and M2 macrophages (Fig.13). Therefore, the M-CSF-differentiated macrophages are likely in an unpolarized state and have the potential to switch their phenotype in response to appropriate stimuli.

Next, I harvested the conditioned media (CM) from HT144 SOX10 KD and NT cells and applied it to the unpolarized macrophages. After 48 hours, qRT-PCR showed that SOX10 KD CM upregulated the expression of pro-inflammatory genes such as CXCL8, CCL4, and the immune-suppressive protein PD-L1 in comparison to NT CM. Then I investigated whether the exosomes were responsible for the induction of the pro-inflammatory phenotype. For this purpose, I used ultracentrifugation to separate the exosomes from the CM, and treated the macrophages with the exosome-free CM. Strikingly, exosome depletion significantly reduced the upregulation of inflammatory markers by SOX10 KD CM. In contrast, exosome-free NT CM did not differ from complete NT CM regarding its effect on macrophages (Fig.14). These data indicate that the phenotypic transition of macrophages after treatment with HT144 SOX10 KD CM likely is mediated by exosomes.

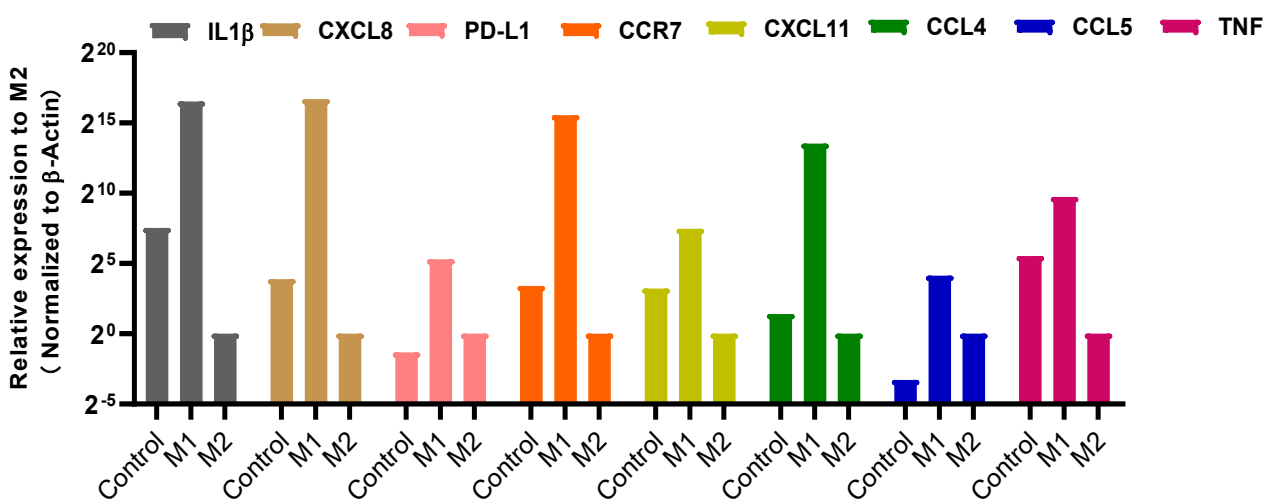


Fig.13 RNA expression of polarization-marker genes in unpolarized (control), M1, and M2-polarized macrophages.

To further characterize exosome-mediated effects on macrophages, I treated macrophages with equal quantities of SOX10 KD and NT exosomes generated from the HT144 and A375 cell lines. The exosomes from both cell lines consistently induced the expression of the pro-inflammatory genes IL1B, CXCL8, TNF- α , CXCL1, CCL4 and PD-L1 more strongly than NT exosomes (Fig.15 and Fig.16). In addition to the melanoma cell lines, I also found the levels of IL1B, CCL2, IL6, CXCL8, CCL4 and CCL5 significantly regulated by treatment with LN229 SOX10 KD compared to NT exosomes (Fig.17). To note, in order to minimize overdosing effects and mimic the pathological condition in tumor, I only applied 2.5ug to 5ug total exosomes to the macrophages, which are approximately produced by 1 to 2 million tumor cells.

To verify that the upregulation of pro-inflammatory genes on RNA level translates to increased cytokine excretion, I performed enzyme-linked immunosorbent assays (ELISA) of IL-1 β and CXCL8 (Fig.18). I found the excretion of both cytokines upregulated for HT144 and A375 SOX10 KD CM-treated macrophages. These results indicate that the effects of SOX10 KD exosomes indeed result in phenotypic adaptations in the treated macrophages.

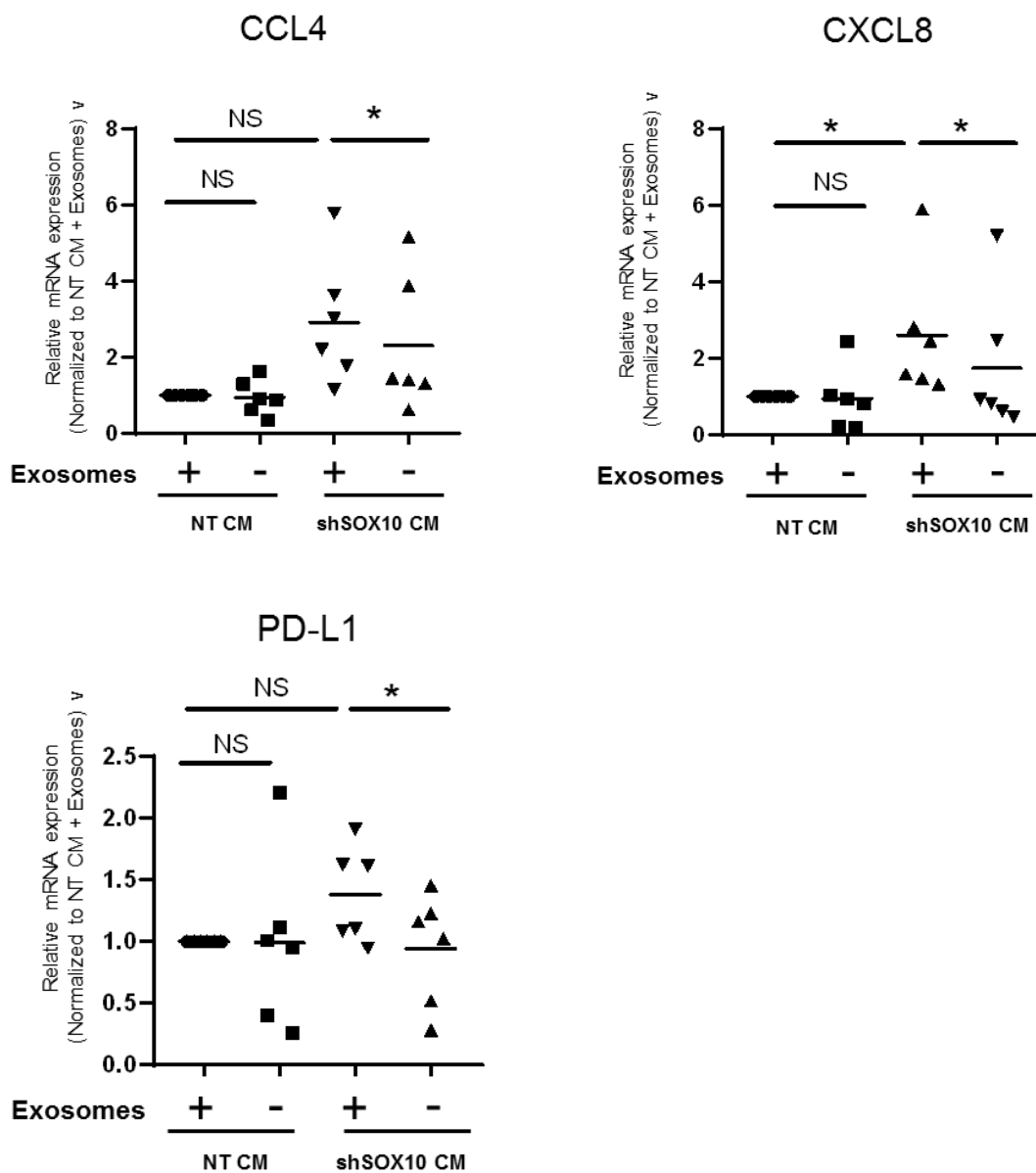


Fig14. Relative RNA expression of the pro-inflammatory genes CXCL8, CCL4, and PD-L1 in macrophages treated with complete and exosome-free CM. RNA expression was analyzed by qRT-PCR and normalized to the β -actin housekeeper gene. +, complete CM; -, exosome-depleted CM. Mean values of N=6 donors are shown. P-values were calculated by paired Wilcoxon signed rank test. *, P value<0.05; ns, not significant.

HT144

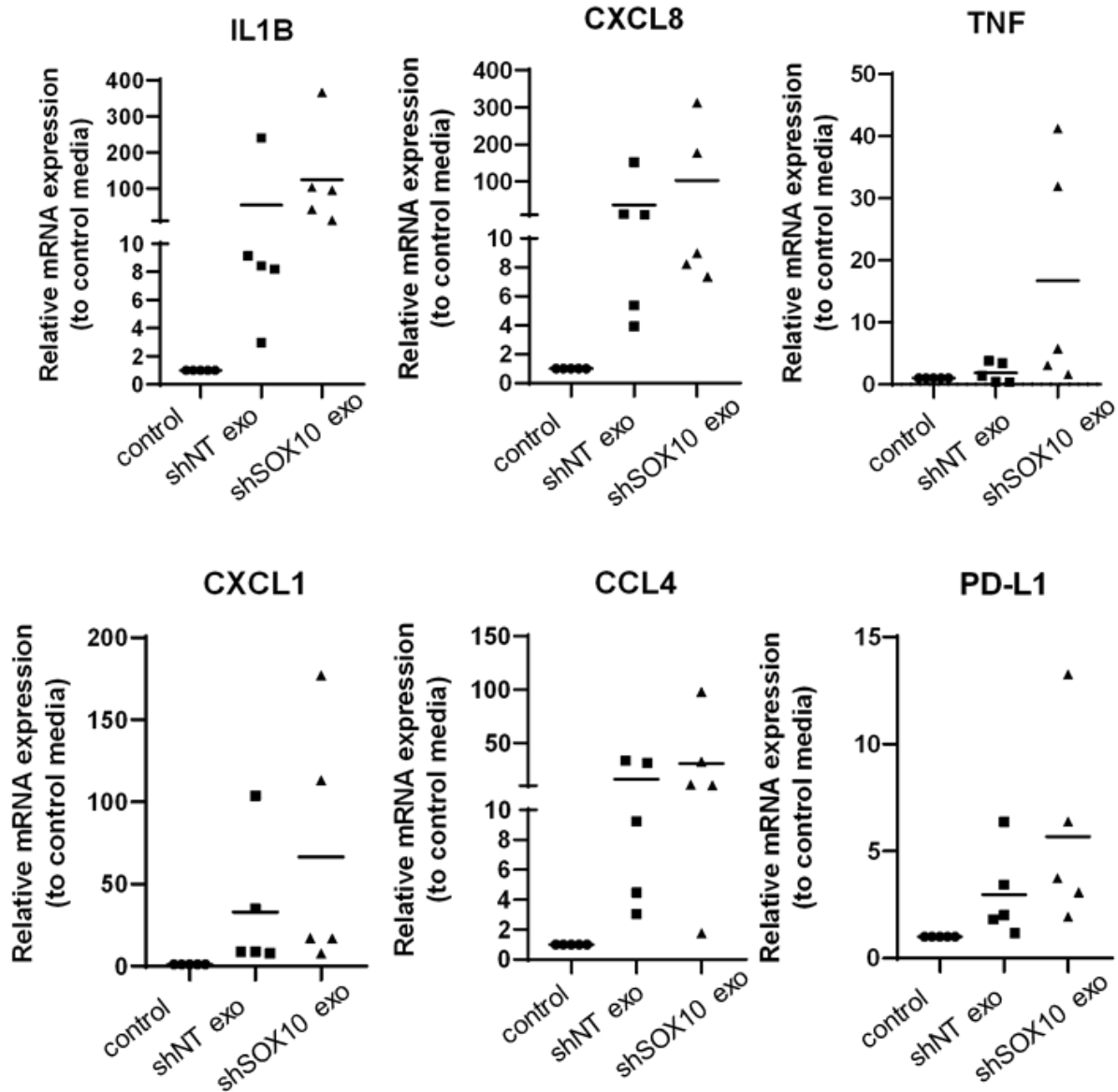


Fig 15. Relative expression of pro-inflammatory genes after exosome treatment. 2.5ug HT144 exosomes were applied to macrophages. Exosomes derived from empty-vector transduced cells were used as controls. RNA expression was analyzed by qRT-PCR and normalized to the β -actin housekeeper gene. Individual and mean values of N=5 biological replicates (PBMC donors) are shown.

A375

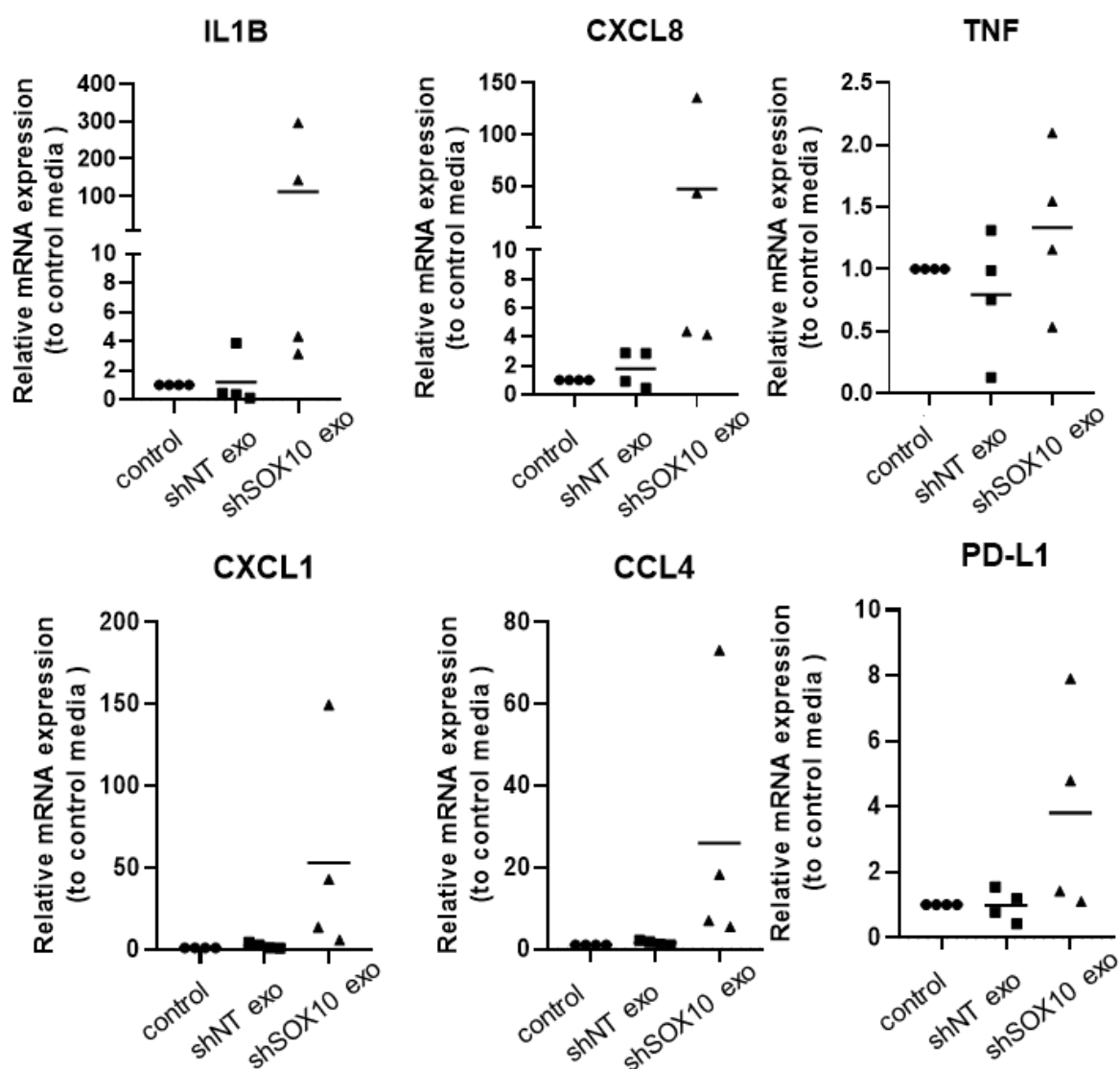


Fig 16. Relative expression of pro-inflammatory genes after exosome treatment. 2.5ug A375 exosomes were applied to macrophages. Exosomes derived from empty-vector transduced cells were used as controls. RNA expression was analyzed by qRT-PCR and normalized to the β -actin housekeeper gene. Individual and mean values of N=4 biological replicates (PBMC donors) are shown.

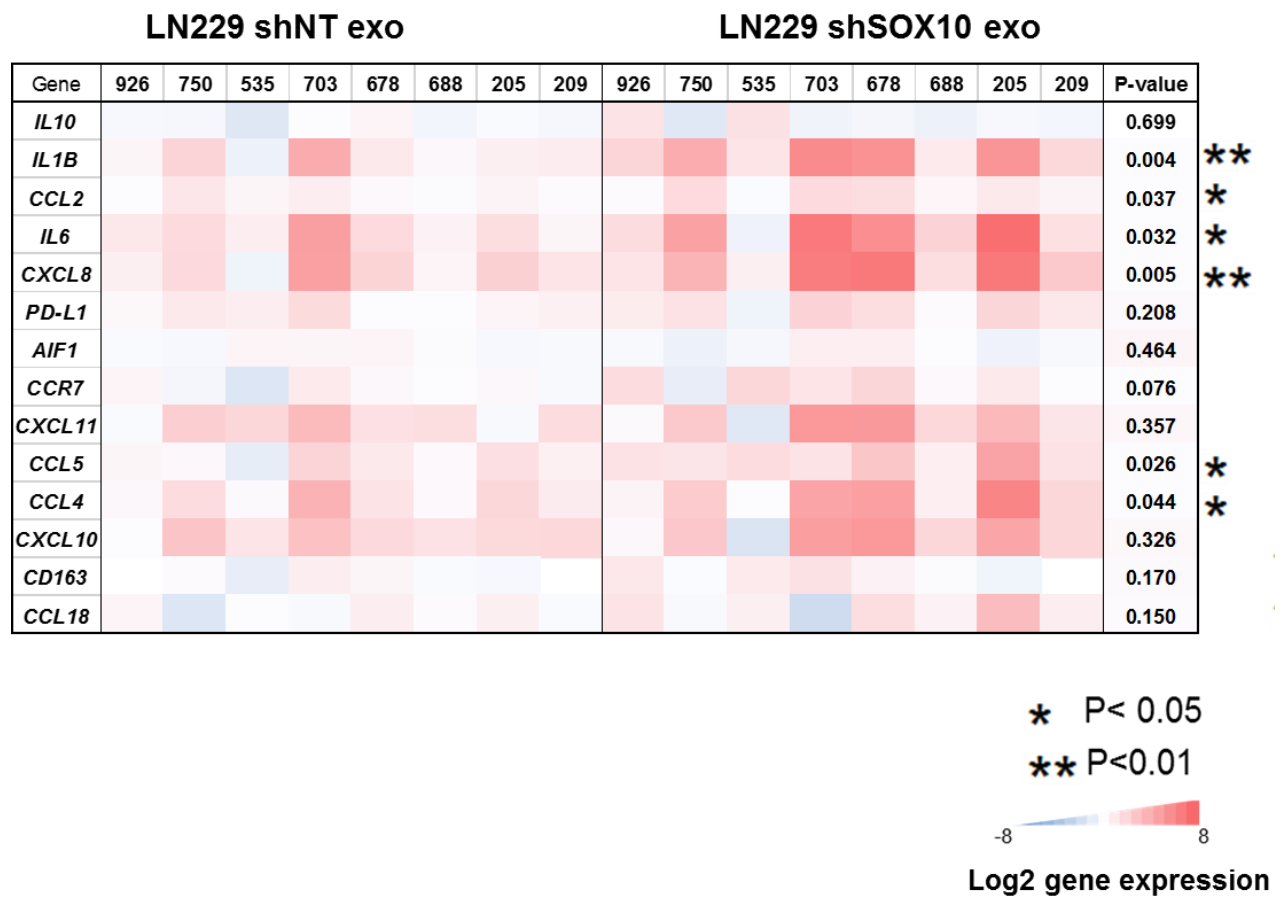


Fig 17. RNA expression of proinflammatory cytokine and receptor genes in LN229 NT and SOX10 KD exosome-treated macrophages. Expression data were determined by qRT-PCR, and normalized using the β -actin housekeeper gene. Log2 fold-ratios relative to controls are represented in the heat map. Each square of the heat map represent one biological sample. The numbers in the top row correspond to individual PBMC donors. The P-values listed to the right of the heat map were obtained by paired Wilcoxon signed rank test. *, P < 0.05; **, P < 0.01.

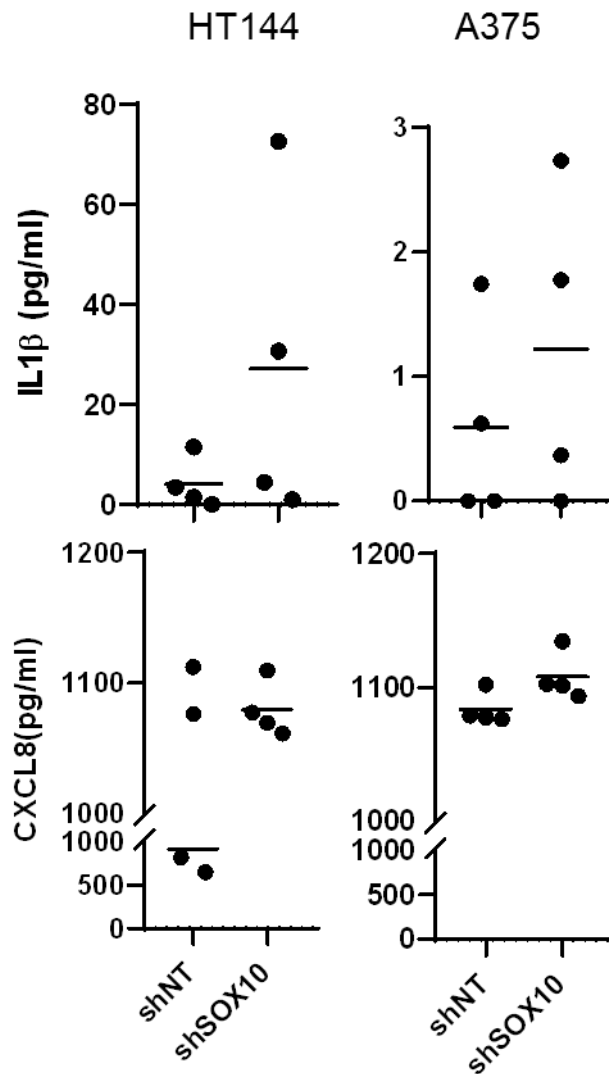
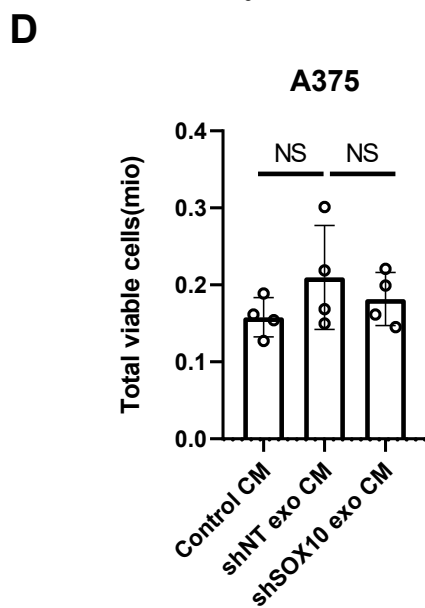
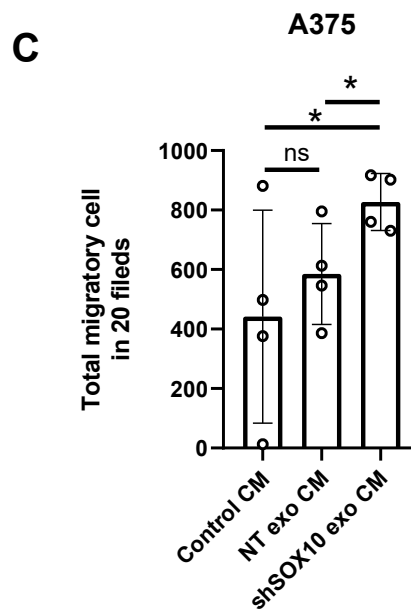
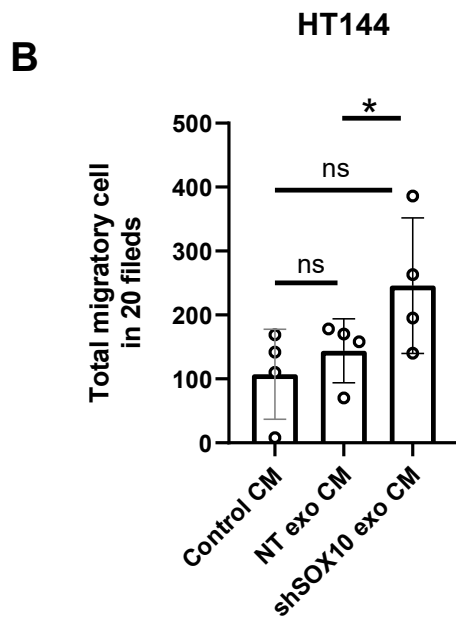
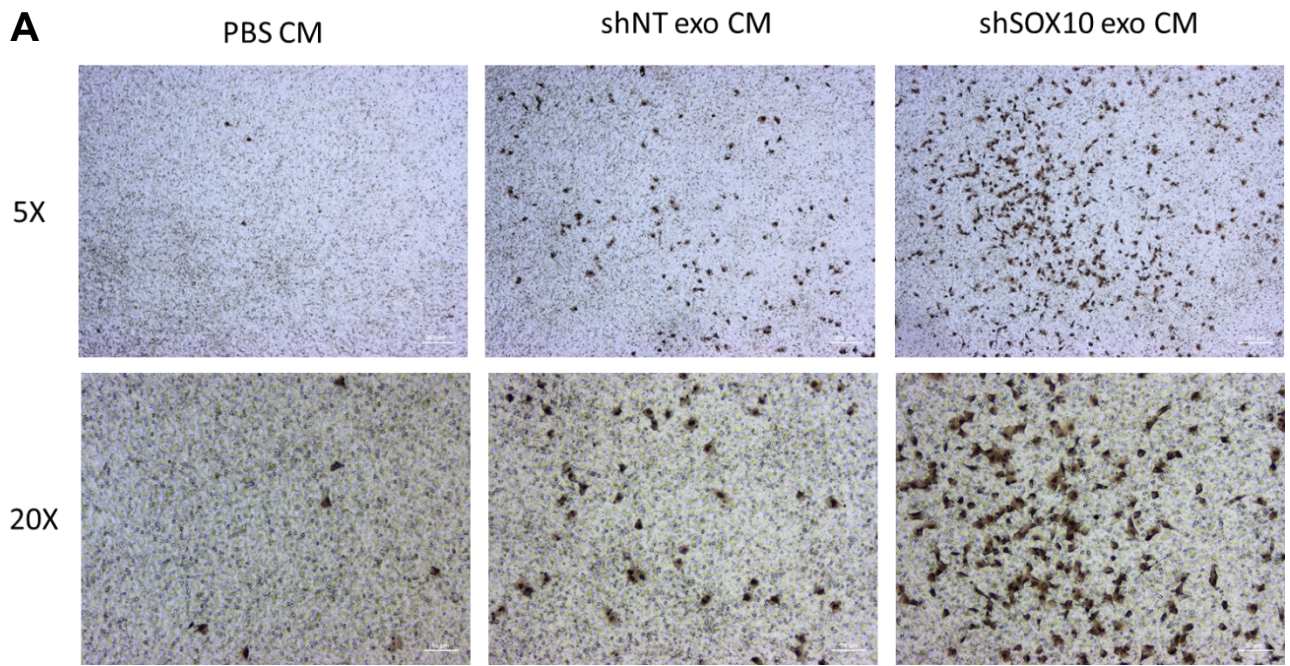


Fig 18. SOX10 KD exosomes induce increased IL-1 β and CXCL8 secretion by macrophages. Quantification of cytokine levels of IL-1 β and CXCL8 from the supernatant of exosome-treated macrophages, shNT and shSOX10 represent the supernatant from corresponding exosome-treated macrophages. Left two plots represent HT144 exosome-treated supernatant, and the right plots represent A375 exosome treated supernatant. Horizontal line in each plot represents the mean value of cytokine concentration and each dot represent macrophages from one biological replicate (PBMC donor), and total replicates n=4. To note, some optical density (OD) values of IL-1 β are lower than the detection limit of the ELISA kit, these values were regarded as 0 pg/ml.

Furthermore, I wanted to investigate the impact of the pro-inflammatory cytokines secreted by the macrophages on tumor cells. I thus collected CM from HT144 and A375 SOX10 KD exosome-treated macrophages, and applied it to wildtype HT144 and A375 for 24 hours and subsequently analyzed tumor cell migration and proliferation. By transwell migration assay, I found that the CM derived from SOX10 KD exosome pre-treated macrophages more effectively induced the migration of tumor cells than the NT exosome pre-treated CM (Fig. 19A-C). However, CM from SOX10 KD exosome treated macrophages exerted no significant impact on tumor cell proliferation (Fig. 19D). These results indicate that exosomes from SOX10-suppressed tumor cells can induce an exosome-mediated pro-inflammatory phenotype-transition in macrophages, which in turn can stimulate the invasiveness of the tumor cells.

Fig 19. (next page). Transwell migration assay with A375 and HT144 WT cells after treatment with CM that was derived from exosome-treated macrophages. A) Representative images of migrated HT144 cells (brown staining) treated with PBS, CM from macrophages treated with HT144 exosomes, and CM from macrophages treated with HT144 SOX10 KD exosomes. HT144 and A375 cells were incubated with macrophage CM for 24h and starved in serum-free medium for another 24h to avoid confounding effects from cell proliferation. Top row: 5x magnification; scale bar 200 μ M; Bottom row: 20x magnification, scale bar 50 μ M. B,C) Quantification of transwell migration assay data. Total number of cells collected from 20 overlapped images are plotted. The height of each column is the mean value and the error bars represent the standard deviation. N = 4 biological replicates. Each biological replicate used CM derived from different PBMC donor. The one-tailed paired Student's t-test was used to compute statistical significance. *, $P < 0.05$; D) Cell viability in dependence on CM treatment. 10.000 A375 cells were seeded and cultured under CM for 5 days then cells are harvested for cell count. Each dot represent a biological replicate. The Y-axis indicates the total number of cells harvested, and the X-axis indicates the types of CM.



3.4 SOX10 KD exosomes induce pro-inflammatory phenotype of macrophages via the TLR8-NF- κ B pathway

To study how SOX10 KD exosomes induce the pro-inflammatory phenotype of macrophages, I first investigated whether the exosomes were internalized by the macrophages. I labelled the exosomes with a general lipophilic dye PHK26 during exosome isolation, and applied 10^9 stained vesicles to macrophages for 2 to 24 hours. Under the confocal microscope, PHK26 positive signals were found localized in the cytoplasm and clustered in structures larger than 800 nm (Fig. 20); however, no accumulation of PHK26 signals was found at the cellular surface of macrophages, which indicates that the internalized exosomes may rely on intracellular organelles to exert the function on macrophages.

Previous reports demonstrated that tumor-derived exosomes contain abundant single strand RNAs (ssRNAs) (Haderk et al., 2017). Small RNAs that contain particular RNA motifs have been shown to activate endosome receptors such as TLR7 and TLR8 (Haderk et al., 2017; Pluta et al., 2019; Zhang et al., 2018b). The activated TLRs subsequently induce downstream signaling including the IRF and NF- κ B signaling pathways (Bender et al., 2020). To validate whether the here observed SOX10-related phenotypic transition of macrophages is triggered by exosomal RNAs, I blocked ssRNA-specific effects of LN229 SOX10 KD exosomes with Chloroquin. The anti-malaria drug Chloroquine has been reported to block the effective epitopes on RNAs and prevent the direct contact of RNAs with the TLRs (Kuznik et al., 2011). After the treatment with Chloroquine, the pro-inflammatory genes of macrophages, such as IL-1 β and CCL5, were less upregulated under LN229 SOX10 KD exosomes treatment (Fig. 21). These results support the hypothesis that exosomal RNA-endosomal TLR signaling contributes to the phenotypic transition of macrophages.

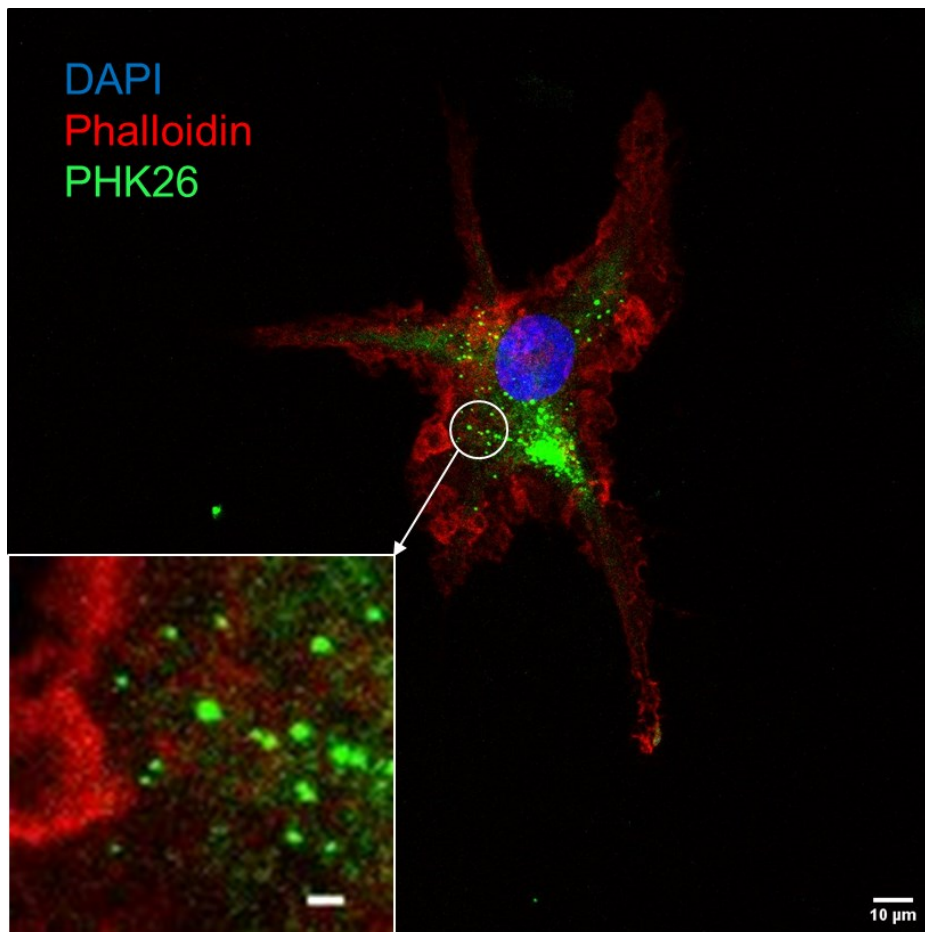


Fig 20. Visualization of exosomes in recipient macrophages. Green: tumor exosomes that were stained with the lipophilic dye PHK26 during isolation; red: Phalloidin staining F-actin; blue, DAPI stain of chromosome DNA. The large picture presents the whole macrophage with the scale bar 10 μm and the inset at the bottom left is a zoom-in image of the encircled macrophage region. The inset scale bar corresponds to a distance of 2 μm .

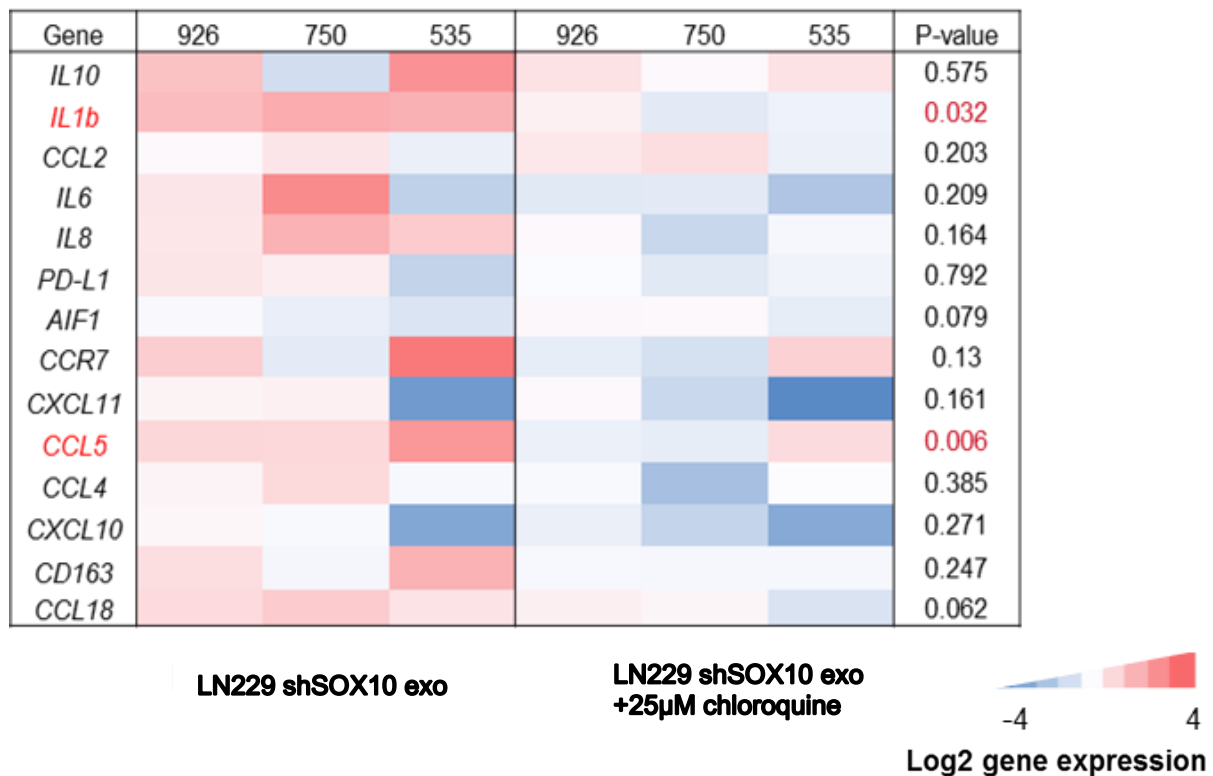


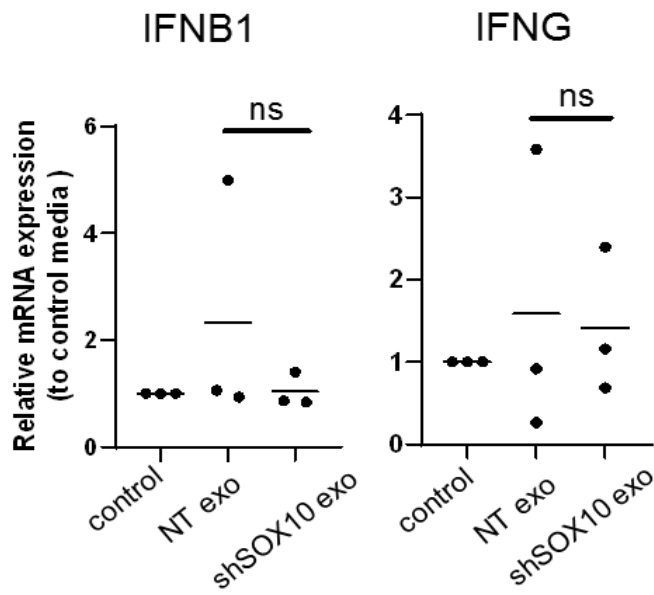
Fig 21. Chloroquine inhibits SOX10 KD exosome-mediated upregulation of pro-inflammatory genes in macrophages. Macrophages were treated with 5ug SOX10 KD exosomes with or without 25 µM chloroquine for 8 hours. Relative gene expression values in treated vs untreated macrophages, normalized to the β -actin housekeeper gene, are represented as a heat map. Each field represents one biological replicate. The numbers on top of the heat map identify individual PBMC donors. Statistical significance was computed by paired Wilcoxon signed rank test. P-values are listed to the right of the heat map. P-values smaller than 0.05 are indicated in red font.

To estimate the relevance of TLR7 and TLR8 for the observed phenotypic transition of macrophages, I tested the gene expression of type I and II interferons such as IFN- β and IFN- γ by qRT-PCR. Recent studies showed that TLR7 activation drives both IRF and NF- κ B signaling while TLR8 preferentially activates NF- κ B and much less affects the production of interferons (Bender et al., 2020). By qRT-PCR analysis I found that SOX10 KD exosomes failed to induce higher IFN- β and IFN- γ expression in macrophages while they significantly upregulated the NF- κ B pathway (Fig 22A-C), consistent with TLR8 activation. To validate this finding, I applied the novel TLR8-specific inhibitor CU-CPT8M to macrophages when treated with SOX10 KD exosomes. As expected, CU-CPT8M significantly inhibited IL1B and CXCL8 upregulation in macrophages under the stimulation of exosomes (Fig 21D). Interestingly, CU-CPT8M did not induce significant downregulation of the TLR8 gene in the absence of exosomes,

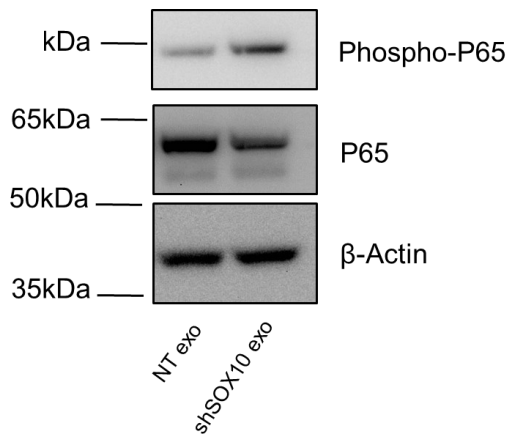
suggesting that stimulation by exosomal single strand RNAs is required to induce the activation of TLR8. Thus, the pro-inflammatory phenotype induced by SOX10 KD exosomes may largely depend on the stimulation of the exosomal ssRNAs – TLR8 pathway.

Fig.22 (next page). SOX10 KD exosomes induce the pro-inflammatory phenotype of macrophages via the TLR8-NF- κ B pathway. A) The relative expressions of type I interferon IFN β and type II interferon IFN γ were identified by qRT-PCR. 2.5 ug HT144 exosomes were administrated to macrophages. The control is exosome vector PBS. qRT-PCR was performed to get Ct value. The value of each gene was first normalized to Ct-value of β -Actin to acquire Δ Ct, then Δ Ct of genes of control macrophages was used to normalize Δ Ct of macrophages, which were treated by NT and SOX10 KD exosomes. Horizontal line in the dots represent the mean value and each dot represent macrophages from one biological replicate (N=3). B) Representative Western blot of NF- κ B expression after A375 exosome treatment. Phosphorylated P65 (Phospho-P65) represents the activation of NF- κ B, β -Actin was used as loading control. C) The quantification of Phospho-P65 was performed by Image J. The intensity of Phospho-P65 was normalized to β -Actin, and afterwards the SOX10 KD group was normalized to the NT group. Each dot represent one biological replicate. D and E) qRT-PCR of typical pro-inflammatory cytokines IL-1 β and CXCL8 from SOX10 KD exosome and TLR8 inhibitor CU-CPT8M- treated macrophages. 2.5ug SOX10 KD exosomes were treated to macrophages for 8 hour with or without 1 μ M CU-CPT8M, +/- represents the existence of treatment. Relative expression of each treatment were normalized to the double negative control. N=6 biological replicates were shown, P-values were acquired by paired Wilcoxon signed rank test. . * represent P<0.05.

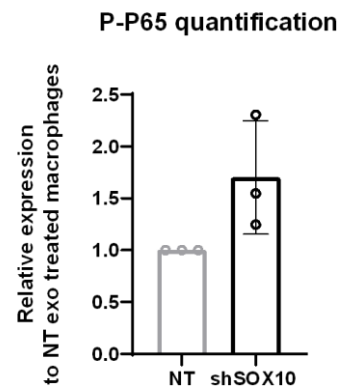
A



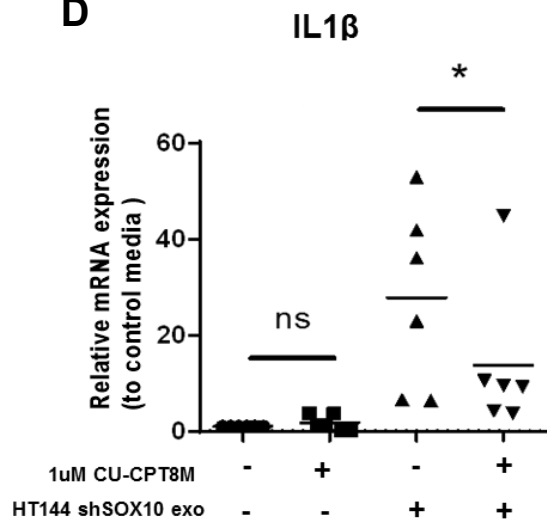
B



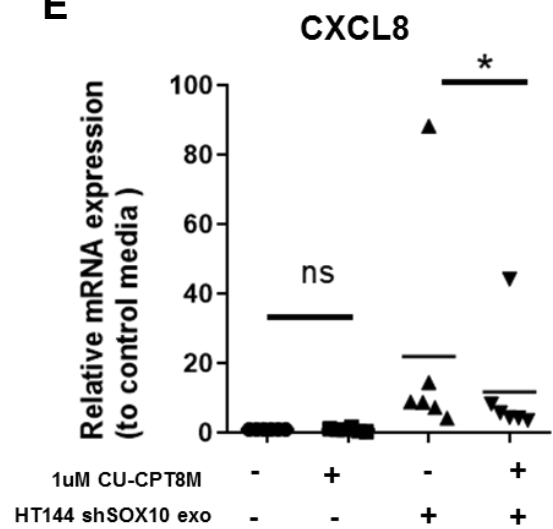
C



D



E



4 DISCUSSION AND OUTLOOK

4.1 Discussion

SOX10 downregulation has been shown to be associated with the development of drug-resistance mechanisms in melanoma and glioblastoma (Lau et al., 2015; Sun et al., 2014). To assess the potential clinical relevance of SOX10 downregulation and its association with standard therapies, I showed that Vemurafenib and TMZ treatment results in the downregulation of SOX10 RNA and protein expression in melanoma and glioblastoma cell lines, respectively. Additional analysis of published patient data revealed that *SOX10* expression is downregulated in biopsies of BRAFi and MEKi-resistant human melanoma, lending further support to the hypothesis that treatment-associated suppression of SOX10 might lead to therapy resistance in a considerable proportion of melanoma and glioblastoma patients. My analyses showed that the SOX10 downregulation was not an instant reaction to drug treatment but established itself after about six days of incubation with the drugs *in vitro*. These results are consistent with the study of Uka *et al.*, who treated melanoma cell lines with Vemurafenib for 24 hours but did not observe SOX10 downregulation (Uka et al., 2020). To further investigate the underlying mechanism of SOX10 inhibition after treatment, I hypothesized that SOX10 downregulation could be a secondary effect of treatment-induced activation of TGF β signaling (Cui et al., 2019; John et al., 2011). The activation of TGF β signaling requires increased secretion of ligands such as TGF β 1, TGF β 2 to bind TGF β RII dimers, which will subsequently phosphorylate the TGF β RI followed by the activation of downstream canonical and non-canonical TGF β signaling (Weiss and Attisano, 2013). In my study, I used the TGF β RI inhibitor Galunisertib to block TGF β signaling and successfully rescued SOX10 downregulation in two melanoma cell lines. I also observed the significant upregulation of TGF β 2 after Vemurafenib treatment in two cell lines, consistent with effects observed in published RNA-seq data of BRAFi-treated melanoma cell line Colo858 (Fallahi-Sichani et al., 2017). In addition to Vemurafenib treatment of melanoma, I also found that TMZ, the first-line chemotherapy agent for glioblastoma treatment, can induce SOX10 downregulation in LN229, a glioblastoma cell line of the RTK I glioblastoma subtype, at the mRNA and protein levels. Together, these data suggest that SOX10 downregulation in response to standard therapy could be a common feature of SOX10^{high} melanoma and glioblastoma.

To study the phenotypic effects of SOX10 suppression, I utilized shRNA and CRISPRi system to efficiently downregulate SOX10 expression. SOX10 KD in the HT144, A375 melanoma, and LN229 glioblastoma cell lines consistently decreased cell proliferation, and increased expression of the senescence marker β -gal, in line with previous studies in human melanoma and murine embryonic development models (Cronin et al., 2013; Mertelmeyer et al., 2020). Typically, β -gal positive cells secrete large quantities of cytokines and EVs, including exosomes (Misawa et al., 2020), suggesting that β -gal positive tumor cells can affect the phenotype of nearby tumor and stroma cells through intercellular signaling; however, the underlying molecular mechanisms and the role of exosomes remain poorly understood. Therefore, I harvested, characterized, and quantified exosomes from SOX10 KD and control cells. Since there is no gold standard to compare the exosome-producing capacities of cells *in vitro*, I used microBCA, EM, and Nanosight analysis (Nanosight data not shown in the thesis) to validate the results and avoid detection method-specific bias. These analyses consistently showed increased exosome production in SOX10 KD compared to control cells. I validated this finding using a Sox10 KD glioblastoma syngeneic graft model, demonstrating that the interstitial fluid of Sox10 KD tumors contained more Cd63-positive EVs than that of control tumors. Notably, the isolated exosome preparations did not contain the cytoplasmic proteins Gapdh and β -Actin, indicating that they were not contaminated by Cd63-positive intracellular vesicles that could have leaked from damaged cells during tissue dissociation.

Previously, our group found that SOX KD induced a glioblastoma subtype transition from the RTK I to the mesenchymal (MES) subtype that was accompanied by the upregulation of the cytokines CCL2, CXCL1, IL-6, and others. Using the same Sox10 KD glioblastoma syngeneic graft model as I used for exosome isolation, Wu et al, found that Sox10 KD tumors are more invasive than control tumors, were extensively infiltrated by Iba1-positive cells, presumably macrophages or microglia. These data suggested that suppression of Sox10 remodels the tumor microenvironment and modulates myeloid-cell phenotypes (Wu et al., 2020). To investigate how SOX10 KD tumor cells affect myeloid cells, I used human PBMCs induced with a low concentration of M-CSF to mimic naïve, non-polarized (M0) tumor-associated macrophages. RNA expression analysis by qRT-PCR validated that the M-CSF induced macrophages harbor the plasticity of transition toward M1 and M2 and thus can be used as a model to study the reprogramming of macrophages in the tumor microenvironment (Tarique et al., 2015). Treatment with CM derived from control and SOX10 KD demonstrated

that SOX10 KD CM induced a pro-inflammatory phenotype of the macrophages. By depletion of exosomes from CM and by treatment of macrophages with purified exosome fractions, I was able to show that exosomes mediated the induction of pro-inflammatory gene expression in macrophages by SOX10 KD CM. To avoid the overdosing of exosomes in the functional assay, I applied only 2.5-5 μg exosomes, approximately corresponding to the concentration of 5 $\mu\text{g}/\text{ml}$ that I observed in CM. The resulting induction of pro-inflammatory gene expression was less pronounced than in IFN- γ and LPS induced anti-tumor M1 macrophages and LN229 SOX10 KD exosomes frequently induced upregulation of the M2 marker CD163. It remains unclear whether the SOX10 KD exosome-dependent pro-inflammatory phenotype has pro-tumoral or anti-tumoral effects in the tumor microenvironment; however, as it is well accepted that chronic inflammation is a hallmark of cancer, such a moderately pro-inflammatory phenotype could also be tumor-supportive (Maru et al., 2014). This has been validated by Fleming *et al.*, who found that melanoma cell line-derived exosomes induce a pro-inflammatory phenotype in monocytes, which in turn inhibit the proliferation of CD8⁺ T cells *in vitro* (Fleming et al., 2019). These data indicate that exosomes-educated myeloid cells may suppress immune surveillance. In addition, my study showed that the CM derived from the exosome-treated macrophages promoted the migration of tumor cells, suggesting they could promote invasive tumor growth and metastasis (Fu et al., 2015; Kawata et al., 2012; Wu et al., 2009).

Exosomal proteins and RNAs have been reported to elicit pro-inflammatory phenotypes of myeloid cells via toll-like receptors and activation of downstream NF- κB signaling (Fabbri et al., 2012; Fleming et al., 2019; Haderk et al., 2017; Madhyastha et al., 2021). Consistent with these findings, my analyses indicated that SOX10 KD more strongly than control exosomes activate NF- κB . Visualization of exosome uptake and localization in macrophages indicated that endosome TLRs may be responsible for NF- κB activation. The human endosome TLRs include TLR3, TLR7/8, TLR9, and TLR13 which sense the double-strand RNA (dsRNA), ssRNA, CpG DNA, and rRNA respectively (Leifer and Medvedev, 2016), the latter three types of nucleic acids likely are present in SOX10 KD exosomes. Using chloroquine, which was reported to mask the epitope of ssRNA and block the contact with TLR7/8, I successfully abolished pro-inflammatory gene expression in macrophages after co-culture with SOX10 KD exosomes. Activation of downstream NF- κB signaling together with the lack of IRF-pathway activation suggests the involvement of the TLR8 receptor signaling, which was further supported by the fact that pharmacologic inhibition of TLR8 attenuated

SOX10 suppression-dependent macrophage inflammatory response. These results suggest that SOX10 KD exosomes induce the macrophage inflammatory response through ssRNAs enriched in adenine and uracil (AU)-enriched motifs (Forsbach et al., 2008) that activate TLR8 and NF- κ B signaling.

4.2 Outlook

The work presented here provides experimental evidence outlining a mechanism for therapy-associated exosome-dependent tumor-microenvironment interactions in SOX10^{high} melanoma and glioblastoma. It provides a basis to address additional aspects of melanoma and glioblastoma biology and therapy in future studies. First, the causative role of exosomes in therapy-induced melanoma and glioblastoma progression should be validated by interfering with exosome production or delivery in animal models. This could involve the knockout of CAV1 and RAB27-family proteins involved in exosome processing in the host cells or the transplantation of Sox10 KD tumors into Tlr7/8 KO mice. Second, the characterization of SOX10 KD exosome cargo by small-RNA sequencing and proteomic analysis can identify the molecular signals driving the phenotypic modulation of the tumor-associated macrophages. Third, based on the integrated analysis of tumor, exosome, and macrophage data, possible points for therapeutic interference can be identified and corresponding targeted therapies developed and tested in pre-clinical animal models.

5 SUMMARY

The transcription factor SRY-Box Transcription Factor 10 (SOX10) is highly expressed in the majority of melanoma and a subtype of glioblastoma. During first-line therapy, SOX10 expression is reduced in many patients. This loss of SOX10 commonly appears to be associated with increased therapy resistance. In my thesis work, I modeled therapy-dependent SOX10 suppression *in vitro* by treating melanoma and glioblastoma cell lines with the BRAF inhibitor Vemurafenib and Temozolomide, respectively. The downregulation of SOX10 expression was rescued by the inhibition of transforming growth factor-beta signaling. Genetic knockdown of SOX10 in the HT144 and A375 melanoma, and LN229 glioblastoma cell lines resulted in reduced cell proliferation, expression of β -galactosidase by a fraction of the cells, and the upregulation of cytokine expression. Furthermore, SOX10 suppression increased exosome production by melanoma and glioblastoma cell lines and in a syngeneic glioblastoma mouse model. Cell culture media conditioned by melanoma HT144-SOX10-knockdown cells were applied to PBMC-derived macrophages to explore the function of SOX10-knockdown exosomes on myeloid cells. Conditioned media and isolated exosome fractions from SOX10-knockdown cells induced the increased secretion of cytokines and upregulated expression of pro-inflammatory and immunosuppressive genes by the macrophages. In contrast, depletion of extracellular vesicles from the conditioned media reduced the expression of pro-inflammatory genes in comparison to conditioned media of control cells. Furthermore, conditioned media of macrophages treated with SOX10-knockdown exosomes promoted cell migration of melanoma cells. Pharmacologic inhibition of Toll-like receptor 8 with the inhibitor CU-CPT8M suppressed the induction of the pro-inflammatory phenotype of macrophages by SOX10 knockdown exosomes. In conclusion, the presented data support the hypothesis that standard melanoma and glioblastoma therapies lead to transforming growth factor-beta-dependent downregulation of SOX10 and the increased production of tumor-cell exosomes, which induce a pro-inflammatory phenotype in macrophages, mediated by Toll-like receptor 8. These data suggest that tumor-exosomes might be essential in therapy-induced progression of melanoma and glioblastoma and provide a basis for the exploration of the underlying mechanisms and the identification of interference points for targeted therapies.

6 REFERENCES

- Admyre, C., Grunewald, J., Thyberg, J., Gripenback, S., Tornling, G., Eklund, A., Scheynius, A., and Gabrielsson, S. (2003). Exosomes with major histocompatibility complex class II and co-stimulatory molecules are present in human BAL fluid. *Eur Respir J* 22, 578-583.
- Ahmed, S.M., Nishida-Fukuda, H., Li, Y., McDonald, W.H., Gradinaru, C.C., and Macara, I.G. (2018). Exocyst dynamics during vesicle tethering and fusion. *Nat Commun* 9, 5140.
- Baietti, M.F., Zhang, Z., Mortier, E., Melchior, A., Degeest, G., Geeraerts, A., Ivarsson, Y., Depoortere, F., Coomans, C., Vermeiren, E., *et al.* (2012). Syndecan-syntenin-ALIX regulates the biogenesis of exosomes. *Nat Cell Biol* 14, 677-685.
- Balaj, L., Lessard, R., Dai, L., Cho, Y.J., Pomeroy, S.L., Breakefield, X.O., and Skog, J. (2011). Tumour microvesicles contain retrotransposon elements and amplified oncogene sequences. *Nat Commun* 2, 180.
- Beach, A., Zhang, H.G., Ratajczak, M.Z., and Kakar, S.S. (2014). Exosomes: an overview of biogenesis, composition and role in ovarian cancer. *J Ovarian Res* 7, 14.
- Bender, A.T., Tzvetkov, E., Pereira, A., Wu, Y., Kasar, S., Przetak, M.M., Vlach, J., Niewold, T.B., Jensen, M.A., and Okitsu, S.L. (2020). TLR7 and TLR8 Differentially Activate the IRF and NF-kappaB Pathways in Specific Cell Types to Promote Inflammation. *Immunohorizons* 4, 93-107.
- Bertolotto, C., Busca, R., Abbe, P., Bille, K., Aberdam, E., Ortonne, J.P., and Ballotti, R. (1998). Different cis-acting elements are involved in the regulation of TRP1 and TRP2 promoter activities by cyclic AMP: pivotal role of M boxes (GTCATGTGCT) and of microphthalmia. *Mol Cell Biol* 18, 694-702.
- Bobrie, A., Krumeich, S., Reyat, F., Recchi, C., Moita, L.F., Seabra, M.C., Ostrowski, M., and Thery, C. (2012). Rab27a supports exosome-dependent and -independent mechanisms that modify the tumor microenvironment and can promote tumor progression. *Cancer Res* 72, 4920-4930.
- Bondurand, N., Dastot-Le Moal, F., Stanchina, L., Collot, N., Baral, V., Marlin, S., Attie-Bitach, T., Giurgea, I., Skopinski, L., Reardon, W., *et al.* (2007). Deletions at the SOX10 gene locus cause Waardenburg syndrome types 2 and 4. *Am J Hum Genet* 81, 1169-1185.
- Bowles, J., Schepers, G., and Koopman, P. (2000). Phylogeny of the SOX family of developmental transcription factors based on sequence and structural indicators. *Dev Biol* 227, 239-255.
- Britsch, S., Goerich, D.E., Riethmacher, D., Peirano, R.I., Rossner, M., Nave, K.A., Birchmeier, C., and Wegner, M. (2001). The transcription factor Sox10 is a key regulator of peripheral glial development. *Genes Dev* 15, 66-78.
- Buonfiglioli, A., Efe, I.E., Guneykaya, D., Ivanov, A., Huang, Y., Orlowski, E., Kruger, C., Deisz, R.A., Markovic, D., Fluh, C., *et al.* (2019). let-7 MicroRNAs Regulate Microglial Function and Suppress Glioma Growth through Toll-Like Receptor 7. *Cell Rep* 29, 3460-3471 e3467.

- Buzas, E.I., Toth, E.A., Sodar, B.W., and Szabo-Taylor, K.E. (2018). Molecular interactions at the surface of extracellular vesicles. *Semin Immunopathol* **40**, 453-464.
- Catalano, M., and O'Driscoll, L. (2020). Inhibiting extracellular vesicles formation and release: a review of EV inhibitors. *J Extracell Vesicles* **9**, 1703244.
- Chairoungdua, A., Smith, D.L., Pochard, P., Hull, M., and Caplan, M.J. (2010). Exosome release of beta-catenin: a novel mechanism that antagonizes Wnt signaling. *J Cell Biol* **190**, 1079-1091.
- Chen, G., Huang, A.C., Zhang, W., Zhang, G., Wu, M., Xu, W., Yu, Z., Yang, J., Wang, B., Sun, H., *et al.* (2018). Exosomal PD-L1 contributes to immunosuppression and is associated with anti-PD-1 response. *Nature* **560**, 382-386.
- Cohen, P.T. (2002). Protein phosphatase 1--targeted in many directions. *J Cell Sci* **115**, 241-256.
- Colombo, M., Moita, C., van Niel, G., Kowal, J., Vigneron, J., Benaroch, P., Manel, N., Moita, L.F., Thery, C., and Raposo, G. (2013). Analysis of ESCRT functions in exosome biogenesis, composition and secretion highlights the heterogeneity of extracellular vesicles. *J Cell Sci* **126**, 5553-5565.
- Colombo, M., Raposo, G., and Thery, C. (2014). Biogenesis, secretion, and intercellular interactions of exosomes and other extracellular vesicles. *Annu Rev Cell Dev Biol* **30**, 255-289.
- Costa, B., Fletcher, M.N.C., Boskovic, P., Ivanova, E.L., Eisemann, T., Lohr, S., Bunse, L., Lower, M., Burchard, S., Korshunov, A., *et al.* (2021). A Set of Cell Lines Derived from a Genetic Murine Glioblastoma Model Recapitulates Molecular and Morphological Characteristics of Human Tumors. *Cancers (Basel)* **13**.
- Cristofalo, V.J. (2005). SA beta Gal staining: biomarker or delusion. *Exp Gerontol* **40**, 836-838.
- Cronin, J.C., Watkins-Chow, D.E., Incao, A., Hasskamp, J.H., Schonewolf, N., Aoude, L.G., Hayward, N.K., Bastian, B.C., Dummer, R., Loftus, S.K., *et al.* (2013). SOX10 ablation arrests cell cycle, induces senescence, and suppresses melanomagenesis. *Cancer Res* **73**, 5709-5718.
- Cui, W., Meng, W., Zhao, L., Cao, H., Chi, W., and Wang, B. (2019). TGF-beta-induced long non-coding RNA MIR155HG promotes the progression and EMT of laryngeal squamous cell carcinoma by regulating the miR-155-5p/SOX10 axis. *Int J Oncol* **54**, 2005-2018.
- Dong, L., Lin, W., Qi, P., Xu, M.D., Wu, X., Ni, S., Huang, D., Weng, W.W., Tan, C., Sheng, W., *et al.* (2016). Circulating Long RNAs in Serum Extracellular Vesicles: Their Characterization and Potential Application as Biomarkers for Diagnosis of Colorectal Cancer. *Cancer Epidemiol Biomarkers Prev* **25**, 1158-1166.
- Du, J., Widlund, H.R., Horstmann, M.A., Ramaswamy, S., Ross, K., Huber, W.E., Nishimura, E.K., Golub, T.R., and Fisher, D.E. (2004). Critical role of CDK2 for melanoma growth linked to its melanocyte-specific transcriptional regulation by MITF. *Cancer Cell* **6**, 565-576.

- Duchler, M., Czernek, L., Peczek, L., Cypriak, W., Sztiller-Sikorska, M., and Czyz, M. (2019). Melanoma-Derived Extracellular Vesicles Bear the Potential for the Induction of Antigen-Specific Tolerance. *Cells* **8**.
- Egea-Jimenez, A.L., and Zimmermann, P. (2020). Lipids in Exosome Biology. *Handb Exp Pharmacol* **259**, 309-336.
- Fabbri, M., Paone, A., Calore, F., Galli, R., Gaudio, E., Santhanam, R., Lovat, F., Fadda, P., Mao, C., Nuovo, G.J., *et al.* (2012). MicroRNAs bind to Toll-like receptors to induce prometastatic inflammatory response. *Proc Natl Acad Sci U S A* **109**, E2110-2116.
- Fallahi-Sichani, M., Becker, V., Izar, B., Baker, G.J., Lin, J.R., Boswell, S.A., Shah, P., Rotem, A., Garraway, L.A., and Sorger, P.K. (2017). Adaptive resistance of melanoma cells to RAF inhibition via reversible induction of a slowly dividing de-differentiated state. *Mol Syst Biol* **13**, 905.
- Felicetti, F., De Feo, A., Coscia, C., Puglisi, R., Pedini, F., Pasquini, L., Bellenghi, M., Errico, M.C., Pagani, E., and Care, A. (2016). Exosome-mediated transfer of miR-222 is sufficient to increase tumor malignancy in melanoma. *J Transl Med* **14**, 56.
- Felicetti, F., Errico, M.C., Bottero, L., Segnalini, P., Stoppacciaro, A., Biffoni, M., Felli, N., Mattia, G., Petrini, M., Colombo, M.P., *et al.* (2008). The promyelocytic leukemia zinc finger-microRNA-221/-222 pathway controls melanoma progression through multiple oncogenic mechanisms. *Cancer Res* **68**, 2745-2754.
- Feng, W., Liu, S., Zhu, R., Li, B., Zhu, Z., Yang, J., and Song, C. (2017). SOX10 induced Nestin expression regulates cancer stem cell properties of TNBC cells. *Biochem Biophys Res Commun* **485**, 522-528.
- Ferletta, M., Uhrbom, L., Olofsson, T., Ponten, F., and Westermarck, B. (2007). Sox10 has a broad expression pattern in gliomas and enhances platelet-derived growth factor-B--induced gliomagenesis. *Mol Cancer Res* **5**, 891-897.
- Fitzner, D., Schnaars, M., van Rossum, D., Krishnamoorthy, G., Dibaj, P., Bakhti, M., Regen, T., Hanisch, U.K., and Simons, M. (2011). Selective transfer of exosomes from oligodendrocytes to microglia by macropinocytosis. *J Cell Sci* **124**, 447-458.
- Fleming, V., Hu, X., Weller, C., Weber, R., Groth, C., Riester, Z., Huser, L., Sun, Q., Nagibin, V., Kirschning, C., *et al.* (2019). Melanoma Extracellular Vesicles Generate Immunosuppressive Myeloid Cells by Upregulating PD-L1 via TLR4 Signaling. *Cancer Res* **79**, 4715-4728.
- Forsbach, A., Nemorin, J.G., Montino, C., Muller, C., Samulowitz, U., Vicari, A.P., Jurk, M., Mutwiri, G.K., Krieg, A.M., Lipford, G.B., *et al.* (2008). Identification of RNA sequence motifs stimulating sequence-specific TLR8-dependent immune responses. *J Immunol* **180**, 3729-3738.
- Fu, X.T., Dai, Z., Song, K., Zhang, Z.J., Zhou, Z.J., Zhou, S.L., Zhao, Y.M., Xiao, Y.S., Sun, Q.M., Ding, Z.B., *et al.* (2015). Macrophage-secreted IL-8 induces epithelial-mesenchymal transition in hepatocellular carcinoma cells by activating the JAK2/STAT3/Snail pathway. *Int J Oncol* **46**, 587-596.

- Geribaldi-Doldan, N., Fernandez-Ponce, C., Quiroz, R.N., Sanchez-Gomar, I., Escorcía, L.G., Velasquez, E.P., and Quiroz, E.N. (2020). The Role of Microglia in Glioblastoma. *Front Oncol* 10, 603495.
- Glebov, O.O., Bright, N.A., and Nichols, B.J. (2006). Flotillin-1 defines a clathrin-independent endocytic pathway in mammalian cells. *Nat Cell Biol* 8, 46-54.
- Glenney, J.R., Jr. (1989). Tyrosine phosphorylation of a 22-kDa protein is correlated with transformation by Rous sarcoma virus. *J Biol Chem* 264, 20163-20166.
- Graf, S.A., Busch, C., Bosserhoff, A.K., Besch, R., and Berking, C. (2014). SOX10 promotes melanoma cell invasion by regulating melanoma inhibitory activity. *J Invest Dermatol* 134, 2212-2220.
- Haderk, F., Schulz, R., Iskar, M., Cid, L.L., Worst, T., Willmund, K.V., Schulz, A., Warnken, U., Seiler, J., Benner, A., *et al.* (2017). Tumor-derived exosomes modulate PD-L1 expression in monocytes. *Sci Immunol* 2.
- Hamidzadeh, K., Belew, A.T., El-Sayed, N.M., and Mosser, D.M. (2020). The transition of M-CSF-derived human macrophages to a growth-promoting phenotype. *Blood Adv* 4, 5460-5472.
- Harjes, U. (2021). Educating macrophages in melanoma. *Nat Rev Cancer* 21, 4.
- Harris, M.L., Baxter, L.L., Loftus, S.K., and Pavan, W.J. (2010). Sox proteins in melanocyte development and melanoma. *Pigment Cell Melanoma Res* 23, 496-513.
- Haseeb, A., and Lefebvre, V. (2019). The SOXE transcription factors-SOX8, SOX9 and SOX10-share a bi-partite transactivation mechanism. *Nucleic Acids Res* 47, 6917-6931.
- Henne, W.M., Stenmark, H., and Emr, S.D. (2013). Molecular mechanisms of the membrane sculpting ESCRT pathway. *Cold Spring Harb Perspect Biol* 5.
- Herbarth, B., Pingault, V., Bondurand, N., Kuhlbrodt, K., Hermans-Borgmeyer, I., Puliti, A., Lemort, N., Goossens, M., and Wegner, M. (1998). Mutation of the Sry-related Sox10 gene in Dominant megacolon, a mouse model for human Hirschsprung disease. *Proc Natl Acad Sci U S A* 95, 5161-5165.
- Hessvik, N.P., and Llorente, A. (2018). Current knowledge on exosome biogenesis and release. *Cell Mol Life Sci* 75, 193-208.
- Hoshino, D., Kirkbride, K.C., Costello, K., Clark, E.S., Sinha, S., Grega-Larson, N., Tyska, M.J., and Weaver, A.M. (2013). Exosome secretion is enhanced by invadopodia and drives invasive behavior. *Cell Rep* 5, 1159-1168.
- Hsu, C., Morohashi, Y., Yoshimura, S., Manrique-Hoyos, N., Jung, S., Lauterbach, M.A., Bakhti, M., Gronborg, M., Mobius, W., Rhee, J., *et al.* (2010). Regulation of exosome secretion by Rab35 and its GTPase-activating proteins TBC1D10A-C. *J Cell Biol* 189, 223-232.
- Huang, X., Yuan, T., Tschannen, M., Sun, Z., Jacob, H., Du, M., Liang, M., Dittmar, R.L., Liu, Y., Liang, M., *et al.* (2013). Characterization of human plasma-derived exosomal RNAs by deep sequencing. *BMC Genomics* 14, 319.

- Hugo, W., Shi, H., Sun, L., Piva, M., Song, C., Kong, X., Moriceau, G., Hong, A., Dahlman, K.B., Johnson, D.B., *et al.* (2015). Non-genomic and Immune Evolution of Melanoma Acquiring MAPKi Resistance. *Cell* *162*, 1271-1285.
- Hurwitz, S.N., Cheerathodi, M.R., Nkosi, D., York, S.B., and Meckes, D.G., Jr. (2018). Tetraspanin CD63 Bridges Autophagic and Endosomal Processes To Regulate Exosomal Secretion and Intracellular Signaling of Epstein-Barr Virus LMP1. *J Virol* *92*.
- Jeppesen, D.K., Fenix, A.M., Franklin, J.L., Higginbotham, J.N., Zhang, Q., Zimmerman, L.J., Liebler, D.C., Ping, J., Liu, Q., Evans, R., *et al.* (2019). Reassessment of Exosome Composition. *Cell* *177*, 428-445 e418.
- Jiang, T., Hou, C.C., She, Z.Y., and Yang, W.X. (2013). The SOX gene family: function and regulation in testis determination and male fertility maintenance. *Mol Biol Rep* *40*, 2187-2194.
- John, N., Cinelli, P., Wegner, M., and Sommer, L. (2011). Transforming growth factor beta-mediated Sox10 suppression controls mesenchymal progenitor generation in neural crest stem cells. *Stem Cells* *29*, 689-699.
- Kahlert, C., Melo, S.A., Protopopov, A., Tang, J., Seth, S., Koch, M., Zhang, J., Weitz, J., Chin, L., Futreal, A., *et al.* (2014). Identification of double-stranded genomic DNA spanning all chromosomes with mutated KRAS and p53 DNA in the serum exosomes of patients with pancreatic cancer. *J Biol Chem* *289*, 3869-3875.
- Kalluri, R., and LeBleu, V.S. (2020). The biology, function, and biomedical applications of exosomes. *Science* *367*.
- Kawasaki, T., and Kawai, T. (2014). Toll-like receptor signaling pathways. *Front Immunol* *5*, 461.
- Kawata, M., Koinuma, D., Ogami, T., Umezawa, K., Iwata, C., Watabe, T., and Miyazono, K. (2012). TGF-beta-induced epithelial-mesenchymal transition of A549 lung adenocarcinoma cells is enhanced by pro-inflammatory cytokines derived from RAW 264.7 macrophage cells. *J Biochem* *151*, 205-216.
- Kiss, A.L., and Botos, E. (2009). Endocytosis via caveolae: alternative pathway with distinct cellular compartments to avoid lysosomal degradation? *J Cell Mol Med* *13*, 1228-1237.
- Koike, S., and Jahn, R. (2019). SNAREs define targeting specificity of trafficking vesicles by combinatorial interaction with tethering factors. *Nat Commun* *10*, 1608.
- Koles, K., Nunnari, J., Korkut, C., Barria, R., Brewer, C., Li, Y., Leszyk, J., Zhang, B., and Budnik, V. (2012). Mechanism of evenness interrupted (Evi)-exosome release at synaptic boutons. *J Biol Chem* *287*, 16820-16834.
- Koppers-Lalic, D., Hackenberg, M., Bijnsdorp, I.V., van Eijndhoven, M.A., Sadek, P., Sie, D., Zini, N., Middeldorp, J.M., Ylstra, B., de Menezes, R.X., *et al.* (2014). Nontemplated nucleotide additions distinguish the small RNA composition in cells from exosomes. *Cell Rep* *8*, 1649-1658.

- Kosgodage, U.S., Uysal-Onganer, P., MacLatchy, A., Mould, R., Nunn, A.V., Guy, G.W., Kraev, I., Chatterton, N.P., Thomas, E.L., Inal, J.M., *et al.* (2019). Cannabidiol Affects Extracellular Vesicle Release, miR21 and miR126, and Reduces Prohibitin Protein in Glioblastoma Multiforme Cells. *Transl Oncol* *12*, 513-522.
- Kurywchak, P., and Kalluri, R. (2017). An evolving function of DNA-containing exosomes in chemotherapy-induced immune response. *Cell Res* *27*, 722-723.
- Kuznik, A., Bencina, M., Svajger, U., Jeras, M., Rozman, B., and Jerala, R. (2011). Mechanism of endosomal TLR inhibition by antimalarial drugs and imidazoquinolines. *J Immunol* *186*, 4794-4804.
- Kwon, A.Y., Heo, I., Lee, H.J., Kim, G., Kang, H., Heo, J.H., Kim, T.H., and An, H.J. (2016). Sox10 expression in ovarian epithelial tumors is associated with poor overall survival. *Virchows Arch* *468*, 597-605.
- Lang, J.K., Young, R.F., Ashraf, H., and Canty, J.M., Jr. (2016). Inhibiting Extracellular Vesicle Release from Human Cardiosphere Derived Cells with Lentiviral Knockdown of nSMase2 Differentially Effects Proliferation and Apoptosis in Cardiomyocytes, Fibroblasts and Endothelial Cells In Vitro. *PLoS One* *11*, e0165926.
- Lau, J., Ilkhanizadeh, S., Wang, S., Miroshnikova, Y.A., Salvatierra, N.A., Wong, R.A., Schmidt, C., Weaver, V.M., Weiss, W.A., and Persson, A.I. (2015). STAT3 Blockade Inhibits Radiation-Induced Malignant Progression in Glioma. *Cancer Res* *75*, 4302-4311.
- Lee, H., Volonte, D., Galbiati, F., Iyengar, P., Lublin, D.M., Bregman, D.B., Wilson, M.T., Campos-Gonzalez, R., Bouzahzah, B., Pestell, R.G., *et al.* (2000). Constitutive and growth factor-regulated phosphorylation of caveolin-1 occurs at the same site (Tyr-14) in vivo: identification of a c-Src/Cav-1/Grb7 signaling cassette. *Mol Endocrinol* *14*, 1750-1775.
- Lefebvre, V., and Dvir-Ginzberg, M. (2017). SOX9 and the many facets of its regulation in the chondrocyte lineage. *Connect Tissue Res* *58*, 2-14.
- Lehmann, B.D., Paine, M.S., Brooks, A.M., McCubrey, J.A., Renegar, R.H., Wang, R., and Terrian, D.M. (2008). Senescence-associated exosome release from human prostate cancer cells. *Cancer Res* *68*, 7864-7871.
- Leifer, C.A., and Medvedev, A.E. (2016). Molecular mechanisms of regulation of Toll-like receptor signaling. *J Leukoc Biol* *100*, 927-941.
- Li, M., Zeringer, E., Barta, T., Schageman, J., Cheng, A., and Vlassov, A.V. (2014a). Analysis of the RNA content of the exosomes derived from blood serum and urine and its potential as biomarkers. *Philos Trans R Soc Lond B Biol Sci* *369*.
- Li, Q., Wang, H., Peng, H., Huyan, T., and Cacalano, N.A. (2019). Exosomes: Versatile Nano Mediators of Immune Regulation. *Cancers (Basel)* *11*.
- Li, Y., Zheng, M., and Lau, Y.F. (2014b). The sex-determining factors SRY and SOX9 regulate similar target genes and promote testis cord formation during testicular differentiation. *Cell Rep* *8*, 723-733.

- Lian, Q., Xu, J., Yan, S., Huang, M., Ding, H., Sun, X., Bi, A., Ding, J., Sun, B., and Geng, M. (2017). Chemotherapy-induced intestinal inflammatory responses are mediated by exosome secretion of double-strand DNA via AIM2 inflammasome activation. *Cell Res* 27, 784-800.
- Liu, R.Y., Zeng, Y., Lei, Z., Wang, L., Yang, H., Liu, Z., Zhao, J., and Zhang, H.T. (2014). JAK/STAT3 signaling is required for TGF-beta-induced epithelial-mesenchymal transition in lung cancer cells. *Int J Oncol* 44, 1643-1651.
- Luebker, S.A., and Koepsell, S.A. (2019). Diverse Mechanisms of BRAF Inhibitor Resistance in Melanoma Identified in Clinical and Preclinical Studies. *Front Oncol* 9, 268.
- Lunavat, T.R., Cheng, L., Kim, D.K., Bhadury, J., Jang, S.C., Lasser, C., Sharples, R.A., Lopez, M.D., Nilsson, J., Gho, Y.S., *et al.* (2015). Small RNA deep sequencing discriminates subsets of extracellular vesicles released by melanoma cells--Evidence of unique microRNA cargos. *RNA Biol* 12, 810-823.
- Madhyastha, R., Madhyastha, H., Nurrahmah, Q.I., Purbasari, B., Maruyama, M., and Nakajima, Y. (2021). MicroRNA 21 Elicits a Pro-inflammatory Response in Macrophages, with Exosomes Functioning as Delivery Vehicles. *Inflammation*.
- Malla, B., Zaugg, K., Vassella, E., Aebersold, D.M., and Dal Pra, A. (2017). Exosomes and Exosomal MicroRNAs in Prostate Cancer Radiation Therapy. *Int J Radiat Oncol Biol Phys* 98, 982-995.
- Maru, G.B., Gandhi, K., Ramchandani, A., and Kumar, G. (2014). The role of inflammation in skin cancer. *Adv Exp Med Biol* 816, 437-469.
- Mathivanan, S., Lim, J.W., Tauro, B.J., Ji, H., Moritz, R.L., and Simpson, R.J. (2010). Proteomics analysis of A33 immunoaffinity-purified exosomes released from the human colon tumor cell line LIM1215 reveals a tissue-specific protein signature. *Mol Cell Proteomics* 9, 197-208.
- Mayor, S., and Pagano, R.E. (2007). Pathways of clathrin-independent endocytosis. *Nat Rev Mol Cell Biol* 8, 603-612.
- Mayor, S., Parton, R.G., and Donaldson, J.G. (2014). Clathrin-independent pathways of endocytosis. *Cold Spring Harb Perspect Biol* 6.
- McGill, G.G., Horstmann, M., Widlund, H.R., Du, J., Motyckova, G., Nishimura, E.K., Lin, Y.L., Ramaswamy, S., Avery, W., Ding, H.F., *et al.* (2002). Bcl2 regulation by the melanocyte master regulator Mitf modulates lineage survival and melanoma cell viability. *Cell* 109, 707-718.
- McKelvey, K.J., Powell, K.L., Ashton, A.W., Morris, J.M., and McCracken, S.A. (2015). Exosomes: Mechanisms of Uptake.
- Mertelmeyer, S., Weider, M., Baroti, T., Reiprich, S., Frob, F., Stolt, C.C., Wagner, K.U., and Wegner, M. (2020). The transcription factor Sox10 is an essential determinant of branching morphogenesis and involution in the mouse mammary gland. *Sci Rep* 10, 17807.

- Misawa, T., Tanaka, Y., Okada, R., and Takahashi, A. (2020). Biology of extracellular vesicles secreted from senescent cells as senescence-associated secretory phenotype factors. *Geriatr Gerontol Int* 20, 539-546.
- Momen-Heravi, F., Balaj, L., Alian, S., Mantel, P.Y., Halleck, A.E., Trachtenberg, A.J., Soria, C.E., Oquin, S., Bonebreak, C.M., Saracoglu, E., *et al.* (2013). Current methods for the isolation of extracellular vesicles. *Biol Chem* 394, 1253-1262.
- Mu, W., Rana, S., and Zoller, M. (2013). Host matrix modulation by tumor exosomes promotes motility and invasiveness. *Neoplasia* 15, 875-887.
- Murisier, F., Guichard, S., and Beermann, F. (2006). A conserved transcriptional enhancer that specifies *Tyrp1* expression to melanocytes. *Dev Biol* 298, 644-655.
- Murisier, F., Guichard, S., and Beermann, F. (2007). The tyrosinase enhancer is activated by *Sox10* and *Mitf* in mouse melanocytes. *Pigment Cell Res* 20, 173-184.
- Nabi, I.R., and Le, P.U. (2003). Caveolae/raft-dependent endocytosis. *J Cell Biol* 161, 673-677.
- Nanbo, A., Kawanishi, E., Yoshida, R., and Yoshiyama, H. (2013). Exosomes derived from Epstein-Barr virus-infected cells are internalized via caveola-dependent endocytosis and promote phenotypic modulation in target cells. *J Virol* 87, 10334-10347.
- Nedaeinia, R., Manian, M., Jazayeri, M.H., Ranjbar, M., Salehi, R., Sharifi, M., Mohaghegh, F., Goli, M., Jahednia, S.H., Avan, A., *et al.* (2017). Circulating exosomes and exosomal microRNAs as biomarkers in gastrointestinal cancer. *Cancer Gene Ther* 24, 48-56.
- Ni, K., Wang, C., Carnino, J.M., and Jin, Y. (2020). The Evolving Role of Caveolin-1: A Critical Regulator of Extracellular Vesicles. *Med Sci (Basel)* 8.
- Nolte-'t Hoen, E.N., Buermans, H.P., Waasdorp, M., Stoorvogel, W., Wauben, M.H., and 't Hoen, P.A. (2012). Deep sequencing of RNA from immune cell-derived vesicles uncovers the selective incorporation of small non-coding RNA biotypes with potential regulatory functions. *Nucleic Acids Res* 40, 9272-9285.
- Olejarz, W., Kubiak-Tomaszewska, G., Chrzanowska, A., and Lorenc, T. (2020). Exosomes in Angiogenesis and Anti-angiogenic Therapy in Cancers. *Int J Mol Sci* 21.
- Orecchioni, M., Ghosheh, Y., Pramod, A.B., and Ley, K. (2019). Macrophage Polarization: Different Gene Signatures in M1(LPS+) vs. Classically and M2(LPS-) vs. Alternatively Activated Macrophages. *Front Immunol* 10, 1084.
- Ostrowski, M., Carmo, N.B., Krumeich, S., Fanget, I., Raposo, G., Savina, A., Moita, C.F., Schauer, K., Hume, A.N., Freitas, R.P., *et al.* (2010). *Rab27a* and *Rab27b* control different steps of the exosome secretion pathway. *Nat Cell Biol* 12, 19-30; sup pp 11-13.
- Paratore, C., Goerich, D.E., Suter, U., Wegner, M., and Sommer, L. (2001). Survival and glial fate acquisition of neural crest cells are regulated by an interplay between the transcription factor *Sox10* and extrinsic combinatorial signaling. *Development* 128, 3949-3961.

- Peinado, H., Aleckovic, M., Lavotshkin, S., Matei, I., Costa-Silva, B., Moreno-Bueno, G., Hergueta-Redondo, M., Williams, C., Garcia-Santos, G., Ghajar, C., *et al.* (2012). Melanoma exosomes educate bone marrow progenitor cells toward a pro-metastatic phenotype through MET. *Nat Med* *18*, 883-891.
- Peng, X., Yang, L., Ma, Y., Li, Y., and Li, H. (2020). Focus on the morphogenesis, fate and the role in tumor progression of multivesicular bodies. *Cell Commun Signal* *18*, 122.
- Pluta, L., Yousefi, B., Damania, B., and Khan, A.A. (2019). Endosomal TLR-8 Senses microRNA-1294 Resulting in the Production of NFkB Dependent Cytokines. *Front Immunol* *10*, 2860.
- Poggio, M., Hu, T., Pai, C.C., Chu, B., Belair, C.D., Chang, A., Montabana, E., Lang, U.E., Fu, Q., Fong, L., *et al.* (2019). Suppression of Exosomal PD-L1 Induces Systemic Anti-tumor Immunity and Memory. *Cell* *177*, 414-427 e413.
- Potterf, S.B., Furumura, M., Dunn, K.J., Arnheiter, H., and Pavan, W.J. (2000). Transcription factor hierarchy in Waardenburg syndrome: regulation of MITF expression by SOX10 and PAX3. *Hum Genet* *107*, 1-6.
- Reddy, V.S., Madala, S.K., Trinath, J., and Reddy, G.B. (2018). Extracellular small heat shock proteins: exosomal biogenesis and function. *Cell Stress Chaperones* *23*, 441-454.
- S, E.L.A., Mager, I., Breakefield, X.O., and Wood, M.J. (2013). Extracellular vesicles: biology and emerging therapeutic opportunities. *Nat Rev Drug Discov* *12*, 347-357.
- Sackmann, V., Sinha, M.S., Sackmann, C., Civitelli, L., Bergstrom, J., Ansell-Schultz, A., and Hallbeck, M. (2019). Inhibition of nSMase2 Reduces the Transfer of Oligomeric alpha-Synuclein Irrespective of Hypoxia. *Front Mol Neurosci* *12*, 200.
- Sahai, E., Astsaturov, I., Cukierman, E., DeNardo, D.G., Egeblad, M., Evans, R.M., Fearon, D., Greten, F.R., Hingorani, S.R., Hunter, T., *et al.* (2020). A framework for advancing our understanding of cancer-associated fibroblasts. *Nat Rev Cancer* *20*, 174-186.
- Sanderson, R.D., Bandari, S.K., and Vlodevsky, I. (2019). Proteases and glycosidases on the surface of exosomes: Newly discovered mechanisms for extracellular remodeling. *Matrix Biol* *75-76*, 160-169.
- Santangelo, L., Giurato, G., Cicchini, C., Montaldo, C., Mancone, C., Tarallo, R., Battistelli, C., Alonzi, T., Weisz, A., and Tripodi, M. (2016). The RNA-Binding Protein SYNCRIP Is a Component of the Hepatocyte Exosomal Machinery Controlling MicroRNA Sorting. *Cell Rep* *17*, 799-808.
- Sapmaz, A., Berlin, I., Bos, E., Wijdeven, R.H., Janssen, H., Konietzny, R., Akkermans, J.J., Erson-Bensan, A.E., Koning, R.I., Kessler, B.M., *et al.* (2019). USP32 regulates late endosomal transport and recycling through deubiquitylation of Rab7. *Nat Commun* *10*, 1454.
- Schneider, B., Schueller, C., Utermoehlen, O., and Haas, A. (2007). Lipid microdomain-dependent macropinocytosis determines compartmentation of Afipia felis. *Traffic* *8*, 226-240.

- Severino, J., Allen, R.G., Balin, S., Balin, A., and Cristofalo, V.J. (2000). Is beta-galactosidase staining a marker of senescence in vitro and in vivo? *Exp Cell Res* 257, 162-171.
- Shakhova, O., Zingg, D., Schaefer, S.M., Hari, L., Civenni, G., Blunschli, J., Claudinot, S., Okoniewski, M., Beermann, F., Mihic-Probst, D., *et al.* (2012). Sox10 promotes the formation and maintenance of giant congenital naevi and melanoma. *Nat Cell Biol* 14, 882-890.
- Shu, S., Yang, Y., Allen, C.L., Maguire, O., Minderman, H., Sen, A., Ciesielski, M.J., Collins, K.A., Bush, P.J., Singh, P., *et al.* (2018). Metabolic reprogramming of stromal fibroblasts by melanoma exosome microRNA favours a pre-metastatic microenvironment. *Sci Rep* 8, 12905.
- Sinha, S., Hoshino, D., Hong, N.H., Kirkbride, K.C., Grega-Larson, N.E., Seiki, M., Tyska, M.J., and Weaver, A.M. (2016). Cortactin promotes exosome secretion by controlling branched actin dynamics. *J Cell Biol* 214, 197-213.
- Skotland, T., Sandvig, K., and Llorente, A. (2017). Lipids in exosomes: Current knowledge and the way forward. *Prog Lipid Res* 66, 30-41.
- Sokolowska, E., and Blachnio-Zabielska, A. (2019). The Role of Ceramides in Insulin Resistance. *Front Endocrinol (Lausanne)* 10, 577.
- Song, L., Tang, S., Han, X., Jiang, Z., Dong, L., Liu, C., Liang, X., Dong, J., Qiu, C., Wang, Y., *et al.* (2019). KIBRA controls exosome secretion via inhibiting the proteasomal degradation of Rab27a. *Nat Commun* 10, 1639.
- Southard-Smith, E.M., Kos, L., and Pavan, W.J. (1998). Sox10 mutation disrupts neural crest development in Dom Hirschsprung mouse model. *Nat Genet* 18, 60-64.
- Stuffers, S., Sem Wegner, C., Stenmark, H., and Brech, A. (2009). Multivesicular endosome biogenesis in the absence of ESCRTs. *Traffic* 10, 925-937.
- Sun, C., Wang, L., Huang, S., Heynen, G.J., Prahallad, A., Robert, C., Haanen, J., Blank, C., Wesseling, J., Willems, S.M., *et al.* (2014). Reversible and adaptive resistance to BRAF(V600E) inhibition in melanoma. *Nature* 508, 118-122.
- Sun, Z., Shi, K., Yang, S., Liu, J., Zhou, Q., Wang, G., Song, J., Li, Z., Zhang, Z., and Yuan, W. (2018). Effect of exosomal miRNA on cancer biology and clinical applications. *Mol Cancer* 17, 147.
- Svensson, K.J., Christianson, H.C., Wittrup, A., Bourseau-Guilmain, E., Lindqvist, E., Svensson, L.M., Morgelin, M., and Belting, M. (2013). Exosome uptake depends on ERK1/2-heat shock protein 27 signaling and lipid Raft-mediated endocytosis negatively regulated by caveolin-1. *J Biol Chem* 288, 17713-17724.
- Takahashi, A., Okada, R., Nagao, K., Kawamata, Y., Hanyu, A., Yoshimoto, S., Takasugi, M., Watanabe, S., Kanemaki, M.T., Obuse, C., *et al.* (2017). Exosomes maintain cellular homeostasis by excreting harmful DNA from cells. *Nat Commun* 8, 15287.

- Tarique, A.A., Logan, J., Thomas, E., Holt, P.G., Sly, P.D., and Fantino, E. (2015). Phenotypic, functional, and plasticity features of classical and alternatively activated human macrophages. *Am J Respir Cell Mol Biol* 53, 676-688.
- Thakur, B.K., Zhang, H., Becker, A., Matei, I., Huang, Y., Costa-Silva, B., Zheng, Y., Hoshino, A., Brazier, H., Xiang, J., *et al.* (2014). Double-stranded DNA in exosomes: a novel biomarker in cancer detection. *Cell Res* 24, 766-769.
- Thery, C., Zitvogel, L., and Amigorena, S. (2002). Exosomes: composition, biogenesis and function. *Nat Rev Immunol* 2, 569-579.
- Tian, T., Zhu, Y.L., Zhou, Y.Y., Liang, G.F., Wang, Y.Y., Hu, F.H., and Xiao, Z.D. (2014). Exosome uptake through clathrin-mediated endocytosis and macropinocytosis and mediating miR-21 delivery. *J Biol Chem* 289, 22258-22267.
- Tosar, J.P., Gambaro, F., Sanguinetti, J., Bonilla, B., Witwer, K.W., and Cayota, A. (2015). Assessment of small RNA sorting into different extracellular fractions revealed by high-throughput sequencing of breast cell lines. *Nucleic Acids Res* 43, 5601-5616.
- Trajkovic, K., Hsu, C., Chiantia, S., Rajendran, L., Wenzel, D., Wieland, F., Schwille, P., Brugger, B., and Simons, M. (2008). Ceramide triggers budding of exosome vesicles into multivesicular endosomes. *Science* 319, 1244-1247.
- Tucci, M., Mannavola, F., Passarelli, A., Stucci, L.S., Cives, M., and Silvestris, F. (2018). Exosomes in melanoma: a role in tumor progression, metastasis and impaired immune system activity. *Oncotarget* 9, 20826-20837.
- Uka, R., Britschgi, C., Krattli, A., Matter, C., Mihic, D., Okoniewski, M.J., Gualandi, M., Stupp, R., Cinelli, P., Dummer, R., *et al.* (2020). Temporal activation of WNT/beta-catenin signaling is sufficient to inhibit SOX10 expression and block melanoma growth. *Oncogene* 39, 4132-4154.
- Uribe-Querol, E., and Rosales, C. (2020). Phagocytosis: Our Current Understanding of a Universal Biological Process. *Front Immunol* 11, 1066.
- Utsugi-Kobukai, S., Fujimaki, H., Hotta, C., Nakazawa, M., and Minami, M. (2003). MHC class I-mediated exogenous antigen presentation by exosomes secreted from immature and mature bone marrow derived dendritic cells. *Immunol Lett* 89, 125-131.
- Vader, P., Breakefield, X.O., and Wood, M.J. (2014). Extracellular vesicles: emerging targets for cancer therapy. *Trends Mol Med* 20, 385-393.
- Valadi, H., Ekstrom, K., Bossios, A., Sjostrand, M., Lee, J.J., and Lotvall, J.O. (2007). Exosome-mediated transfer of mRNAs and microRNAs is a novel mechanism of genetic exchange between cells. *Nat Cell Biol* 9, 654-659.
- Valentino, A., Reclusa, P., Sirera, R., Giallombardo, M., Camps, C., Pauwels, P., Crispi, S., and Rolfo, C. (2017). Exosomal microRNAs in liquid biopsies: future biomarkers for prostate cancer. *Clin Transl Oncol* 19, 651-657.
- van Meer, G., Voelker, D.R., and Feigenson, G.W. (2008). Membrane lipids: where they are and how they behave. *Nat Rev Mol Cell Biol* 9, 112-124.

- Vanni, I., Tanda, E.T., Spagnolo, F., Andreotti, V., Bruno, W., and Ghiorzo, P. (2020). The Current State of Molecular Testing in the BRAF-Mutated Melanoma Landscape. *Front Mol Biosci* 7, 113.
- Villarroya-Beltri, C., Baixauli, F., Mittelbrunn, M., Fernandez-Delgado, I., Torralba, D., Moreno-Gonzalo, O., Baldanta, S., Enrich, C., Guerra, S., and Sanchez-Madrid, F. (2016). ISGylation controls exosome secretion by promoting lysosomal degradation of MVB proteins. *Nat Commun* 7, 13588.
- Villarroya-Beltri, C., Gutierrez-Vazquez, C., Sanchez-Cabo, F., Perez-Hernandez, D., Vazquez, J., Martin-Cofreces, N., Martinez-Herrera, D.J., Pascual-Montano, A., Mittelbrunn, M., and Sanchez-Madrid, F. (2013). Sumoylated hnRNPA2B1 controls the sorting of miRNAs into exosomes through binding to specific motifs. *Nat Commun* 4, 2980.
- Wang, L., Leite de Oliveira, R., Wang, C., Fernandes Neto, J.M., Mainardi, S., Evers, B., Lieftink, C., Morris, B., Jochems, F., Willemsen, L., *et al.* (2017). High-Throughput Functional Genetic and Compound Screens Identify Targets for Senescence Induction in Cancer. *Cell Rep* 21, 773-783.
- Webber, J.P., Spary, L.K., Sanders, A.J., Chowdhury, R., Jiang, W.G., Steadman, R., Wymant, J., Jones, A.T., Kynaston, H., Mason, M.D., *et al.* (2015). Differentiation of tumour-promoting stromal myofibroblasts by cancer exosomes. *Oncogene* 34, 290-302.
- Wei, H., Chen, Q., Lin, L., Sha, C., Li, T., Liu, Y., Yin, X., Xu, Y., Chen, L., Gao, W., *et al.* (2021). Regulation of exosome production and cargo sorting. *Int J Biol Sci* 17, 163-177.
- Wei, Z., Batagov, A.O., Schinelli, S., Wang, J., Wang, Y., El Fatimy, R., Rabinovsky, R., Balaj, L., Chen, C.C., Hochberg, F., *et al.* (2017). Coding and noncoding landscape of extracellular RNA released by human glioma stem cells. *Nat Commun* 8, 1145.
- Weider, M., and Wegner, M. (2017). SoxE factors: Transcriptional regulators of neural differentiation and nervous system development. *Semin Cell Dev Biol* 63, 35-42.
- Weiss, A., and Attisano, L. (2013). The TGFbeta superfamily signaling pathway. *Wiley Interdiscip Rev Dev Biol* 2, 47-63.
- Wen, P.J., Grenklo, S., Arpino, G., Tan, X., Liao, H.S., Heureaux, J., Peng, S.Y., Chiang, H.C., Hamid, E., Zhao, W.D., *et al.* (2016). Actin dynamics provides membrane tension to merge fusing vesicles into the plasma membrane. *Nat Commun* 7, 12604.
- Wu, B., Su, S., Patil, D.P., Liu, H., Gan, J., Jaffrey, S.R., and Ma, J. (2018). Molecular basis for the specific and multivalent recognitions of RNA substrates by human hnRNP A2/B1. *Nat Commun* 9, 420.
- Wu, Y., Deng, J., Rychahou, P.G., Qiu, S., Evers, B.M., and Zhou, B.P. (2009). Stabilization of snail by NF-kappaB is required for inflammation-induced cell migration and invasion. *Cancer Cell* 15, 416-428.

- Wu, Y., Deng, W., McGinley, E.C., and Klinker, D.J., 2nd (2017). Melanoma exosomes deliver a complex biological payload that upregulates PTPN11 to suppress T lymphocyte function. *Pigment Cell Melanoma Res* 30, 203-218.
- Wu, Y., Fletcher, M., Gu, Z., Wang, Q., Costa, B., Bertoni, A., Man, K.H., Schlotter, M., Felsberg, J., Mangei, J., *et al.* (2020). Glioblastoma epigenome profiling identifies SOX10 as a master regulator of molecular tumour subtype. *Nat Commun* 11, 6434.
- Xiao, D., Barry, S., Kmetz, D., Egger, M., Pan, J., Rai, S.N., Qu, J., McMasters, K.M., and Hao, H. (2016). Melanoma cell-derived exosomes promote epithelial-mesenchymal transition in primary melanocytes through paracrine/autocrine signaling in the tumor microenvironment. *Cancer Lett* 376, 318-327.
- Yang, E., Wang, X., Gong, Z., Yu, M., Wu, H., and Zhang, D. (2020). Exosome-mediated metabolic reprogramming: the emerging role in tumor microenvironment remodeling and its influence on cancer progression. *Signal Transduct Target Ther* 5, 242.
- Yang, S., Che, S.P., Kurywchak, P., Tavormina, J.L., Gansmo, L.B., Correa de Sampaio, P., Tachezy, M., Bockhorn, M., Gebauer, F., Haltom, A.R., *et al.* (2017). Detection of mutant KRAS and TP53 DNA in circulating exosomes from healthy individuals and patients with pancreatic cancer. *Cancer Biol Ther* 18, 158-165.
- Yasumoto, K., Yokoyama, K., Shibata, K., Tomita, Y., and Shibahara, S. (1994). Microphthalmia-associated transcription factor as a regulator for melanocyte-specific transcription of the human tyrosinase gene. *Mol Cell Biol* 14, 8058-8070.
- Yin, H., Qin, C., Zhao, Y., Du, Y., Sheng, Z., Wang, Q., Song, Q., Chen, L., Liu, C., and Xu, T. (2017). SOX10 is over-expressed in bladder cancer and contributes to the malignant bladder cancer cell behaviors. *Clin Transl Oncol* 19, 1035-1044.
- Yin, J., Zeng, A., Zhang, Z., Shi, Z., Yan, W., and You, Y. (2019). Exosomal transfer of miR-1238 contributes to temozolomide-resistance in glioblastoma. *EBioMedicine* 42, 238-251.
- Yokoi, A., Villar-Prados, A., Oliphint, P.A., Zhang, J., Song, X., De Hoff, P., Morey, R., Liu, J., Roszik, J., Clise-Dwyer, K., *et al.* (2019). Mechanisms of nuclear content loading to exosomes. *Sci Adv* 5, eaax8849.
- Yu, L.L., Zhu, J., Liu, J.X., Jiang, F., Ni, W.K., Qu, L.S., Ni, R.Z., Lu, C.H., and Xiao, M.B. (2018). A Comparison of Traditional and Novel Methods for the Separation of Exosomes from Human Samples. *Biomed Res Int* 2018, 3634563.
- Yue, K.Y., Zhang, P.R., Zheng, M.H., Cao, X.L., Cao, Y., Zhang, Y.Z., Zhang, Y.F., Wu, H.N., Lu, Z.H., Liang, L., *et al.* (2019). Neurons can upregulate Cav-1 to increase intake of endothelial cells-derived extracellular vesicles that attenuate apoptosis via miR-1290. *Cell Death Dis* 10, 869.
- Zeng, A., Wei, Z., Rabinovsky, R., Jun, H.J., El Fatimy, R., Deforz, E., Arora, R., Yao, Y., Yao, S., Yan, W., *et al.* (2020). Glioblastoma-Derived Extracellular Vesicles Facilitate Transformation of Astrocytes via Reprogramming Oncogenic Metabolism. *iScience* 23, 101420.

- Zhang, H., Deng, T., Liu, R., Ning, T., Yang, H., Liu, D., Zhang, Q., Lin, D., Ge, S., Bai, M., *et al.* (2020). CAF secreted miR-522 suppresses ferroptosis and promotes acquired chemo-resistance in gastric cancer. *Mol Cancer* 19, 43.
- Zhang, H., Freitas, D., Kim, H.S., Fabijanic, K., Li, Z., Chen, H., Mark, M.T., Molina, H., Martin, A.B., Bojmar, L., *et al.* (2018a). Identification of distinct nanoparticles and subsets of extracellular vesicles by asymmetric flow field-flow fractionation. *Nat Cell Biol* 20, 332-343.
- Zhang, W., Zhou, X., Zhang, H., Yao, Q., Liu, Y., and Dong, Z. (2016). Extracellular vesicles in diagnosis and therapy of kidney diseases. *Am J Physiol Renal Physiol* 311, F844-F851.
- Zhang, Y., Liu, Y., Liu, H., and Tang, W.H. (2019). Exosomes: biogenesis, biologic function and clinical potential. *Cell Biosci* 9, 19.
- Zhang, Z.J., Guo, J.S., Li, S.S., Wu, X.B., Cao, D.L., Jiang, B.C., Jing, P.B., Bai, X.Q., Li, C.H., Wu, Z.H., *et al.* (2018b). TLR8 and its endogenous ligand miR-21 contribute to neuropathic pain in murine DRG. *J Exp Med* 215, 3019-3037.
- Zhao, L., and Koopman, P. (2012). SRY protein function in sex determination: thinking outside the box. *Chromosome Res* 20, 153-162.
- Zhou, X., Yan, T., Huang, C., Xu, Z., Wang, L., Jiang, E., Wang, H., Chen, Y., Liu, K., Shao, Z., *et al.* (2018). Melanoma cell-secreted exosomal miR-155-5p induce proangiogenic switch of cancer-associated fibroblasts via SOCS1/JAK2/STAT3 signaling pathway. *J Exp Clin Cancer Res* 37, 242.
- Zhuang, G., Wu, X., Jiang, Z., Kasman, I., Yao, J., Guan, Y., Oeh, J., Modrusan, Z., Bais, C., Sampath, D., *et al.* (2012). Tumour-secreted miR-9 promotes endothelial cell migration and angiogenesis by activating the JAK-STAT pathway. *EMBO J* 31, 3513-3523.

7 CURRICULUM VITAE

Personal information

Name: Peng Yuan
Date of birth: April, 13th, 1991
Place of birth: Anhui, China
Nationality: Chinese
Email: yp19911000@gmail.com
Address: INF 681, 69120, Heidelberg

Education:

Oct 2017 – present M.D. student(Dr. med)
Ruprecht-Karls-University Heidelberg
MD project : The impact of SOX10 downregulation in modulating the extracellular vesicles

Sep. 2016 – Sep. 2017 M.Sc. Translational Medical Research
Ruprecht-Karls-University Heidelberg
Thesis: Functional characterization of exosomes in murine B cell lymphoma

Sep. 2014 – July 2016 Master of Medicine
Anhui Medical University
Thesis: System evaluation of antiviral therapy performed after curative therapy on patients with HBV-related hepatocellular carcinoma

Sep.2009 – June.2016 Bachelor of Medicine
Anhui Medical University

Scholarship: Scholarship from China Scholarship Council (CSC)

Publications:

Yuan,P, Chen,P, Qian, Yeben. Evaluation of antiviral therapy performed after curative therapy in patients with hepatitis B virus-related hepatocellular carcinoma: An updated meta-analysis. Can J Gastroenterol Hepatol 2016;2016:5234969

Chen P, **Yuan P**, Chen B, Sun J, Shen H, Qian Y. Evaluation of drug-eluting beads versus conventional transcatheter arterial chemoembolization in patients with unresectable hepatocellular carcinoma: a systematic review and meta-analysis. *Clin Res Hepatol Gastroenterol*. 2017;41(1):75–85

8 ACKNOWLEDGEMENT

Firstly I would like to thank Prof. Dr. Peter Lichter and Dr. Bernhard Radlwimmer for supervising me in my 4-year MD study. And I would specially like to thank Dr. Bernhard Radlwimmer for the direct supervision of my doctoral thesis and constant support of my work on SOX10 and exosome project during the years.

I would like to thank my colleagues Dr. Yonghe Wu and Ka Hou Man to work with me on the SOX10 project, sharing me with their valuable experience and expertise on scientific research. And I would also like to thank my colleagues, Liliana Francois Martin del Campo, Magdalena Schlotter, Jasmin Mangei, Pavle Boskovic, Petra Schroeter and Theresa Schmid for always being patient and nice to me and making a wonderful working atmosphere in the lab.

In addition, I would like to thank Dr. Martina Seiffert to accept me to work on exosomes when I was a master student in B060.

Special thanks to Prof. Dr. Jochen Sven Utikal and Prof. Dr. Viktor Umansky for giving me so many valuable suggestions on my project and thesis.

I would also thank the Chinese Scholarship Council for financing me to finish the doctoral study in Germany.

At last but most importantly, I would like to thank my wife Shanshan Wu for her deep love, patience and supports during the years, I love you forever. And I would thank my parents and grandparents for supporting me all the time whenever I need help, I love them forever too.